Blue-green catastrophe: remote sensing of mass viral lysis of cyanobacteria

Simis, S.G.H.

2006

BLUE-GREEN CATASTROPHE

remote sensing of mass viral lysis of cyanobacteria

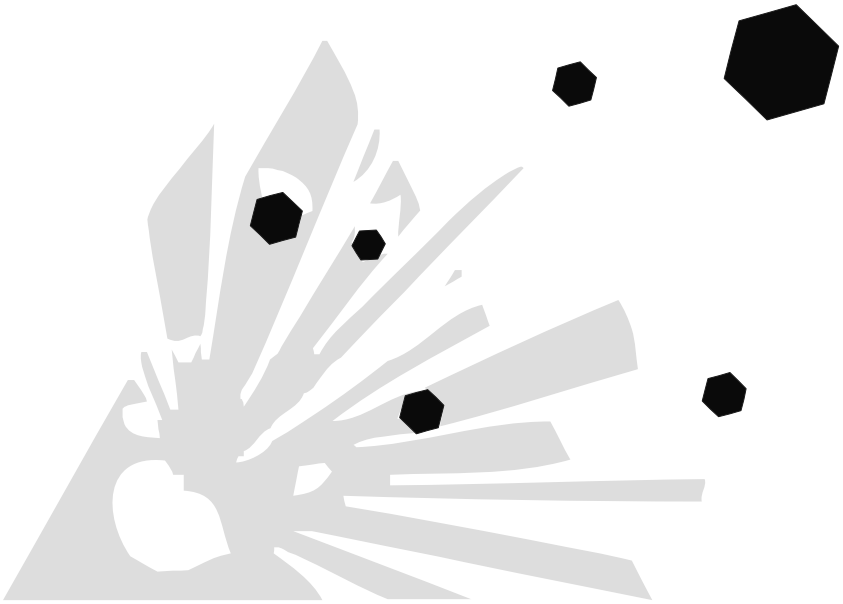

Blue-green catastrophe: remote sensing of mass viral lysis of cyanobacteria.
[Ph. D. Thesis, Vrije Universiteit Amsterdam]

In Dutch:
Blauwgroene catastrofe: remote sensing van massale virussterfte van cyanobacteriën
[ac. proefschrift, Vrije Universiteit Amsterdam]

NIOO Thesis 48

ISBN-10: 90-8659-039-X
ISBN-13: 978-90-8659-039-1

Cover: Caution: lysis hazard.

This research was financially supported through grant EO-053 from the User Support Programme managed by the programme office External Research of the Netherlands Organization for Scientific Research—National Institute for Space Research (NWO-SRON).

The work for this thesis was carried out at the Netherlands Institute of Ecology (NIOO-KNAW), Centre for Limnology, department Microbial Wetland Ecology, and at the Institute for Environmental Studies (IVM), Vrije Universiteit Amsterdam.

NETHERLANDS INSTITUTE OF ECOLOGY

vrije Universiteit *amsterdam*

VRIJE UNIVERSITEIT

BLUE-GREEN CATASTROPHE

remote sensing of mass viral lysis of cyanobacteria

ACADEMISCH PROEFSCHRIFT

ter verkrijging van de graad Doctor aan
de Vrije Universiteit Amsterdam,
op gezag van de rector magnificus
prof.dr. L.M. Bouter,
in het openbaar te verdedigen
ten overstaan van de promotiecommissie
van de faculteit der Aard- en Levenswetenschappen
op woensdag 29 november 2006 om 10.45 uur
in het auditorium van de universiteit,
De Boelelaan 1005

door

Stefan Gerardus Henricus Simis

geboren te Purmerend

promotoren:	prof.dr. A. Brouwer
	prof.dr. H.J. Laanbroek
copromotoren:	dr. H.J. Gons
	dr. S.W.M. Peters

TABLE OF CONTENTS

1. GENERAL INTRODUCTION

"It came to pass before that great war in which nearly all this province was destroyed by the sons of Jestin, that the large lake and the river Leveni which flows from it into the Wye opposite Glasbury, were tinged with deep green colour. The old people of the country were consulted and answered that a short time before the great desolation caused by Howel, son of Meredyth, the water had been coloured in a similar manner. […]

The lake also (according to the testimony of the inhabitants) is endued with miraculous powers; for, as we have before observed, it sometimes assumed a greenish hue, so in our day, it has appeared to be tinged with red, not universally, but as if blood flowed partially through certain veins and small channels."

Giraldus Cambrensis, 1188, according to Griffiths, 1938.

"Am 8. Januar zeigte das über dem grünen schlammigen Bodensatz stehende Wasser ein sehr schönes und auffallendes Farbenspiel. Es war von oben betrachtet blutroth und gegen das Licht gehalten sehr schön himmelblau. [...] Wenn wir diesen Stoff mit einem Namen bezeichnen wollen, so würde ich dafür das Wort "Saprocyanin," oder weil die Farbe blau und roth erscheint."

Nees v. Esenbeck, 1836.

"Being very light, it floats on the water except during breezes, when it becomes diffused. Thus floating, it is wafted to the lee shores, and forming a thick scum like green oil paint, some two to six inches thick, and as thick and pasty as porridge, it is swallowed by cattle when drinking, especially such as suck their drink at the surface like horses. This acts poisonously, and rapidly causes death; symptoms—stupor and unconsciousness, falling and remaining quiet, as if asleep, unless touched, when convulsions come on, with head and neck drawn back by rigid spasm, which subsides before death. Time—sheep, from one to six or eight hours; horses, eight to twenty-four hours; dogs, four to five hours; pigs, three or four hours. […] There exudes from this decomposing matter a blue pigment which has remarkable properties. […] This fluid is remarkably red, fluorescent by reflected light, being blue by transmitted light. Spectrum a broad and deep band total at top in the red, but shading off to green, quite cutting off orange and yellow."

George Francis, 1878.

"In welke plas kun je veilig zwemmen?"

De Volkskrant, 26 July 2006.

Abstract

This thesis presents an analysis of optical characteristics of epidemic infection and death of cyanobacteria by viruses, applied to the field of optical remote sensing. The main objective of the research was to investigate whether current remote sensors, in particular the Medium Resolution Imaging Spectrometer onboard the ENVISAT satellite mission, can be used to detect mass viral lysis of cyanobacteria in well mixed, turbid, eutrophic water bodies. It is expected that catastrophic viral lysis of a dominant cyanobacterial population brings about optical changes that can be detected with optical sensors mounted on satellite platforms in space. This chapter provides a general introduction on the occurrence of cyanobacteria in inland water bodies, the role of viruses as agents of cyanobacterial population control, and the use of remote sensing instruments to monitor water colour.

1.1. Cyanobacteria

Fossil records date the earliest cyanobacteria back over 3 billion years (Des Marais 2000, Schopf 2000). Primitive cyanobacteria are attributed the early production of oxygen on Earth, as well as a key role in the evolution of intracellular structure. Cyanobacteria are found in diverse and extreme environments, ranging from the Antarctic ice to hot springs, bare rock, arid soil, salt lakes, corals, polar bears, and golf greens (Lewin and Robinson 1979, Whitton and Potts 2000). When speculating on the existence of extraterrestrial life, cyanobacteria-like life forms make a pretty good candidate.

The name ‘cyanobacteria’ derives from their colour, commonly blue-green (cyan), due to the presence of water-soluble phycobilin pigments. These pigments, mainly forms of phycoerythrin (pink) and phycocyanin (blue) are able to harvest light for photosynthesis in a part of the spectrum that is little used by other photosynthetic organisms. All cyanobacteria produce at least some phycocyanin; phycoerythrin-rich species are known to occasionally give the water a blood-like appearance, inspiring some sinister legends (cf. Griffiths 1939).

Cyanobacteria are widely discredited for their negative impact on water quality, mainly due to the formation of surface scums and the ability of some species to produce toxic substances. Symptoms can range from skin irritation to fever, intestinal problems, and various allergic reactions (Chorus and Bartram 1999). High cyanotoxin levels have lead to poisoning of birds, fish and livestock on a number of occasions. Rapid tests for toxin presence are not yet available, so common policy is to issue a health warning as soon as dense cyanobacterial populations are suspected in any

Table 1.1. Observations of cyanobacterial population collapse in the Netherlands. Data from Water Management Board of Rijnland, Leiden (unpubl.), and Limnological Institute, Oosterzee (unpubl.).

Lake	Year	Collapsed	Recovered
Langeraar Lakes (Noordplas, Geerplas)	1985	26 June	13 November
Nieuwkoop Lakes (Zuideinderplas)	1985	24 July	18 September
Lake Tjeukemeer	1985	8 October	Spring 1986
Lake Amstelveense Poel	1993	24 June	22 July
Lake Amstelveense Poel	1999	3 June	29 July
Nieuwkoop Lakes (Zuideinderplas)	1999	23 June	21 July
Langeraar Lakes (Geerplas)	2003	16 June	unknown
Reeuwijk Lakes (Ravensbergse plas)	2005	early June	unknown

recreational water body. However, some cyanotoxins can pose a health risk even at relatively low concentrations and population densities. Adding to the problem, cyanobacterial dominance is promoted by high nutrient loading. Intensive land use and untreated wastewater discharge lead to increased nutrient concentrations, a process called eutrophication, although some lakes are naturally eutrophic. Several species are able to fix gaseous nitrogen, an energy-consuming process, but allowing access to a virtually unlimited nitrogen supply, the atmosphere. The unique pigmentation of the cyanobacteria allows them to efficiently harvest sunlight even in turbid waters. Several species are able to trace the right environment of light and other resources by regulating their buoyancy to actively migrate vertically in the water column, which can lead to very high population densities near or at the water surface. Dense populations of cyanobacteria decrease water transparency, reducing the recreational value of the water body and preventing the growth of submerged vegetation, which could compete for light and nutrients. In general cyanobacteria are a less valuable food source and may suffer less grazing losses than most algae, hampering top-down control of their growth (Porter 1973, Richman and Dodson 1983).

Death of cyanobacteria releases organic material, which is recycled by heterotrophic bacteria that use oxygen in the process. Sudden death and degradation of a whole cyanobacterial population can cause oxygen depletion, resulting in fish kills. The death of toxin-producing cells may be particularly dangerous. Provided that the population loss is substantial, a lethal dose of harmful substances could be released into the water, which at the same time loses the murky appearance that intuitively holds back most swimmers. Therefore it is not sufficient to know only the current state of cyanobacteria in public water bodies; it is best to monitor continuously.

The risks of cyanobacterial growth and mortality are substantial, and it has been well established that cyanobacteria thrive in eutrophic lakes and reservoirs. As to whether mass mortality, as discussed above, is very likely to occur in nature, is less well known and the mechanisms behind such events are not very clear. Mortality may be caused by

many factors, such as grazing, nutrient starvation or programmed cell death (Berman-Frank *et al*. 2004). One scenario, however, stands out when it comes to the sudden death of an otherwise productive population: the role of viruses. The impact of viruses on the phytoplankton has long been underestimated but is now considered an unparalleled route to rapid termination of a dominating species. Viral infection is a density-dependent process and a dominant cyanobacterial population could thus be very susceptible—obviously being big comes with a price.

1.2. Viruses

Billions of viruses are found per litre of natural water (Bergh *et al.* 1989), making viruses the most numerous biological particles on Earth. All viruses are obligate parasites—no propagation without a host. Infection of a unicellular alga or a cyanobacterium leads to the reproduction of the viral genome, production of a new generation of virus particles, and eventually death of the host and release of viral progeny. In any water body a multitude of viral strains may be found to coexist with their hosts, promoting population turnover, nutrient recycling, and possibly gene transfer. Most viruses in the aquatic environment are considered host-specific, relying heavily on a chance encounter with a suitable host, suggesting that a dominant host species is likely to suffer the largest losses—viruses will 'kill the winner' of the competition for resources (Thingstad and Lignell 1997). Thus, viruses may limit the growth of dominating species and sustain higher biodiversity. Assemblages of viruses and hosts can easily co-exist in Lotka-Volterra (lynxes vs. hares) type population models (Levin *et al.* 1977, Thingstad 2000). This density-dependent behaviour may be compared with the passing of the common cold viruses between humans. Instinctively, when you're standing in a cramped elevator, you'd prefer the person behind you not to sneeze; the more crowded that elevator, the more likely that you will be the next to suffer from the common cold (Dick *et al*. 1987).

It has been demonstrated that phytoplankton blooms are susceptible to viral lysis up to epidemical proportions (Bratbak *et al.* 1993, Beltrami and Carroll 1994, Brussaard *et al.* 1996). However, it is largely unknown under which circumstances and how often bloom termination by viruses occurs in nature. Nutrient enrichment, resulting from flood events or wastewater spills, may induce the phenomenon by promoting the rapid growth of cyanobacterial hosts with a good capacity for viral reproduction (Gons *et al.* 2006).

Several observations of sudden, catastrophic death of cyanobacterial populations have been made in nature (Table 1.1). Unfortunately, these cases were not adequately documented to reveal the cause of the cyanobacterial collapse. In the laboratory environment, complete lysis of a bloom-forming cyanobacterial population has been repeatedly found to take only a few days (Van Hannen *et al.* 1999, Gons *et al.* 2002*a*,

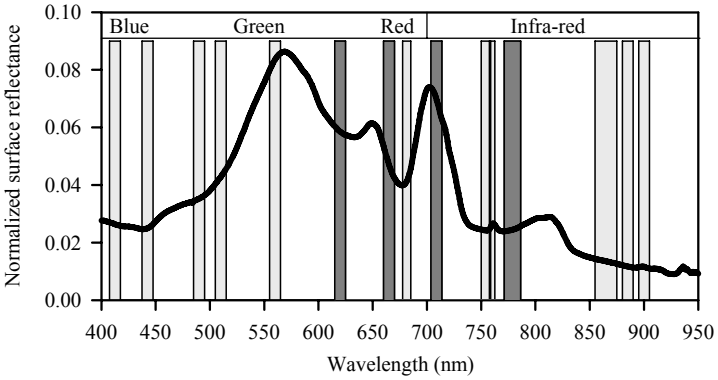

Figure 1.1. Reflectance spectrum of a cyanobacteria-dominated, turbid lake, measured in Spain. The valleys in the spectrum around 675 and 625 nm indicate the absorption maxima of the phytoplankton pigments chlorophyll *a* (algae and cyanobacteria) and phycocyanin (cyanobacteria), respectively. MERIS band positions are indicated by the vertical bars. The dark bands are used to estimate chlorophyll *a* and phycocyanin concentrations (Gons *et al*. 2002*b*, Simis *et al*. 2005*a*).

Simis *et al.* 2005*b*). Although the short time span of these events suggests that the phenomenon is easily overlooked in nature, the studies did reveal that the process of viral lysis was accompanied by marked changes in the appearance of the water column. The typical 'pea soup' of cyanobacteria-dominated lake water turned rapidly into a transparent, pale yellow mixture of cell debris and dissolved organic matter. When viral activity is so hard to monitor during mass mortality events that occur in nature, could these changes in water colour be used as an indicator, and if so, how could they be detected?

1.3. Water colour

When sunlight penetrates the water surface and interacts with water molecules and dissolved and particulate water constituents, the intensity and spectral quality of the light change with depth. Pure water appears blue, since light is mainly scattered at short wavelengths (blue light) and absorbed at longer wavelengths (red to infrared) in water. In turbid water, the downwelling light is mainly attenuated due to the absorption by phytoplankton pigments, coloured dissolved organic matter, cell tissue, suspended sediments, and detrital matter. The downwelling light is additionally attenuated by molecular scattering of the water, and particulate scattering by colloids, viruses, bacteria, cyanobacteria, algae, flagellates, and larger planktonic organisms (Stramski and Kiefer 1991, Kirk 1994).

A small part of the downwelling light is eventually scattered back to, and emerges from, the water surface. The ratio of upwelling light relative to downwelling light is

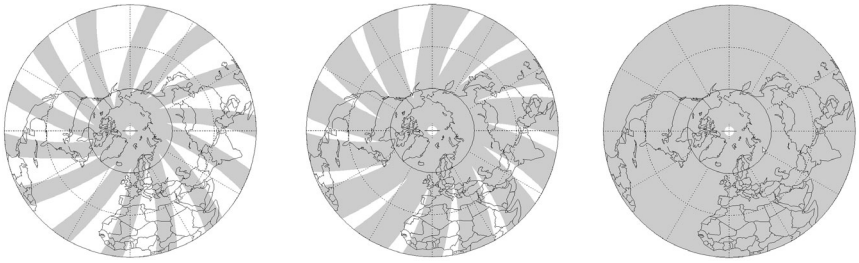

Figure 1.2. Coverage of the Earth by MERIS. In one day, 14 orbits are completed out of a repeat cycle of 35 orbits. Only descending (illuminated) pathway shown.

referred to as reflectance. The perception of water colour is a function of reflectance just above the water surface, in those parts of the electromagnetic spectrum to which our eyes are sensitive. In order to analyze the contribution of different water constituents to the appearance of a water body, dedicated sensors are needed. Such sensors register the intensity of reflected light in narrow wavebands, e.g. for a band covering the wavelength of maximum light absorption by the pigment phycocyanin (Figure 1.1).

1.4. Remote sensing

"Remote sensing is the science of deriving information about the Earth's land and water areas from images acquired at a distance. It usually relies upon measurement of electromagnetic energy reflected or emitted from the features of interest" (Campbell 1987). Remote sensing instruments are commonly mounted on aircraft or satellites, allowing the simultaneous registration of water colour for a large number of water bodies, simultaneously. For airborne campaigns the operational costs are repeated for every flight, and obtaining time-series to document cyanobacterial dynamics quickly becomes very expensive. Satellite missions require more funding to launch, but can be expected to deliver imagery for a period up to ten years, on a global scale. The advance of technology is the main limiting factor determining the spatial and spectral resolution of the images that remote sensors provide.

In March 2002, the European Space Agency launched the ENVISAT satellite mission to observe environmental processes from space. One of the ten instruments in the ENVISAT payload is the Medium Resolution Imaging Spectrometer (MERIS). MERIS' purpose is to record the surface reflectance of oceans, coastal waters, and land (Rast 1999). The sensor is particularly interesting for monitoring turbid waters because it provides a number of spectral bands that target the absorption maxima of the main

phytoplankton pigment, chlorophyll *a*, as well as the cyanobacterial pigment phycocyanin at an unparalleled radiometric sensitivity. Figure 1.1 shows a reflectance spectrum typical of a water body with cyanobacteria dominating the phytoplankton, as well as the MERIS bands, which can be seen to overlap with several spectral features. MERIS has a pixel size of 260 × 290 m and global coverage every 2 to 3 days, following a polar orbit as illustrated in Figure 1.2. Atmospheric conditions can significantly reduce the amount of available imagery: the annual and winter averages of clear sky in the Netherlands are 32 % and 18 % of the daytime, respectively.

1.5. Thesis objectives and outline

This thesis is a compilation of scientific papers produced under a common theme. The question that prompted the research was whether dramatic optical changes, associated with the sudden viral lysis of the dominant cyanobacterial population in a turbid, eutrophic lake, could be observed using remote sensing techniques, in particular with MERIS. The answer is sought over the following chapters, dealing with the subtopics as given below.

Optical changes associated with cyanobacterial bloom termination

In **Chapter 2** the focus is on a description of changes in inherent optical properties of enclosed lake water upon mass viral lysis of the dominant filamentous cyanobacterial population. Potential optical indicators for mass viral lysis in nature are presented. A tentative upscaling of results towards reflectance, before and after the collapse of the dominant cyanobacterial population, is given. **Chapter 3** is an optical modelling study that was carried out to quantify changes in reflectance that result during mass viral lysis of a cultured cyanobacterium.

Remote sensing of cyanobacterial biomass

A remote sensing algorithm for the quantification of absorption by accessory photosynthetic pigments, focused on the cyanobacterial pigment phycocyanin, is presented in **Chapter 4**. The application of the algorithm is for cyanobacteria-dominated, well mixed, turbid, eutrophic lakes, using wavebands that are available from MERIS imagery. The concentration of phycocyanin in the surface layer serves as a proxy for cyanobacterial biomass. In **Chapter 5** the algorithm is validated with field observations on Lake IJsselmeer (The Netherlands) and a large number of Spanish lakes and reservoirs.

MERIS potential for inland water quality monitoring

Chapter 6 focuses on the suitability of MERIS to monitor the cyanobacterial state of turbid inland water bodies, in terms of adequate retrieval of reflectance data from several turbid lakes. Since neither the MERIS instrument nor the data processing chain

were designed to deal with turbid inland water bodies, several problems with the quality of the output products arise. Recommendations for the treatment of MERIS data are given in this chapter.

A summarizing discussion of the results from the research carried out for this thesis, and an outlook for further research and application of the remote sensing tools that have been developed during this study, are given in **Chapter 7**. Interested readers who are not familiar with hydrologic optics may prefer to first direct their attention to this chapter.

2. OPTICAL CHANGES ASSOCIATED WITH CYANOBACTERIAL BLOOM TERMINATION BY VIRAL LYSIS

Stefan G.H. Simis, Marjolijn Tijdens, Hans L. Hoogveld & Herman J. Gons

Journal of Plankton Research (2005) 27: 937-949

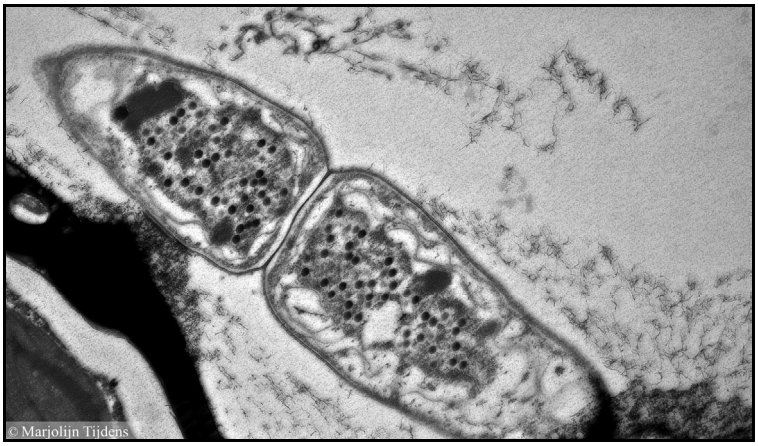

Electron micrograph of the virus-infected cells of a filamentous cyanobacterium, recorded during a laboratory-scale enclosure experiment. Figure by M. Tijdens.

Abstract

Optical changes that accompanied a collapse of the population of filamentous cyanobacteria from a shallow, eutrophic lake were studied in laboratory-scale enclosures. The experimental conditions are known, from previous work on these systems, to cause a dramatic collapse of the dominant algal or cyanobacterial species, which in turn can be associated with viral activity. Within 2 weeks of continuous addition of nutrient-rich growth medium, near-complete collapse of the dominant population occurred over the span of a few days. The collapse was repeatedly and reproducibly observed and was primarily characterized by a marked increase in water transparency. Scattering of light decreased by ≈ 80%, absorption decreased by 20-80%. There was high similarity in optical changes between several experiments, carried out in different seasons. An increase of dissolved material and submicron-sized particles that showed chlorophyll *a* absorption was observed during the collapse. The phycocyanin : chlorophyll *a* ratio and phaeopigment : chlorophyll *a* ratio proved to be good indicators of the observed collapse. Reflectance spectra that were modelled using a constant volume-scattering function indicated that mass mortality of this magnitude can be detected in natural systems using current remote sensors.

2.1. Introduction

Eutrophication has caused an increase in the occurrence of cyanobacterial blooms, mainly in coastal and inland water bodies. Blooms of cyanobacteria are of a relatively persistent nature and can lead to surface scums, especially under calm weather conditions. Toxin-producing strains pose an immediate health risk at high population densities. In water with a recreational function a public warning is often issued as soon as blooms of cyanobacteria are reported. Although reports of cyanobacterial bloom abound, there is little information on the environmental effects of cyanobacterial bloom decay. Anoxia resulting from increased activity by heterotrophic bacteria upon termination of a phytoplankton bloom can lead to fish kills and loss of recreational and economic value. Cyanobacterial blooms that produce toxins may introduce a high concentration of harmful substances into the environment upon sudden collapse. Increasing efforts are being made by local water quality managers and national governments to predict and prevent cyanobacterial blooms.

Viruses may be a primary mortality factor determining population turnover in phytoplankton communities (Bergh *et al.* 1989, Proctor and Fuhrman 1990, Suttle 1994, Brussaard 2004). Phytoplankton blooms offer dense host populations, often monospecific, and due to the population density-dependent nature of virus-host interactions, phytoplankton blooms are susceptible to viral lysis up to epidemical

Table 2.1. Relevant facts concerning starting conditions (t = 0 after filling the LSEs) and time of lysis in the experiments. The Chl a concentrations, depth of the euphotic zone z_{eu} (where 1 % of downwelling photosynthetically active radiation is available), pH, and temperature values were typical for the time of year.

Date	Lysis			Starting conditions			
	LSEs	Start (day)	End (day)	Chl *a* (mg m^{-3})	z_{eu} (m)	pH	Temperature (°C)
6 November 2002	1	12	19	86	1.6	8.3	9.5
24 March 2003	3	9	14	50	1.9	8.3	9.5
17 June 2003	1	6	13	60	1.5	8.4	22.0

proportions (Bratbak *et al.* 1993, Beltrami and Carroll 1994, Brussaard *et al.* 1996). However, it is largely unknown under which circumstances and at which frequency bloom termination by viruses occurs in nature. During experiments with nutrient-enriched lake water in laboratory-scale enclosures (LSEs) it was observed that the dominant filamentous cyanobacteria present in the water from a turbid, eutrophic lake, suffered a sudden collapse after a period of steady growth (Van Hannen *et al.* 1999, Gons *et al*. 2002*a*). The exclusive collapse of the filamentous cyanobacteria, the lack of large numbers of grazing zooplankton, observations of maturing cyanophages by transmission electron microscopy, and an increased number of virus-like particles suggested that the mortality of cyanobacteria was primarily due to viral lysis.

For a series of LSE experiments, the current aim was to describe changes in the optical properties upon the collapse of the dominant species as a result of viral lysis. It is expected that upon lysis of the dominant species, inherent optical properties (absorption and scattering) of the water body will change drastically. The changes in bulk optical properties are caused by the disruption (lysis) of infected cells, which causes the release of soluble and non-soluble matter into the surrounding medium. As a result, absorption processes by photosynthetic pigments are not restricted to cells and absorption of light by photosynthetic pigments does not lead to photosynthetic energy conversion. During the phase of lysis of the host population scattering and absorption by living cells or colonies are thus largely replaced by scattering and absorption due to small particles and soluble material. Additionally, a positive response of heterotrophic bacteria, ciliates, nanoflagellates, etc. can be expected as a result of the release of fresh organic material, causing further changes in the observed water colour.

A description of the optical changes that are found upon mass lysis could in the future be used to identify lytic events in nature from optical remote sensing data derived from spaceborn instruments or sensors moored on ships or buoys. An optical model linked to remotely sensed imagery of a high spatial scale offers the possibility to monitor a large number of water bodies simultaneously. With time-series of remotely sensed data, the possibility to identify bloom termination in natural systems is further

Table 2.2. Composition of the culture medium used in the experiments (concentrations in mg L^{-1} in the medium reservoirs, compounds added to distilled water). The medium was continuously added using peristaltic pumps at 7 L d^{-1}. The phosphate and Fe/EDTA compounds were added from separate containers at 0.25 L d^{-1}. Medium added to replace extracted samples did not contain phosphate and Fe/EDTA compounds. Concentrations (µmol L^{-1} d^{-1}) added to the LSEs daily are given in the last column.

Compound	In medium reservoir (mg L^{-1})	Daily addition to LSE (µmol L-LSE^{-1} d^{-1})
Combined in medium reservoir:		
$NaNO_3$	250	158.4
$NaHCO_3$	201	128.8
$MgSO_4 \cdot 7H_2O$	25	5.5
$CaCl_2 \cdot 2H_2O$	6.5	2.4
Trace elements:		
H_3BO_3	1.430	1.2
$MnCl_2 \cdot 4H_2O$	0.905	0.2
$CuSO_4 \cdot 5H_2O$	0.040	< 0.01
$Co(NO_3)_2 \cdot 6H_2O$	0.040	< 0.01
$ZnSO_4 \cdot 7H_2O$	0.011	< 0.01
NH_4VO_3	0.005	< 0.01
$(NH_4)_6Mo_7O_{24} \cdot 4H_2O$	0.001	< 0.01
Introduced from separate containers:		
K_2HPO_4	295	3.3
$Na_2EDTA + FeCl_2 \cdot 4H_2O$	40.0 + 33.3	0.2 + 0.3

increased. The temporal resolution of remotely sensed data with a wide spatial coverage is, however, limited. This study therefore focuses on a description of the 'pre-lysis' or bloom-situation and the 'post-lysis' situation, which were observed in the experimental systems. The optical changes between these moments describe the largest optical changes that could be found in the field situation.

Until now, only changes in single-wavelength scattering and backscattering upon viral lysis of cultured heterotrophic bacterial species, and of the cyanobacterium *Synechococcus marinus* have been described (Balch *et al.* 2002). This study is the first to describe the changes in spectral absorption and scattering upon viral lysis of phototrophic aquatic micro-organisms, in this case a filamentous cyanobacterium belonging to a group of *Limnothrix*/*Pseudanabaena* species common to shallow, eutrophic lakes (Zwart *et al.* 2005). This is also the first study to describe these optical changes with respect to enclosed lake water rather than cultured material. Although changes in the backscattering coefficient are still lacking, an attempt was made to describe changes in the remote-sensing reflectance of a water body undergoing mass collapse. The experimental system, the experimental conditions and the source of the lake water were unchanged with regard to the previous studies in which the collapse was attributed to viral activity (Van Hannen *et al.* 1999, Gons *et al.* 2002*a*).

2.2. Method

Experimental setup

Three mass lysis experiments were conducted in LSEs in November 2002, March 2003 and June 2003 (Table 2.1). From hereon, these experiments will be referred to as November, March, and June, respectively. The March experiment was carried out in triplicate. A detailed description of construction, operation and light climate of the enclosures is given elsewhere (Rijkeboer *et al.* 1990, Gons *et al.* 1992). In short, the LSEs are Perspex cylinders of 2 meters length and a volume of 130 L each. They are illuminated at one end and coated in reflective foil to avoid light losses through the walls. The enclosures are placed horizontally in a tank filled with water of regulated temperature. Sealable ports are located at the top and are used for sampling, a stirring mechanism (continuously active) and oxygen, pH and temperature probes. Nutrient medium can be fed to the column dropwise using peristaltic pumps. Water from the shallow (mean depth < 2 m), turbid (Secchi-disc depth ≈ 0.6 m), and highly eutrophic Lake Loosdrecht (The Netherlands) was used to fill the enclosures. The phytoplankton in this lake is typically predominated by filamentous cyanobacteria (Van Tongeren *et al.* 1992). See Table 2.2 for the composition of the growth medium, which was added dropwise at 7 L d^{-1}, causing excess fluid to spill from the exit port located at the far end of the column, at the same rate, thus obtaining a slow flow-through system (dilution rate 5.4 % of total volume d^{-1}). Phosphate and Fe/EDTA compounds were fed to the system from separate containers in order to avoid contamination of the growth medium, at a rate of 0.25 L d^{-1}. The systems received white light from high-intensity daylight-lamps (Osram, Metallogen HMI 1200W/GS) at 360 µmol m^{-2} s^{-1} photosynthetically active radiation (PAR) during a 16 : 8 h light-dark cycle. Temperature was maintained at 20 °C and periodic bubbling with CO_2 was carried out to maintain pH 8 – 9. For the experiments conducted in November and March it took approximately one day for the column to reach the experimental temperature. Dissolved oxygen levels were kept below 130% saturation and adjusted by bubbling with N_2. Table 2.1 lists several physical and biochemical parameters of each experiment at time zero in the laboratory (after filling the enclosures), including the Chlorophyll *a* (Chl *a*) concentration, pH, temperature, and depth of the euphotic zone (depth where 99% of downwelling irradiance is attenuated, calculated from vertical profiles of downwelling PAR measured at the sampling location).

During the experiment, dissolved oxygen and nutrient levels were monitored daily, while samples for optical measurements, pigment analyses and particulate organic matter (POM) were taken every 2-3 days. The samples (3 L = 2.3% of LSE volume) for optical and biochemical measurements were replaced by growth medium that lacked the phosphate and Fe/EDTA compounds. During lysis, the sampling frequency was intensified to a maximum of 3 times per day. For the present study, data from the first

20 - 25 days of the experiments are presented, spanning one cycle of growth, collapse and (in part) recovery of phototrophic biomass.

Total suspended matter was concentrated on Whatman GF/F filters (approximate pore size 0.7 μm). Subsequently, POM was obtained from the difference in weight of the dried filter before and after combustion of organic material at 550 °C for 2 h, with correction for the ignition loss of blank filters.

Inherent optical properties

Optical measurements of the materials in different size fractions (see further) were performed using a Lambda 800 UV/Vis spectrophotometer (PerkinElmer, Wellesley, MA, USA) in the 350 – 800 nm wavelength (denoted λ) range. A 150-mm integrating sphere (Labsphere Inc., North Sutton, NH, USA) was used for filterpad measurements (Yentsch, 1962, Maske and Haardt, 1987), with the filters positioned in the centre of the sphere using a clip-style centre mount accessory. Absorption was measured at 1-nm intervals, using 2-nm slit width at an integration time of 0.12 sec nm^{-1}. Spectra were not corrected for fluorescence. A scattering correction by subtracting far-red absorption values was not needed because scattering loss was minimal in this optical configuration.

The absorption values of different size fractions were obtained by filtration of the samples over filters of various pore sizes. Whatman GF/F filters were used to differentiate the > 0.7 μm and < 0.7 μm fractions [$a_{>0.7}(\lambda)$ and $a_{<0.7}(\lambda)$, respectively] and cellulose acetate filters (Schleicher & Schuell) were used to obtain the fraction < 0.2 μm [$a_{<0.2}(\lambda)$]. Care was taken to exert only mild vacuum pressure during filtration. The absorption by the fraction between 0.2 - 0.7 μm [$a_{0.2\text{-}0.7}(\lambda)$] was derived from $a_{<0.7}(\lambda) - a_{<0.2}(\lambda)$. For the $a_{>0.7}(\lambda)$ measurements, Whatman GF/F filters (Ø 25 mm) were placed in the sphere at a 100° angle from the incident beam. Reference and sample filters were wetted in the sample's filtrate prior to measurement. Equal moisture content of filters was obtained by shortly placing them on a tissue, without exerting pressure.

The optical densities measured using the quantitative filter technique (QFT) were corrected for path length amplification (Butler 1962, Kiefer and SooHoo 1982) as shown further below. The $a_{<0.7}(\lambda)$ and $a_{<0.2}(\lambda)$ spectra were measured without the integrating sphere accessory, in 5-cm optical-grade glass cells, against a reference of filtered distilled water. The attenuation coefficient of the total suspended matter $c(\lambda)$ was measured in the same way, but in a 1-cm geometrical path length optical-grade glass cell to minimize the effect of multiple scattering without diluting the sample. From the optical geometry of this setup it was estimated that the detector accepts light scattered at an angle < 1.3° with respect to the direction of incident light, thus approximating proper configuration for the measurement of beam attenuation, although

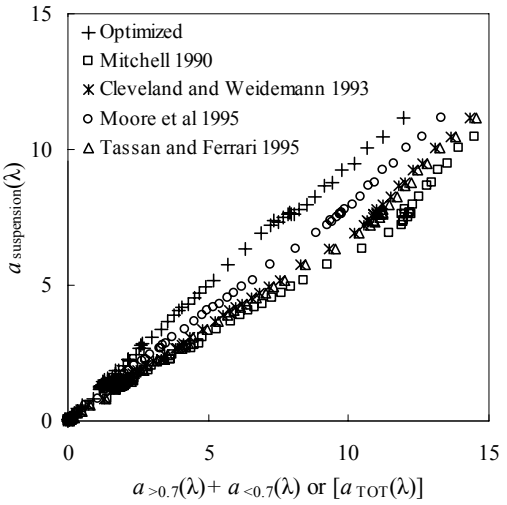

Figure 2.1. Absorption by particle suspension plotted against the sum of $a_{>0.7}(\lambda)$ (Eq. 2.1) and $a_{<0.7}(\lambda)$. Data obtained by averaging absorption spectra of the 8 samples used for the optimization (see text). Values plotted at 5-nm intervals in the region 350 – 800 nm.

underestimation may result when scattering is sharply peaked in the forward direction. The measurement of $c(\lambda)$ lacked for the November experiment.

Because the lysis experiments constitute a wide range of combinations of optically active water constituents, a correction for path length amplification in the QFT was established by comparing measurements on filters and filtrates to measurements of suspensions. Samples taken throughout the last of the experiments (n = 8) were used to optimize the relationship (Mitchell 1990, Hoepffner and Sathyendranath 1992, Cleveland and Weidemann 1993, Tassan *et al.* 2000):

$$a_{>0.7}(\lambda) = 2.3 \times \frac{\left[a\ \mathrm{OD_f}(\lambda) + b\ \mathrm{OD_f}(\lambda)^2\right]}{V \times A} \tag{2.1}$$

where $\mathrm{OD_f}(\lambda)$, V, and A are the optical density of the particles on the filter, filtered volume (L), and filter loading area (m^2), respectively, while a and b are empirical constants. The factor 2.3 is used to convert OD values from a base 10 log to a natural log scale.

Filtered samples were measured as described above, while untreated suspensions of the sample were measured inside the integrating sphere unit in a 1-cm quartz cell, resulting in noisy (due to low signal), but for the comparison, usable spectra. The absorbance values of the suspensions ranged between 0 and 0.066 and were considered

the 'true' absorbance values of the suspension. The absorbance values of the material retained on filters ranged between 0.010 and 1.340. The absorption at 750 nm was subtracted from $a_{<0.7}(\lambda)$ spectra to correct for a low amount of scattering by sub-micron sized particles present in some post-lysis filtrates (these spectra were not recorded inside the sphere for this exercise).

The absorption measured from suspensions was fitted to the sum of $a_{>0.7}(\lambda)$ and $a_{<0.7}(\lambda)$ spectra, optimizing a and b in Eq. 2.1. This resulted in $a = 0.26$ and $b = 0.27$ (8 samples, 3600 data points) with a mean root square error (MRSE) of the obtained absorption of 0.41 with standard deviation of 0.15. Some values of a and b were obtained from literature and used for comparison, although all were higher than the values reported here. The results obtained with literature a and b values were MRSE = 2.13 (± 0.64) for $a = 0.392$, $b = 0.655$ (Mitchell 1990), MRSE = 1.55 (± 0.52) for $a = 0.378$, $b = 0.523$ (Cleveland and Weidemann 1993), MRSE = 0.92 (± 0.41) for $a = 0.304$, $b = 0.450$ (for *Synechococcus* WH8103, Moore *et al.* 1995), and MRSE = 1.68 (± 0.96) for $a = 0.406$, $b = 0.519$ (Tassan and Ferrari 1995). The absorption spectra of the 8 samples that were obtained using the different methods were averaged, and values plotted against the absorption by the suspension (also averaged), at 5-nm intervals (Figure 2.1).

It is noted that the referred studies (except Tassan and Ferrari 1995) were exclusively based on cultured material and not turbid water samples, and these studies do not always clarify whether the absorbance of the sample filtrate has been taken into account. The currently used dataset includes samples of material known to undergo viral lysis, which was not available from literature. An additional test of Eq. 2.1 with the optimized values was performed on a set of 43 water samples from two turbid lakes sampled at various times, measured in the same configuration. The MRSE was 0.34 (± 0.21) and increased towards 0.6 from $\lambda = 400$ to 350 nm. It is therefore concluded that the values of a and b found with the test dataset can also be applied to other turbid waters when using the described optical geometry.

The absorption coefficient of all water constituents [$a_{TOT}(\lambda)$] was defined as:

$$a_{TOT}(\lambda) = a_{<0.7}(\lambda) + a_{>0.7}(\lambda) \tag{2.2}$$

The total scattering coefficient for particles in suspension [$b(\lambda)$] was obtained from the difference between attenuation and absorption of all water constituents:

$$b(\lambda) = c(\lambda) - a_{TOT}(\lambda) \tag{2.3}$$

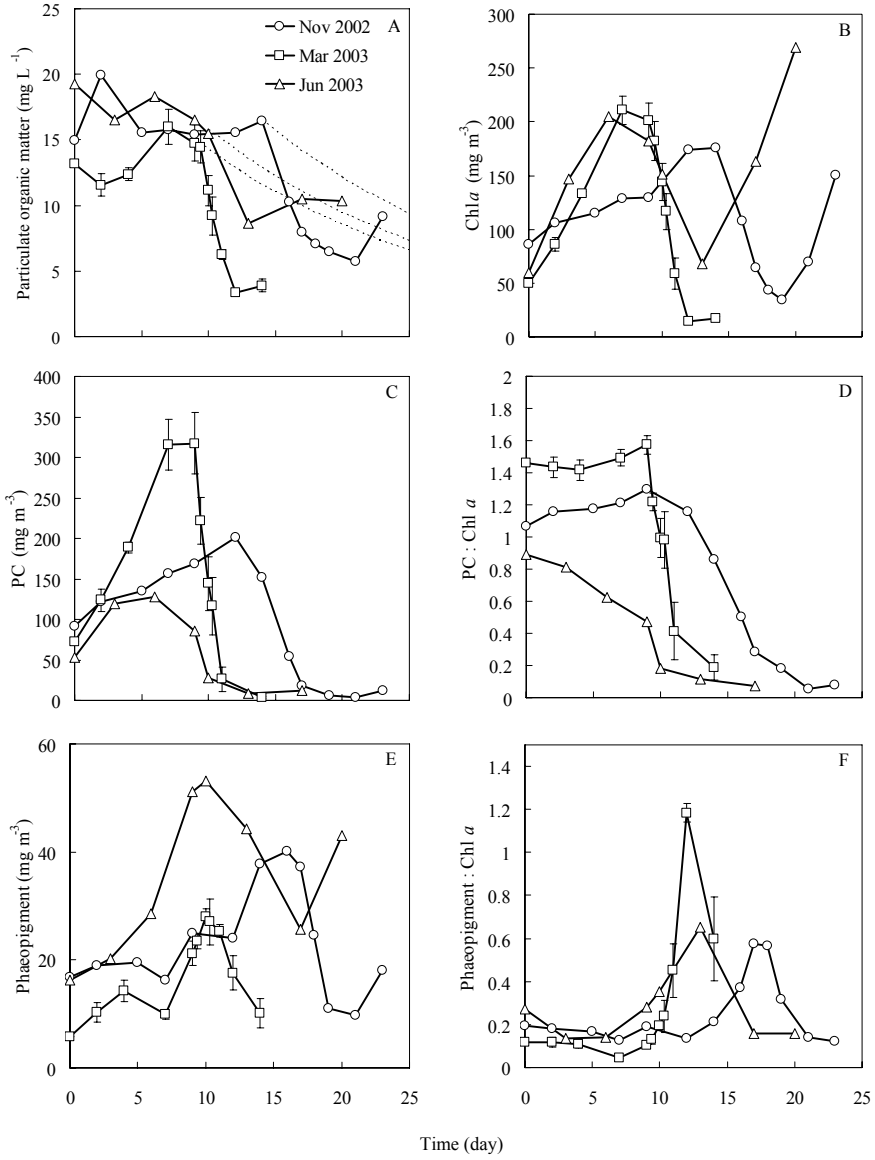

Figure 2.2. Dynamics of (**A**) POM (mg L^{-1}); (**B**) Chl *a* (mg m^{-3}); (**C**) PC (mg m^{-3}); (**D**) PC : Chl *a* ratio; (**E**) Phaeopigments (mg m^{-3}); and (**F**) Phaeopigment : Chl *a* ratio. Error bars given for the March experiment. Dashed lines starting from the onset of collapse in panel A describe the loss of inert compounds due to continuous flow in the enclosures (caused by addition of growth medium).

Pigments

Pigment concentrations were obtained using methods described elsewhere (Simis *et al.* 2005*a*). In short: Chl *a* concentrations were measured spectrophotometrically after 5 min extraction in 80% ethanol at 70-75 °C; subsequently phaeopigments were quantified after acidification (NEN 1981). It is noted that quantification of phaeopigments is compromised in the presence of Chlorophyll *b* when using this method. Additionally, the quantification of phaeopigments is somewhat artificial, since they consist of several degradation products of Chl *a* with different molecular weights. Care should be taken regarding the interpretation of these concentrations. Phycobilipigments (Phycocyanin – PC, Phycoerythrin – PE, and Allophycocyanin – APC) were measured spectrophotometrically using published trichromatic equations (Bennett and Bogorad 1973), after concentration of the samples by high-speed centrifugation, extraction through 9 freeze-thaw cycles, and purification by prolonged high-speed centrifugation (Sarada *et al.* 1999, Simis *et al.* 2005*a*). Since PC was the major accessory pigment and it is most indicative of cyanobacterial presence, only the PC data are currently used.

Virus-like particles

To assess the number of free virus-like particles (VLP), diluted samples were filtered over 0.02-µm pore size, 25-mm diameter Anodisc (Whatman) filters and stained with SYBR Green I (Molecular Probes), following published protocol (Noble and Fuhrman 1998). Enumeration of VLP was carried out using an epifluorescence microscope at blue excitation, counting at least 200 VLP.

Definition of occurrence of mass lysis

The period of mass lysis was defined by the time of highest biomass after the start of the experiment (day 0), and the subsequent time of lowest biomass. POM and Chl *a* dynamics (Figure 2.2A, B) were used to identify the following periods of lysis: days 12 - 19 for the November experiment, days 9 - 14 for the March experiment, and days 6 - 13 for the June experiment (Table 2.1). Measurements referring to ‘pre-lysis’ and ‘post-lysis’ refer to the start and end of the periods mentioned above.

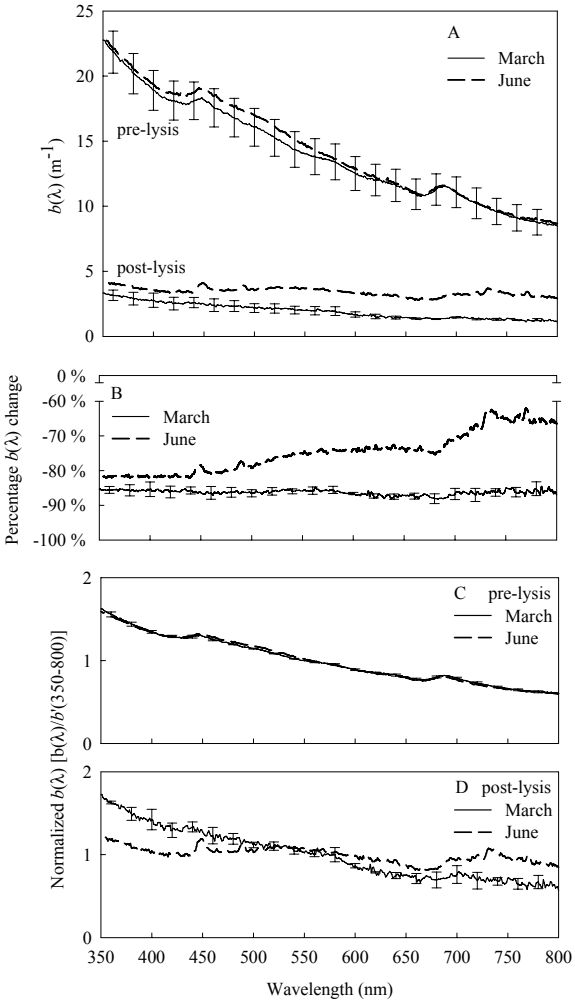

Figure 2.3. Changes upon lysis of the spectral scattering coefficient [$b(\lambda)$]. (**A**) Pre- and post-lysis $b(\lambda)$; (**B**) percentage change upon lysis [(post-lysis – pre-lysis) / pre-lysis] of $b(\lambda)$; (**C**) normalized $b(\lambda)$ (pre-lysis); (**D**) normalized $b(\lambda)$ (post-lysis). Normalized values (C, D) were obtained after dividing spectra by the spectral average [$b(\lambda)/b'(350\text{-}800)$]. Standard deviation for the March experiment shown at 20-nm intervals.

Remote-sensing reflectance

Remote-sensing reflectance was modelled at 5-nm intervals from measured inherent optical properties of the pre- and post-lysis situation, during the March and June experiments, using the Hydrolight 4.1 radiative transfer model (Sequoia Scientific, Inc.). Since no description of changes of the volume-scattering function (VSF) upon lysis currently exists, calculations were based on the VSF measured for San Diego harbour waters (Petzold 1972, Mobley 1994) for both the pre- and post-lysis situation. Absorption by water was taken from literature (Smith and Baker 1981, Pope and Fry 1997, Sogandares and Fry 1997) combining sources to cover the spectrum from 350 – 800 nm. A sun-zenith angle of 0°, clear sky conditions, no waves, full mixing, and no effect of bottom reflectance were selected.

2.3. Results

Biomass and pigments

Steady growth of the cyanobacteria-dominated population was observed from the start of all experiments. POM kept pace with the flow-through rate of the system (Figure 2.2A) while Chl *a* showed an increase, until lysis started (Figure 2.2B). The dominant species belonged to the group of filamentous *Limnothrix/Pseudanabaena* (formerly *Oscillatoria* cf. *limnetica*) species that is commonly found in L. Loosdrecht (Van Tongeren *et al.* 1992, Zwart *et al.* 2005). Reproducibility of growth and collapse of the cyanobacterial biomass was demonstrated by the March experiment, carried out in triplicate (error bars in all figures denote standard deviation between replicates in March). It was illustrated in Figure 2.2A that the decrease of biomass during the collapse differed markedly from the dilution of the systems as caused by nutrient medium addition (dashed lines, rate of 0.29 L h^{-1} = 5.4 % of total volume d^{-1}). The POM losses in the period marked as lysis were 59 %, 74 % (± 1.3 %), and 53 % for the experiments in November, March and June, respectively. VLP enumerated for the March experiment showed that the collapse of the dominant phytoplankton species co-occurred with an over threefold increase of the number of free VLP, similar to the results reported for previous experiments (Van Hannen *et al.* 1999, Gons *et al.* 2002*a*). VLP increased upon lysis from 7.2×10^7 ($\pm 3.1 \times 10^6$) to 2.3×10^8 ($\pm 1.4 \times 10^7$) mL^{-1}. At the start of the experiments, free VLP amounted to 8.9×10^7 ($\pm 3.1 \times 10^6$) mL^{-1}.

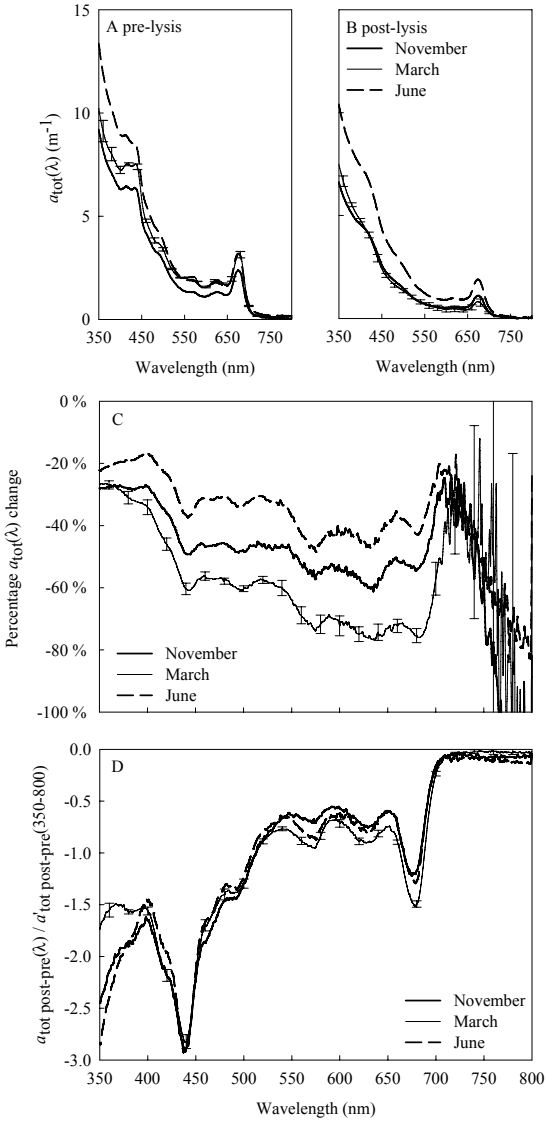

Figure 2.4. Changes upon lysis of the total absorption coefficient [$a_{TOT}(\lambda)$]. (**A**) Pre-lysis $a_{TOT}(\lambda)$; (**B**) post-lysis $a_{TOT}(\lambda)$; (**C**) percentage change upon lysis [(post-lysis – pre-lysis) / pre-lysis] of $a_{TOT}(\lambda)$; (**D**) normalized changes in $a_{TOT}(\lambda)$. Normalized values (D) were obtained after dividing relative change spectra in panel C by the spectral average [$a_{TOT\ post\text{-}pre}(\lambda)$ / $a'_{TOT\ post\text{-}pre}(350\text{-}800)$]. Standard deviation for the March experiment shown at 20-nm intervals.

The main accessory pigment in the cyanobacterial community, PC, increased at the start of all experiments, and dropped simultaneously with the decrease of POM (Figure 2.2C). The ratio of PC to Chl *a* (Figure 2.2D) was steady in November and March, and decreased slowly in June, until the collapse of the filamentous cyanobacteria caused a sharp drop in the ratio in all experiments. PC disappeared from the systems at a higher rate than Chl *a*, and the resulting drop in the PC : Chl *a* ratio indicates that the decrease of POM involved specifically the disappearance of PC-containing cyanobacteria. The PC : Chl *a* ratio of particulate matter that remained after lysis was very low compared to the pre-lysis situation and accordingly, a recovery of filamentous cyanobacteria was not observed. Instead, growth of mainly green algal species followed the collapse of the filamentous cyanobacteria.

An indication of the health of the cyanobacterial community could be obtained from the concentration of phaeopigments (Figure 2.2E) and the ratio of phaeopigments to Chl *a* (Figure 2.2F). A sharp peak in the latter indicated that strong degradation of Chl *a* occurred during the lysis phase in all experiments. Increase in phaeopigments after the lysis phase (during the succession by green algae) can be explained by the presence of chlorophyll *b*, which compromises the assessment of phaeopigments by acidification (see Method).

Bulk optical properties

Mass lysis caused a sharp decline of the inherent optical properties of the water constituents in all experiments, the exception being that scattering was not recorded during the November experiment. At the start of lysis, similar $b(\lambda)$ spectra were measured in the March and June experiments (Figure 2.3A). Relative differences [(post-lysis – pre-lysis) / pre-lysis] around -80% were found for $b(\lambda)$ (Figure 2.3B). Spectra of $b(\lambda)$, each normalized to their spectral average [$b(\lambda)/b'(350\text{-}800)$] showed a slightly more gradual slope in the June experiment while in March no change in slope could be discerned (Figure 2.3C, D).

The foremost change in $a_{TOT}(\lambda)$ that followed the lytic event was a flattening of the spectra (Figure 2.4A, B). Before lysis, the spectra showed the absorption features of the Chl *a* (around 440 and 675 nm) and phycobilin pigments (mainly PC around 615 nm, and some phycoerythrin around 565 nm) whereas after lysis Chl *a* absorption was less visible while phycobilin pigment absorption features almost disappeared. Relative changes in $a_{TOT}(\lambda)$, expressed as (post-lysis – pre-lysis) / pre-lysis, varied from -20% to -80% depending on wavelength and between the experiments (Figure 2.4C). The relative changes were largest in the red spectral region and decreased with shorter wavelengths. Note that the absolute absorption change was higher in the blue region where phytoplankton absorption was highest. Plots of spectral change of $a_{TOT}(\lambda)$ were normalized to their average values in the 350-800 nm wavelength range [$a_{TOT\ post\text{-}pre}(\lambda)$ /

$a'_{TOT\ post\text{-}pre}(350\text{-}800)$] in Figure 2.4D. These plots show that the shape of the change in $a_{TOT}(\lambda)$ was nearly identical between experiments. These spectra resemble mirror images of absorption spectra of cyanobacteria, indicating that this was the main constituent to disappear from the columns.

The decrease of $a_{TOT}(\lambda)$ is outlined in more detail in Figure 2.5, as the post-lysis absorption subtracted from the pre-lysis absorption for the various size fractions. In all experiments (Figure 2.5A, B, and C for November, March and June, respectively) it can be seen that although $a_{>0.7}(\lambda)$ decreased, there was a simultaneous increase in absorption by the small size fractions, highest in the blue part of the spectrum and in the areas of Chl *a* absorption. The net result was still a decreased $a_{TOT}(\lambda)$.

The dissolved pool and submicron-sized particles

The filtrate from 0.7 µm pore size filters includes dissolved organic matter (DOM) and submicron-sized particles (SMP). From Figure 2.5 it can be seen that as a result of cell lysis, increased absorption also occurs in the <0.2 µm fraction which is commonly used to obtain the absorption by coloured DOM. Time series of $a_{<0.7}(\lambda)$ curves (Figure 2.6) show a gradual decline of absorption before and also after lysis, more or less equal to the rate of dilution of the system with nutrient medium. Upon lysis, an increase of $a_{<0.7}(\lambda)$ was observed over the whole spectrum marking the release of coloured material from lysed cells. A small absorption peak in the red region close to the red absorption maximum of Chl *a* occurred upon collapse and faded after a few days. This increased absorption in the red region was present in the samples that had passed 0.7 µm as well as 0.2 µm filters, although the peak was less intense in the latter case (Figure 2.7). The peak was no longer clearly visible after prolonged high-speed centrifugation of the sample (15000 × *g*, 0:40 h), proving that it was associated with SMP. PC from lysed cells was not observed as absorption around 615 nm in the spectra of $a_{<0.2}(\lambda)$ or $a_{<0.7}(\lambda)$ (Figures 2.5–2.7).

Apparent optical properties

Remote-sensing reflectance for the pre- and post-lysis situation during the March and June experiments were plotted in Figure 2.8 for 5-nm intervals in the 350 – 800 nm region. Because no information exists on changes in the VSF upon lysis the same VSF was applied to all situations. Pre-lysis reflectance in the March experiment showed stronger absorption features of photosynthetic pigments ('valleys' in the spectra around the absorption maxima of PE, PC, and Chl *a*) compared to the June experiment. Otherwise, the pre-lysis spectra of the March and June experiments were highly similar. After lysis, reflectance in both experiments lost most of the characteristic features for absorption by accessory pigments. The 'green peak' around 580 nm became more expressed upon lysis, while reflectance in the blue region increased only slightly.

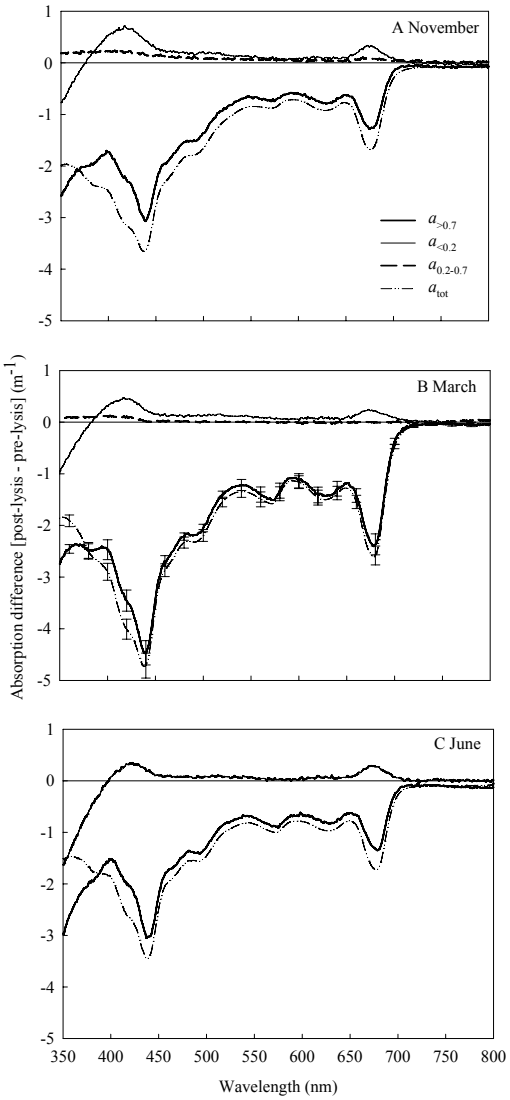

Figure 2.5. Difference spectra (post-lysis – pre-lysis) of absorption by the indicated size fractions for the experiments in (**A**) November; (**B**) March; (**C**) June. Error bars for the small size fractions in the March experiment omitted, for clarity.

2.4. Discussion

Changes in inherent optical properties were studied upon sudden collapse of a predominant filamentous cyanobacterial community, using enclosed lake water. Treatment of the lake water with saturating nutrient medium and high light resulted first in steady growth in terms of POM, and strong production of the main photosynthetic pigment Chl *a* and accessory pigment PC. After a period of 6 – 12 days, the population of filamentous cyanobacteria collapsed suddenly, exhibiting cell lysis in all experiments. In previous experiments, viruses that naturally occur in the lake water could be associated with the collapse (Van Hannen *et al.* 1999; Gons *et al.* 2002*a*). Enumeration of VLP during the March experiment of the present work confirmed once more that the collapse is closely coupled to viral dynamics. No elevated numbers of grazers were observed during the collapse, nutrients were available in high quantity, and exclusively the filamentous cyanobacteria suffered collapse. Further evidence for the viral nature of the collapse is provided by earlier experiments with LSEs, where filamentous cyanobacteria from cultured strains reached high population densities without suffering collapse (Rijkeboer *et al.* 1990).

The starting conditions of the three experiments differed due to seasonal differences in biomass, water temperature (Table 2.1), nutrient availability, and suspended sediment load *in situ*. The experiments in November and March started with a short period of increase in water temperature until the experimental value of 20 °C was reached. In the June experiment the *in situ* water temperature was 22 °C, which explains a short lag time compared to the other experiments as well as a more rapid succession by the green algal species after lysis of the dominant cyanobacteria. Duration of the adaptation and growth phase (varying from 6 to 12 days) and of the lytic event (4-7 days) was thus probably effected by different starting conditions. Even so, collapse of the filamentous cyanobacterial community was observed in all experiments, and therefore the current experimental setup proves to be a reliable method to obtain mass viral lysis of enclosed lake water. Results from the March experiment (carried out in triplicate) showed that the method was highly reproducible.

Optical changes upon mass lysis

Drastic changes in the inherent optical properties were observed in all experiments. The release of dissolved substances from lysed cells caused a relatively lower decrease in absorption in the blue part of the spectrum compared to longer wavelengths. During the first days of the collapse, absorption in the <0.7 μm fraction showed a temporary increase (Figure 2.6). Among the lysed substances was a fraction of SMP exhibiting absorption, characteristic of Chl *a*. Although the particulate nature of this fraction was demonstrated through high-speed centrifugation, it partly passed a 0.2 μm filter. Upon

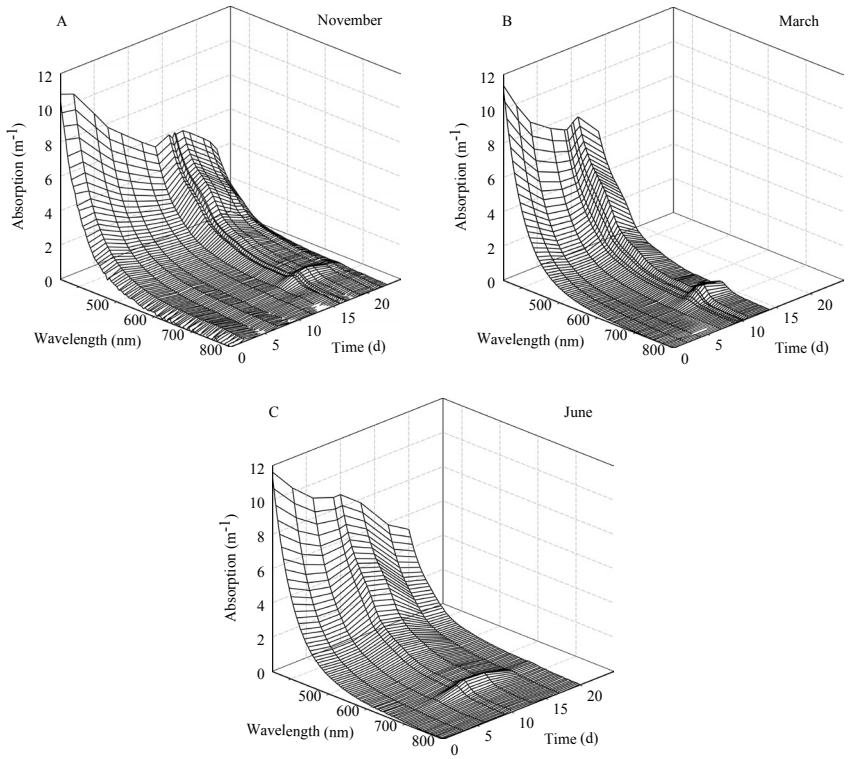

Figure 2.6. Time series of spectral absorption by the size fraction <0.7 µm [$a_{<0.7}(\lambda)$]. An initial decrease of $a_{<0.7}(\lambda)$ due to flow-through in the system was followed by an increase caused by cell lysis. Submicron-sized particles with Chl *a* absorption features (peak near 675 nm) appeared during lysis.

mass lysis, this fraction can thus be observed from routine measurements of absorption by coloured DOM.

From Figures 2.6 – 2.7 it can be seen that the Chl *a* absorption feature in SMP was one of the indicators of mass collapse, and that it faded quickly after the collapse passed. It has been suggested that these small particles and colloids are of a very unstable nature and that they may be fragmented into even smaller units or aggregated into flocks (Shibata *et al.* 1997), used as substrate by bacterioplankton (cf. Wetzel 2001), or degraded by sunlight (Kramer 1979, Kieber *et al.* 1990). Increased SMP has been reported previously in studies of viral lysis of bacteria (Shibata *et al.* 1997, Balch *et al.* 2002). For photosynthetic plankton, the Chl *a* associated with the SMP may exhibit a clear fluorescence signal, since the disruption of the photosynthetic energy pathway will allow only conversion of absorbed energy into heat or fluorescence. However, it is probable that the SMP have a high content of Chl *a* degradation products, with low fluorescence yield.

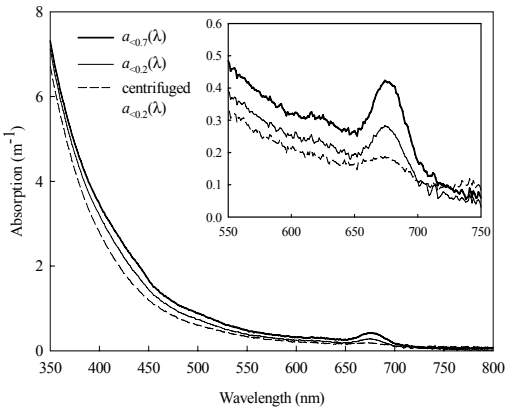

Figure 2.7. Plots of spectral absorption by the size fractions <0.7 µm and <0.2 µm before centrifugation, and by the <0.2 µm fraction after centrifugation (15000 × *g*, 0:40 h). The particulate origin of absorption in the 'yellow substance' domain is demonstrated. Sample taken during the March experiment (day 9, second sampling, average of three enclosures). Inset: magnification of the area 550 – 750 nm. The anomalies in the spectrum conform to the *in vivo* absorption spectrum of Chl *a*.

Absorption by water-soluble phycobilipigments could not be observed in the small size fractions during or after the lysis phase. Possibly, these pigments (mainly PC) were rapidly degraded by heterotrophic organisms, light, or too high pH of the surrounding medium, upon lysis. Alternatively, these pigments were broken down soon after infection of the cells, yet before lysis. In either case, the fact that Chl *a* fragments linger in the water column for a number of days after mass collapse, while the accessory pigments disappear quickly, seems to serve well as a prime indicator for the cyanobacterial collapse.

Scattering in the water column decreased drastically upon lysis (Figure 2.4A, B), while the shape of the scattering spectrum did not change much (Figure 2.4C, D). The observed decline in bulk scattering contributes to an increase in water transparency. Drastic changes in water transparency can be retrieved from remote sensing imagery, even for low spectral resolution. From scattering theory, it is known that particles smaller than the wavelength of incident light have a strong contribution to the fraction of backscattered light, whereas the backscattering ratio of cyanobacteria is lower (Morel and Bricaud 1986, Kirk, 1994).

Even if the refractive index of pre- and post-lysis particulate matter remains unchanged by lysis, an increase in the backscattering ratio can be expected as a result of a shift in the particle size distribution towards smaller particles. Empirical evidence for an increased backscattering ratio is not available, as earlier work also suffered from a lack of signal strength for the determination of the VSF of post-lysis suspensions of

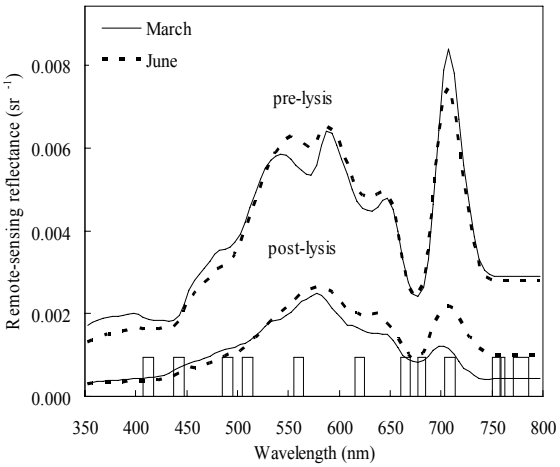

Figure 2.8. Remote-sensing reflectance modelled for the pre- and post-lysis situation during the March and June experiments. Reflectance calculated and plotted at 5-nm intervals. The location of wavebands of the MERIS instrument are given as vertical bars.

cyanobacteria (Balch *et al.* 2002). Therefore, modelling of the scattering function for the pre- and post-lysis situation currently seems the best approach. For a modelling approach, knowledge of the particle size distribution and the complex refractive index of the material, is essential.

The VSF for San Diego harbour waters (Petzold 1972) was applied on both the pre- and post-lysis situations to obtain remote-sensing reflectance spectra. Thus, an unknown error in the estimation of the backscattering coefficient was introduced. It is most likely that the VSF of a post-lysis environment dominated by very small particles will be less strongly peaked in the forward direction, thus resulting in higher reflectance at all wavelengths. The post-lysis spectra of reflectance in Figure 2.8 may thus be too low. It was estimated that, to obtain post- and pre-lysis reflectance of approximately the same magnitude, a three-fold increase of the backscattering ratio would be required upon lysis, which seems very large. Besides lowered reflectance, most spectral features characteristic of cyanobacterial presence, e.g. reflectance 'valleys' around the maxima of phycobilin absorption, were no longer recognizable from post-lysis spectra. Additionally, the green peak of the reflectance spectra became more pronounced while blue reflectance remained almost unaffected, as would be expected from the changes in bulk absorption. For unstratified and optically deep waters, these changes in the shape of the reflectance spectrum can easily be monitored using band ratios of remote sensing instruments with various bands in the visible and near-infrared spectrum, such as the Medium Resolution Imaging Spectrometer onboard ENVISAT-1 (band locations shown in Figure 2.8). Vertically stratified water bodies

may display more complex reflectance behaviour upon increased transparency of the layer affected by mass lysis, while shallow waters may exhibit bottom reflectance. These possibilities require further study.

Optical markers of bloom termination by viral lysis

Several optical markers of viral lysis of cyanobacteria can be defined based on the present results. These are, in decreasing order of importance: (1) decrease of coefficients $b(\lambda)$ and $a_{TOT}(\lambda)$; (2) a shift from high to low PC : Chl *a* ratio; (3) increase in the phaeopigment : Chl *a* ratio; and (4) increase in absorption by the small size fraction, which includes dissolved substances and SMP carrying the Chl *a* absorption signature. These optical markers may prove useful for monitoring of cyanobacterial mortality in general, but not necessarily for mass viral lysis nor specifically from remotely sensed imagery. For satellite-based optical remote sensing, the results presented under (1) are most important: beam attenuation at 550 nm decreased from approximately 16 to 4 m^{-1}, which is equivalent to a fourfold increase in transparency for constant VSF, even though the shape of the VSF after lysis is debatable. If the absorption signal of PC around 615 nm can be adequately retrieved from remotely sensed imagery (see Simis *et al.* 2005*a*), the PC : Chl *a* ratio mentioned under (2) is the second-most important indicator. Moreover, the PC : Chl *a* ratio would be specific for mass mortality of PC-containing cyanobacteria and may even be a clear indicator of mass lysis. Both signals are sufficiently strong to be resolved from spectral reflectance data, and would have to be observed simultaneously to exclude the possibility of a succession to species that do not contain PC. On the contrary, the changes mentioned under (3 - 4) are too weak to be detectable from current remotely sensed data, but these signals, perhaps together with fluorescence detection methods, may be applied *in situ*, for instance using equipment mounted on buoys.

It cannot be determined with certainty that the optical markers are indicative of viral lysis of a cyanobacterial host, or whether other mortality factors would display similar optical behaviour of the water column. If time-series of remotely sensed material are available, then the rate of change of these parameters might be used to indicate whether viral lysis is the most likely mechanism to have caused the observed optical changes. When, as in our experiments, a population loss up to 75% is witnessed within days, an outbreak of viruses is more likely the cause of these dynamics than other mortality factors such as zooplankton grazers or benthic filter-feeders, since the life-histories of the latter are incompatible with such drastic population dynamics. However, when time-series of remotely sensed data are not available, optical indicators that are specific to viral lysis are a prerequisite. Flattening of the absorption spectrum and a much stronger decrease of absorption in the red spectral region than in the blue, due to the release of yellow substance, were also shown as effects of grazing (Stramski *et al.* 1992), but the optical changes were much slower in those experiments. Degradation of

Chl *a* into phaeopigments upon grazing was demonstrated in other reports (cf. Cartaxana *et al.* 2003). Apart from the current work, there have been no publications on the disappearance of the PC absorption signal upon mortality of cyanobacteria. It is evident that changes in the backscattering coefficient and the particle size distribution should be explored in more detail to complete the current observations. The backscattering to scattering ratio holds important information on the ratio of phytoplankton to detritus and minerals caused by differences in the refractive indices of these water constituents and the particle size distribution. Changes in the directional aspect of the scattering coefficient might markedly differ between a post-lysis, cell debris-rich suspension and a 'healthy' aquatic community with a large number of photosynthetically active filamentous cyanobacteria. Finally, the impact of elevated numbers of heterotrophic bacteria, ciliates, and other grazers after mass lysis on the underwater light field, should be taken into account (Stramski and Kiefer 1991, Balch *et al.* 2000). Nonetheless, the current results demonstrate the principles of optical behaviour as a result of mass viral lysis, and therefore optical monitoring of water bodies for such viral impact is a logical next step.

2.5. Acknowledgments

Several anonymous reviewers are thanked for their comments that lead to the final manuscript. Part of the work was carried out at the Institute for Environmental Studies, Vrije Universiteit, Amsterdam.

3. OPTICAL SIGNATURES OF THE FILAMENTOUS CYANOBACTERIUM *LEPTOLYNGBYA BORYANA* DURING MASS VIRAL LYSIS

Stefan G. H. Simis, Marjolijn Tijdens, Hans L. Hoogveld & Herman J. Gons

Limnology and Oceangraphy, in press

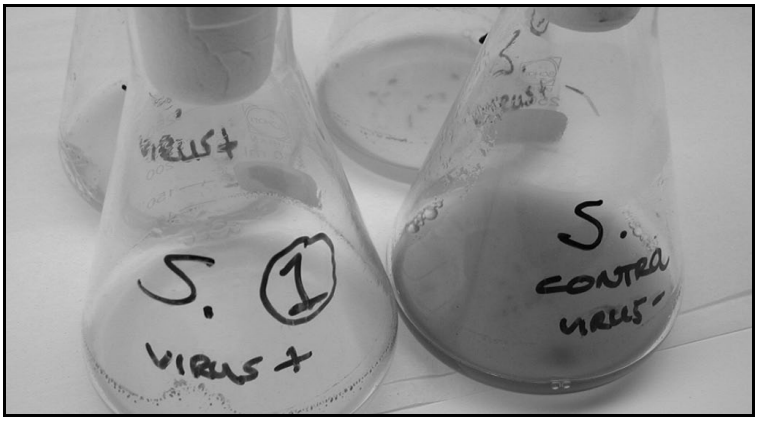

Cultures of *Leptolyngbya boryana* infected (left) and uninfected (right) with LPP-1.

Abstract

The inherent optical properties absorption and scattering, the population density of virus-like particles, and the particle size distribution (PSD) for particles > 0.7 µm of the filamentous cyanobacterium *Leptolyngbya boryana*, were monitored for 72 h at 9-h intervals following infection with cyanophage LPP-1. Lorenz-Mie scattering theory and the anomalous diffraction approximation were used to derive the refractive index representative of the bulk of particles, and particulate backscattering [$b_{bp}(\lambda)$]. Upon lysis, particulate absorption [$a_p(\lambda)$] and scattering [$b_p(\lambda)$] decreased, the number of free virus-like particles increased drastically, the PSD shifted to relative abundance of small particles, and average trichome length decreased sharply. The complex refractive index was comparable with literature values. Modelled $b_{bp}(\lambda)$ spectra were lowered upon lysis while backscattering probability increased. The effect of underrepresentation of particles below the measurement limit of the particle sizer was studied; more small particles in the PSD resulted in higher, but still relatively low, backscattering probability. The consequences of the studied optical behaviour on reflectance was explored. Significant dynamics at longer wavelengths were mostly masked by water absorption at nominal population densities. However, strongly reduced $a_p(\lambda)$ in the red pigment absorption bands also resulted in a pronounced green peak in reflectance spectra. It was concluded that reflectance band ratio algorithms targeted at the absorption of the pigments phycocyanin and chlorophyll *a* should be used to detect mass lysis. The integrated intensity of reflected light may be too variable to serve as optical indicator for mass lysis events.

3.1. Introduction

General

Cyanobacterial blooms occur with increasing frequency in response to eutrophication of aquatic ecosystems and pose environmental, economical, and health threats. A potentially important role of viruses as controlling agents of phytoplankton growth has emerged from field studies on viral abundance and activity carried out in the last decades (Bergh *et al.* 1989, Suttle 1994, Brussaard, 2004). It has become clear that cyanophagy can be an important mortality factor for cyanobacteria (Proctor and Fuhrman 1990, Wilson *et al.* 1996, 1997, 1998). In experimental conditions a semi-natural cyanobacterial bloom can be lysed by viruses in the course of a few days (Van Hannen *et al.* 1999, Gons *et al.* 2002*a*). In such experiments, changes in the inherent optical properties particulate absorption [$a_p(\lambda)$] and scattering [$b_p(\lambda)$] were dramatic and sudden. Given the magnitude of observed optical changes, optical monitoring for catastrophic viral lysis of natural cyanobacterial populations using current remote

sensing instruments seems feasible (Simis *et al.* 2005*b*). Remote sensing offers the possibility to track optical changes in a large number of water bodies simultaneously, and could thus greatly increase understanding of frequency and circumstance of mass lysis events. However, to evaluate mass lysis effects on remotely sensed reflectance, knowledge of the backscattering coefficient [$b_b(\lambda)$] is still required, as reflectance is mainly a function of $b_b(\lambda)$ and the absorption by water plus its constituents [$a_{TOT}(\lambda)$] (Gordon *et al.* 1975). Measurement of the particulate backscattering $b_{bp}(\lambda)$ during lysis of cultured cyanobacteria is compromised by low signal intensity, although single-wavelength scattering functions may be obtained using dedicated light scattering measurements. Balch *et al.* (2002) carried out such measurements on *Synechococcus* 1331 and found a decrease in $b_{bp}(514)$ but no change in the shape of the VSF, upon lysis.

Upon cell lysis, a shift in the particle size distribution (PSD) from several large to many small particles can be observed (Shibata *et al.* 1997, Balch *et al.* 2002). In general, particles that are small with regard to the wavelength of incident light show a high backscattering ratio $B(\lambda) = b_{bp}(\lambda) : b_p(\lambda)$ in comparison with larger particles of the same shape and material. The complex refractive index [$m(\lambda) = n(\lambda) + in'(\lambda)$] of the cell material, and the particle size relative to the wavelength of incident light, jointly define the volume scattering function (VSF). Increased $B(514)$ was recorded for bacterial cultures, but not for cyanobacteria (Balch *et al.* 2002). For phototrophs, changes in $m(\lambda)$ as a result of cell lysis have not yet been reported.

The scenario of mass lysis of a bloom-forming species that dominates the optical properties of the water column can be approached experimentally. The present study focuses on the optical changes of the cultured filamentous cyanobacterium *Leptolyngbya boryana* that is exposed to the cyanophage LPP-1. Measurements of $a_p(\lambda)$, $b_p(\lambda)$, and the PSD are carried out at regular intervals following infection up until clearing of the infected cultures. Subsequently $b_{bp}(\lambda)$ is obtained from the best fit of the measured and modelled optical properties through a Mie-Lorenz scattering model for homogeneous spherical particles, that uses $m(\lambda)$ and relative particle size as input. The approach was first described by Morel and Bricaud (1986) and adapted as described below.

Scattering model

Lorenz-Mie theory and its later formulations commonly referred to as Mie theory (Mie 1908), can be used to describe light propagation by simultaneously scattering and absorbing spherical particles, through electromagnetic wave theory. For a single spherical particle with known diameter and $m(\lambda)$, the Mie model yields the efficiency of light absorption and angular scattering. For a polydisperse population of irregularly shaped particles in random orientation, the assumption that particles are perfect spheres

may be relaxed (Latimer *et al.* 1978, Bohren and Hufmann 1983, Morel and Bricaud 1986). This generalization has been repeatedly put to use in hydrologic optics to explain the scattering contributions of the various biological elements of aquatic ecosystems (Morel and Ahn 1991, Stramski and Kiefer 1991, Stramski and Mobley 1997). To speed up rigorous Mie calculations, the approximation of anomalous diffraction theory (ADT) may be used (Van de Hulst, 1957). However, it is not possible to calculate the angular distribution of propagated light with ADT, so its use is restricted to fitting $m(\lambda)$ to the optical and PSD measurements. Combining Mie theory and ADT, Morel and Bricaud (1986) modelled the light propagation by picoplanktonic cyanobacteria. Ahn *et al.* (1992) extended their use to cultured phytoplankton species of various shape, size, and plankton subgroups. In Volten *et al.* (1998), a wide range of phytoplankton groups and some silt samples were described both with Mie scattering calculations and VSF measurements at wavelength (λ) = 633 nm. The latter study pointed out some of the difficulties with fitting the Mie model to optical measurements. This was particularly apparent for filamentous and other colony-forming species, where some values of $m(\lambda)$ fitted by the model would be implausibly high. The present study also applies the Mie-approach to filamentous cyanobacteria. However, instead of using volume-equivalent spheres to represent the whole trichomes, spheres are entered into the model to represent the individual cells included in the trichomes, irrespective of their position in a colony structure. This approach may result in more realistic values of $m(\lambda)$.

Mass lysis of host cells is expected to cause a shift in the PSD towards smaller particles. With smaller particle size relative to the wavelength of incident light, the scattered light field becomes more diffuse. In many natural situations, sub-micron sized particles (SMP) and colloids have a significant contribution to the total backscattering (Morel and Ahn 1991, Stramski and Kiefer 1991, Ulloa *et al.* 2004, Stramski and Wozniak 2005). The role of SMP on $b_{bp}(\lambda)$ during dense cyanobacterial bloom has not been studied, but may become important as a result of cell mortality, particularly sudden mass lysis. The number of particles released per lysed cell was estimated to be around 20 for bacterial cells (Shibata *et al.* 1997). In the present study, the effect of SMP on calculated $b_{bp}(\lambda)$ and $B(\lambda)$ is investigated, prompted by the fact that the used particle sizer was insensitive to SMP < 0.7 µm. Considering cases during mass lysis with limited and exaggerated numbers of expected SMP, it is possible to explore the sensitivity of modelled $b_{bp}(\lambda)$ and $B(\lambda)$ to the changes in the PSD.

Finally, using both measured $a_p(\lambda)$ and modelled $b_{bp}(\lambda)$, the effect of mass viral lysis on remotely sensed reflectance of inland and coastal waters exhibiting cyanobacterial blooms can be assessed.

3.2. Method

Cell cultures and experimental conditions

The cyanobacterial host *Leptolyngbya boryana* (Gomont) Anagnostidis et Komárek (1988), previously *Plectonema boryanum*, and the cyanophage LPP-1 were obtained from the American Type Culture Collection (Manassas, VA, USA). The host was grown on modified Chu 10 medium and LPP-1 stock was regularly harvested from infected cultures and kept in a magnesium salt solution (Safferman and Morris, 1964). A week before, and again several days before the start of the experiment, the host was transferred to fresh culture medium and kept at the same temperature and ambient light that applied to the experiment. During the experiment the culture flasks were placed on an orbital shaker in an incubator, supplied with continuous light (Sylvania Britegro fluorescent tubes) at approximately 95 μmol quanta m^{-2} s^{-1} photosynthetically active radiation. Temperature was maintained at 20 °C. Several hours before the start of the experiment, 50 mL of the culture stock and 50 mL fresh culture medium were added to 250-mL Erlenmeyer flasks. At $t = 0$, three replicate flasks received 0.750 mL of LPP-1 phage stock (adding approximately 1×10^8 viruses mL^{-1} $flask^{-1}$). As a negative control treatment, one flask received 0.750 mL phage-free magnesium salt solution. Low densities of heterotrophic bacteria were maintained in the host cultures, growing on dying *L. boryana* cells and exudates; the culture medium alone did not support them. They were included in the experiment to cause degradation of the lytic material, above all the water-soluble phycobilin pigments that can be released from lysing cells. The heterotrophic bacteria were rod-shaped with a narrow size distribution around a volume-equivalent sphere diameter (ESD) of 0.95 (± 0.11) μm. The cultures were treated under sterile conditions and it was periodically checked that no phototrophic species other than *L. boryana* were present.

Virus-like particles

Free virus-like particles (VLP) were enumerated according to Noble and Fuhrman (1998). Diluted samples were filtered over 0.02-μm pore size, 25-mm diameter Anodisc (Whatman) filters and stained with SYBR Green I (Molecular Probes). At least 200 VLP were counted using a Zeiss Axiophot epifluorescence microscope at blue excitation.

Measured inherent optical properties

Measurements of the inherent optical properties were made on a Lambda 800 UV/Vis spectrophotometer (PerkinElmer, Wellesley, MA, USA) in the 350 – 800 nm wavelength (denoted λ, refer to Table 3.1 for a lists of recurring symbols) range. Spectra of $a_p(\lambda)$ were measured by placing a 1-cm path length quartz cell, with clear panes on all sides, in the centre of a 150-mm integrating sphere accessory (Labsphere Inc, North Sutton, NH, USA). The measured absorbance spectra were obtained from

Table 3.1. List of recurrent symbols.

Symbol	Description	Units
λ	wavelength of light in air	µm
a_p	particulate absorption coefficient, assuming negligible absorption by dissolved matter	m^{-1}
a_w	absorption coefficient of pure water	m^{-1}
a_{TOT}	sum of a_p and a_w	m^{-1}
b_p	particulate scattering coefficient	m^{-1}
b_b	backscattering coefficient	m^{-1}
b_{bp}	particulate backscattering coefficient	m^{-1}
c	beam attenuation coefficient	m^{-1}
B	backscattering probability, ratio $b_{bp} : b_p$	dimensionless
$R(0^-)$	subsurface irradiance reflectance at depth 0	dimensionless
ω_b	backscattering albedo, $b_{bp}(\lambda) / (a_{TOT}(\lambda) + b_{bp}(\lambda))$	dimensionless
m	complex refractive index relative to water	dimensionless
n	real part of m	dimensionless
n'	imaginary part of m	dimensionless
Q_j	optical efficiency factor of a particle ($j = a, b, c,$ or b_b)	dimensionless
$\overline{Q}_j$	optical efficiency factor of the 'average' particle ($j = a, b, c,$ or b_b)	dimensionless
d	particle diameter	µm or m (Eq. 1)
x	particle size relative to wavelength of light in surrounding medium	dimensionless
S	geometric shape factor of bulk of particles	m^{-1}
$S(d)$	geometric shape factor of particle with diameter d	m^{-1}

the spectral difference between the sample and the cuvette filled with 0.2-µm filtered distilled water. The spectra were subsequently scaled to absorption units to yield $a_p(\lambda)$. Various papers discuss the method of measuring absorption inside an integrating sphere in detail (Maske and Haardt 1987, Babin and Stramski 2002, 2004).

Beam attenuation [$c(\lambda)$] was measured in a 1-cm path length cuvette against a reference of filtered distilled water. The spectrophotometer was set up in dual-beam mode for this measurement, the cuvette positioned at relatively large distance from the detector to exclude detection of light scattered at angles above an estimated 1.3°. Details on the spectrophotometric determination of $c(\lambda)$ and dependence on detector acceptance angle may be found elsewhere (Bricaud *et al.* 1983, Stramski and Reynolds 1993). Spectra of $b_p(\lambda)$ were obtained from the difference between $c(\lambda)$ and $a_p(\lambda)$.

To minimize the possibility of multiple scattering during measurement of $a_p(\lambda)$ and $c(\lambda)$, dilutions of the sample were made until the optical thickness (the product of $c(\lambda)$ and path length) was below 0.3 (Bricaud *et al.* 1988). All spectrophotometric measurements were made at 1-nm intervals with an integration time of 0.24 s nm^{-1} and slit width of 2 nm. A correction of $a_p(\lambda)$ by subtracting near-infra red values was not

needed, as scattering losses were negligible when the sample was placed in the centre of the sphere.

The absorption by coloured dissolved organic matter (CDOM) was obtained from the filtrate of samples passed over a 0.2 µm Schleicher & Schuell FP30 cellulose acetate membrane filter, pre-rinsed with the sample. These measurements were carried out as described for measurement of $a_p(\lambda)$, inside the integrating sphere. CDOM absorption was very low throughout the experiment and only used in test runs of the model.

Particle size distribution

The PSD was obtained from a combination of microscopic observations and size distribution measurements using a Casy TTC particle sizer (Schärfe System GmbH, Reutlingen, Germany). This particle sizer detects particle volumes by integrating changes in an electromagnetic field at a frequency of 1 MHz as particles pass through a capillary. Lower and upper detection limits were 0.18 μm^3 (0.7 µm ESD) and 14137 μm^3 (30 µm ESD) which amply covers the range of expected volumes of *L. boryana* trichomes as well as the heterotrophic bacteria.

Cyanobacterial trichomes were detected as single particles with a large ESD. Individual cells conform better to the assumption of sphericity by the model than trichomes. The PSD obtained by the particle sizer (Figure 3.1A for t = 0 h) was therefore converted, so that the PSD ultimately used as model input (Figure 3.1B) included individual *L. boryana* cells besides cell debris and heterotrophic bacteria. Microscopical examination of the samples yielded the distribution of cyanobacterial cell volume, which was fitted by a Gaussian curve (Figure 3.1C). Cell volumes and ESD were calculated from cell length and diameter, assuming cylindrical cell shape. A probability function was constructed from the fitted ESD distribution, to separate the total volume measured by the particle sizer into the volumes contained in small particles (debris, bacteria) and *L. boryana* cells (Figure 3.1D). Per size class, the product of total volume (particle sizer) and the probability of any *L. boryana* cells present, yielded the volume contained in *L. boryana* cells, and the number of *L. boryana* cells, using the average cell volume obtained from microscopy. The final PSD (Figure 3.1B), used as model input, now consisted of the sum of individual *L. boryana* cells and all smaller matter, repeated for each size class. It is noted that the samples for microscopic determination of cell dimensions were fixed with a minimal amount of Lugol's solution. The samples were kept at 4 °C and analysed within 3 weeks after the experiment. No marked effect of the fixative on cell size was observed compared to regular observations of fresh *L. boryana* cultures.

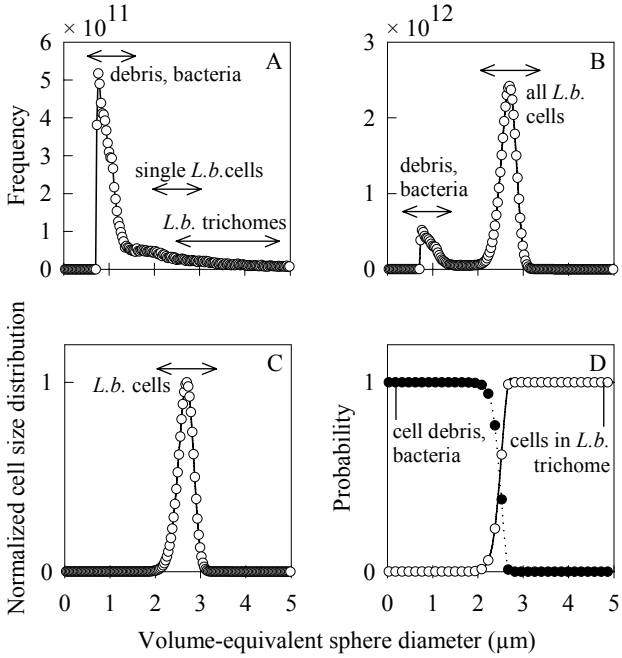

Figure 3.1. Procedure followed to obtain the particle size distribution (PSD) from microscopic observations of cell size, and from automated particle counts that include *L. boryana* trichomes. The displayed results are expressed in volume-equivalent sphere diameter at the size classes used as input for the scattering model, for the average of infected cultures at $t = 0$. (**A**) Particle sizer output showing peaked distribution towards smaller diameters. Heterotrophic bacteria constitute part of the peak, with an ESD of approximately 1 μm. (**B**) Final PSD, combining particle sizer output and microscopically observed cell size distribution. The sum of single *L. boryana* cells and cells organized in trichomes yields the peak at 2-3 μm, the peak that constitutes smaller particles is the same as in panel A (note difference in scale). (**C**) Normalized size distribution of *L. boryana* cells, based on Gaussian fit of microscopic observations of cells organized in trichomes of ≥ 1 cells length. (**D**) Probability functions used to distinguish *L. boryana* cells (either single or organized in trichomes) from smaller particles like cell debris and heterotrophic bacteria.

In order to reduce computation time of the scattering model, the PSD data were reduced to 44 size classes in the range 0-7 µm ESD. Values of ESD given in the text and figures of this paper refer to the midpoint of these classes, which are plotted as symbols in Figure 3.1.

Optimization of the refractive index

The optical efficiency factor of the 'average' particle, $\overline{Q}_j(\lambda)$ (j = a, b, c, or b_b), can be determined from the PSD and the optical coefficients $a_p(\lambda)$ and $b_p(\lambda)$. The PSD is first converted into the geometrical shape factor for the whole population [S] following

$$S = \sum_{C=1}^{n} (\pi / 4) \cdot d_C^2 \cdot N_C \tag{3.1}$$

where C is size class number, d_C the particle diameter describing the size class, and N_C the number of particles in a size class per unit volume of medium. The unit of S is m^{-1}. By convention, the unit for particle diameter d is µm, however exclusively in Eq. 3.1 d is expressed in m.

For the whole population of suspended particles,

$$\overline{Q}_j(\lambda) = j(\lambda) / S \tag{3.2}$$

The ADT and Mie models operate with the input parameters relative particle size and $m(\lambda)$. The relative particle size is expressed as the dimensionless size parameter x

$$x = \pi\, d\, n_w(\lambda) / \lambda \tag{3.3}$$

where $n_w(\lambda)$ is the refractive index of the medium (water) and λ the wavelength in µm of the light in air. Only the real part of $n_w(\lambda)$ is used here, as the imaginary part amounts to $<1.6 \times 10^{-7}$ (for λ = 750 nm) over the entire 350-800 nm range. The real part of $n_w(\lambda)$ was interpolated from Segelstein (1981), although a fixed value of 1.33 did not yield significantly different results. The values of $m(\lambda)$ are also expressed relative to the refractive index of the medium.

ADT calculations gave the optical efficiency factors for a single size class, $Q_j(\lambda)$. To obtain $\overline{Q}_j(\lambda)$, calculations for every size class were made and weighted according to their shape factors (from Eq. 3.1 it follows that $S(d) = \pi/4\, d^2\, N$). Because $\overline{Q}_j(\lambda)$ could thus be derived from both measured and modelled optical properties, it was possible to optimize the value of $m(\lambda)$ for the best fit of measured and modelled optical efficiencies. If $\Delta Q_j(\lambda)$ is the absolute difference between measured and modelled $\overline{Q}_j(\lambda)$, then the optimal value of $m(\lambda)$ lead to the smallest value of $[\Delta Q_a(\lambda) + \Delta Q_b(\lambda)]$. The optimization routine outlined below was mainly adapted from earlier publications (Morel and Bricaud 1986, Stramski *et al.* 1988), to quickly retrieve $m(\lambda)$ for the

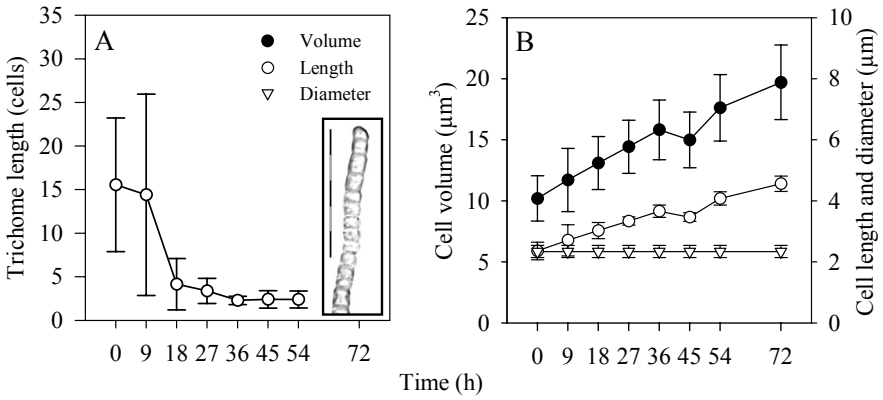

Figure 3.2. Microscopical observations of (**A**) Average and standard deviation of trichome length, for infected cultures, and (**B**) average and standard deviation of cell volumes, cell length, and cell diameter for a combination of infected (n = 3) and control (n =1) cultures. Cell morphology was not different for infected and control cultures. The data at t = 72 h is based only on the cells in the control culture as no cells were found in the infected cultures. The inset in panel A shows a light microscope image of a fragment of a *L. boryana* trichome; the scale bar is 20 μm.

wavelength range 350 – 800 nm at 1-nm intervals. All calculations were made for the polydisperse population. First, a plausible value of $m(\lambda)$ was chosen as a starting value, and after every iteration, the optimized value was used as a starting point for the next wavelength in the series. This approach speeds up the optimization process as differences in $m(\lambda)$ are typically small at 1-nm intervals. Convergence of modelled and measured optical efficiency factors was reached for all samples at all wavelengths when starting from 800 nm with m = 1.02 + 0.003i and proceeding towards shorter wavelengths using the optimized value of the last step. The optimization routine itself was structured so that a 5 × 5 matrix around the initial value of $m(\lambda)$ was constructed, with a variation of 10% and 20 % around $m(\lambda)$ for both the imaginary part [n'], and the real part above 1 [n – 1]. In case negative values of n – 1 or n' occurred, these were zeroed. The value from the m-matrix that yielded the best fit of modelled and measured efficiency factors was selected and a new matrix around this value constructed. The procedure was then repeated until no change in the optimal value of $m(\lambda)$ was found. Variation in the m-matrix was subsequently reduced to 1% and 2% around $m(\lambda)$ until the procedure again yielded no change, at which point the optimal value of $m(\lambda)$was stored and the routine run for the next wavelength in the series.

The optimization procedure was carried out using the ADT routine, after it was checked from test-runs that ADT and Mie models gave the same optimized value of the refractive index, within 1%, for selected samples, using 10-nm intervals. The ADT routine does not yield angular scattering coefficients, so the Mie routine was still

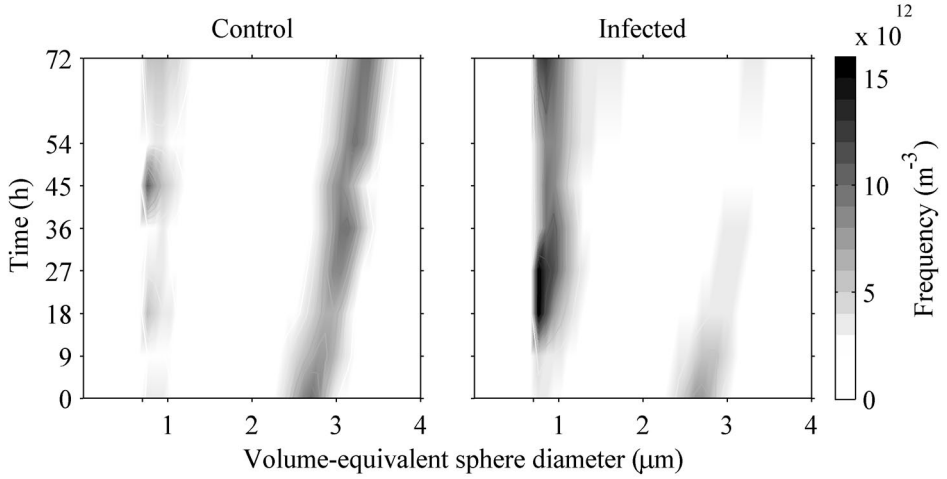

Figure 3.3. Particle size distributions, after conversion of trichomes to individual cells (see Method and Figure 3.1). Cells are visible as a band around ESD = 3 μm, cell fragments and heterotrophic bacteria are visible around 1 μm. Frequencies (gray scale) were linearly interpolated between sampling times and size classes.

operated on the optimized values of $m(\lambda)$, for every sample, wavelength, and size class. The obtained efficiency factors for every size class were multiplied by the size class respective shape factor and particle density, yielding the modelled inherent optical property $b_{bp}(\lambda)$.

The measurements of $a_p(\lambda)$, $b_p(\lambda)$, and PSD for the replicate infected samples were averaged before operating the scattering models. No smoothing of spectral data was carried out except for plotting some of the figures (as indicated).

Reflectance

For the interpretation of remotely sensed signals it has been established that the reflectance of solar irradiance at zero depth $[R(0^-, \lambda)]$ is related to the inherent optical properties of the water column through (Gordon *et al.* 1975)

$$\mathrm{R}(0^-, \lambda) = f \frac{b_b}{a_{\mathrm{TOT}} + b_b} \tag{3.4}$$

where f is a scaling factor dependent on the incident light field (Morel and Gentili, 1991, 1993). The term $a_{\mathrm{TOT}}(\lambda)$ sums the absorption by water and its constituents, $[a_w(\lambda) + a_p(\lambda)]$, whereas $a_{\mathrm{CDOM}}(\lambda)$ did not significantly contribute and was omitted. The absorption by pure water $[a_w(\lambda)]$ was obtained from Buiteveld *et al.* (1994). The dimensionless bracketed term can be considered an inherent optical property of the

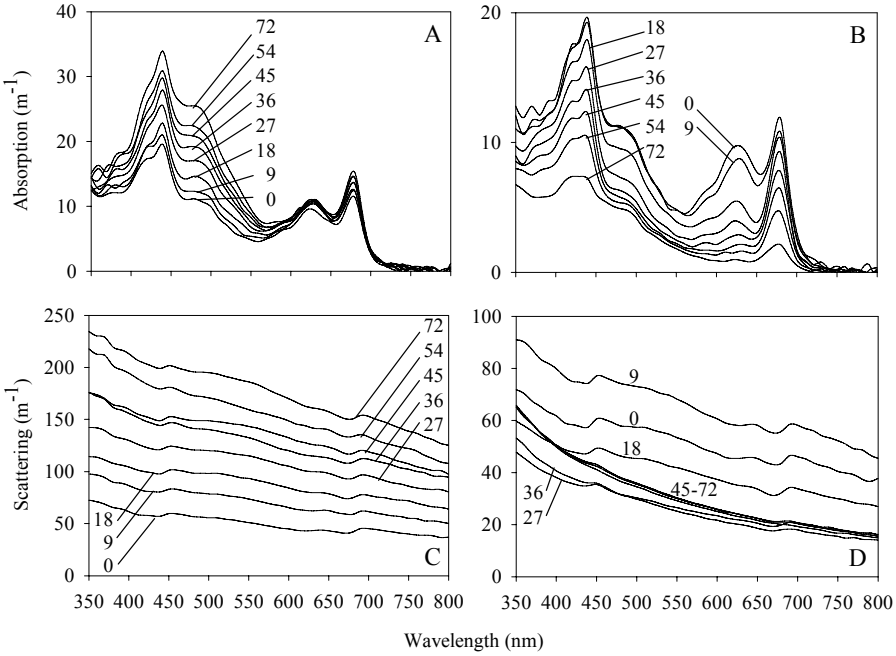

Figure 3.4. (**A**, **B**) Spectra of the measured inherent optical properties absorption [$a_p(\lambda)$] and (**C**, **D**) scattering [$b_p(\lambda)$] for the infected cultures (B, D) and control culture (A, C). Sample time indicated in the plots. Spectra were smoothed over 10 nm. Note the different scales for plots of infected and control cultures.

water body, closely related to subsurface reflectance but independent of the incident light field. By analogy to the scattering albedo $\omega(\lambda)$, the term is defined here as the backscattering albedo, calculated as [$\omega_b(\lambda) = b_{bp}(\lambda) / (a_{TOT}(\lambda) + b_{bp}(\lambda))$]. Spectra of $\omega_b(\lambda)$ were calculated from modelled $b_{bp}(\lambda)$ and measured $a_p(\lambda)$.

3.3. Results

As soon as 18 hours after infection trichome length in the infected cultures decreased drastically (Figure 3.2A). Average trichome length of the control culture exceeded 100 cells per trichome nearing the end of the experiment, while the average was < 5 cells per trichome in infected cultures from 18 hours after infection onward. After 36 h, average filament length was ≤ 3 cells, and at t = 72 h no intact cyanobacterial cells were observed. Both the infected cultures and the control culture exhibited an increase in average cell volume from the start of the experiment, caused by an increase in average cell length while average diameter remained constant (Figure 3.2B). The increase in length may be attributed to two processes. First, in infected cultures, trichomes split up into many smaller sections and thus relatively many cells were

located at the apical ends of trichomes, which are slightly elongated. Second, growth of *L. boryana*, which mainly affects the control culture, follows a regular pattern of increase in cell length and subsequent cell division. The culture medium was refreshed twice shortly before the start of the experiment and cell division could have been synchronized. Although the two processes affected the treatments differently, no significant difference in the trend of cell length and volume was found between control and infected cultures.

Temporal changes in PSD differed markedly between the control and infected cultures. The progression of the PSD for both treatments has been plotted in Figure 3.3, where a band around ESD = 3 μm represents the *L. boryana* cells and the band around ESD = 1 μm represents heterotrophic bacteria and cell debris. Some variation in peak height was observed in the control treatment for the smaller particles, close to the detection limit of the particle counter at ESD = 0.7 μm. This variation could be attributed to instrument noise—it was also present between replicate counts of the same sample. The infected cultures consisted of three replicate samples instead of one for the control treatment, which cancelled out most instrument noise. The increase with time of average cell length and volume, discussed above, was reflected in the PSDs, as the band around ESD = 3 μm shows a shift to larger ESD for both infected and control cultures.

Optical measurements showed differences between control and infected treatments from t = 9 h. Absorption by coloured dissolved organic matter (CDOM) increased slightly upon lysis but remained low (results not shown). The lack of CDOM increase may be attributed to the presence of the heterotrophic bacteria, which are also held responsible for a lack of water-soluble pigments visible in the dissolved fraction. Only around t =18 weak absorption was observed around the absorption peaks of the pigments phycocyanin (PC, around 615 nm) and chlorophyll *a* (Chl *a*, around 440 nm and 675 nm), close to the detection limit of the spectrophotometer. It was previously described that Chl *a*-like absorption patterns in the CDOM fraction (< 0.2 μm) during mass lysis of cyanobacteria have a particulate nature (Simis *et al.* 2005*b*). The absence of significant absorption in this experiment thus suggests that the degradation of lytic matter either took place very rapidly, or that released cell fragments were mostly larger than 0.2 μm. It was also tested whether the scattering models gave different results when CDOM absorption was included in the imaginary part of n_w, which was not the case. Therefore, CDOM absorption was further neglected.

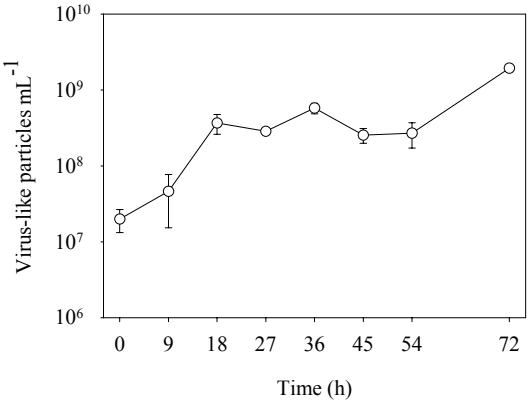

Figure 3.5. Free virus-like particles (VLP) counted in the infected cultures by epifluorescence microscopy after SYBR-green staining. Error bars indicate standard deviation between replicate infected cultures (n = 3). The approximate number of phages added at t = 0 was 1.0×10^8 mL^{-1} The first count, immediately after infection (t = 0), yielded 2.0×10^7 VLP mL^{-1}.

The measured inherent optical properties $a_p(\lambda)$ and $b_p(\lambda)$ continuously increased in the control culture (Figure 3.4A, C). Marked increase in the blue to green domain was observed, whereas the increase in the red part of the spectrum was small. This indicated that the culture was light-saturated and produced more photoprotective carotenoid pigments than photosynthetic pigments. In contrast, the infected cultures showed a drastic decline of both $a_p(\lambda)$ and $b_p(\lambda)$ (Figure 3.4B, D). The first change appeared to be loss of PC, which showed at t = 9 h when absorption around 620 nm decreased while the rest of the spectrum appeared unaffected. From t = 9 h towards the end of the experiment an overall decrease and flattening of $a_p(\lambda)$ was observed. The infected cultures showed an initial increase in measured $b_p(\lambda)$ at t = 9 h, after which $b_p(\lambda)$ dropped until t = 27 h. Subsequently, features around the major pigment absorption peaks disappeared from the $b_p(\lambda)$ spectra. From t = 27 to 45 h post-infection, $b_p(\lambda)$ increased, especially towards shorter wavelengths. Between t = 45 and 72 h, no further changes were observed.

The number of VLP first increased sharply after 9 h post-infection (Figure 3.5). Approximately 1×10^8 VLP mL^{-1} were initially added. The first measurement at t = 0 yielded 2×10^7 VLP mL^{-1}, suggesting that most VLP rapidly attached to a host. Subsequently, VLP increased 18-fold within 18 h, coinciding with a drastic increase in the number of small particles (Figure 3.3). Another outbreak of VLP occurred between 27 and 36 h post-infection. Both initial peaks in the VLP count were followed by a decline in VLP, suggesting that several cycles of infection and lysis took place. At t = 72 the VLP count was 97 times higher than at t = 0. During the last 24 h interval (54

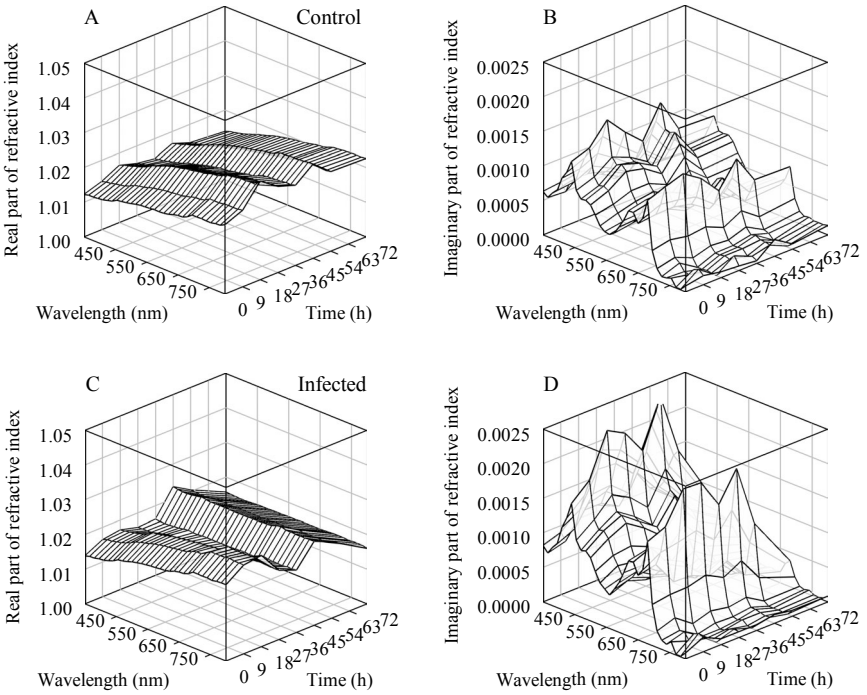

Figure 3.6. (**A**, **C**) Optimized values of $m(\lambda)$, split up in real part $n(\lambda)$, and (**B**, **C**) imaginary part $n'(\lambda)$ for control and infected cultures (panels A-B and C-D, respectively).

– 72 h following infection) the number of VLP increased with a factor 7. At this point the host population was so sparse that very few infections could take place.

The optimization of $m(\lambda)$ through ADT modelling yielded the values of $m(\lambda)$ plotted in Figure 3.6. Spectral variation of the real part n was small, showing a gentle positive slope with wavelength found for all samples of the control culture and the early samples of the infected cultures. Over time, the $n(\lambda)$ spectra flattened in the infected cultures. The average and standard deviation (SD) of $n(\lambda)$ calculated over all cultures ($n = 4$) was 1.02 ± 0.003. The imaginary part n' varied between 0 and 0.0026 with average and SD of 0.0007 ± 0.0005. These values of $n(\lambda)$ compare well with literature values, e.g., $n = 1.04 - 1.05$ for *Synechocystis* sp. and *Synechococcus* sp. (Ahn *et al.* 1992), $n = 1.02 - 1.04$ ($\lambda = 633$) for *Microcystis* species and $n = 1.05$ for species of the filamentous *Oscillatoria* genus (Volten *et al.* 1998). In the latter study values of n as high as 1.24 ($\lambda = 633$ nm) were found for *Prochlorothrix hollandica* (a filamentous prochlorophyte) and other colony-forming phytoplankton. Similarly high values (spectral average of $n > 1.15$) could be obtained with the present data when using a

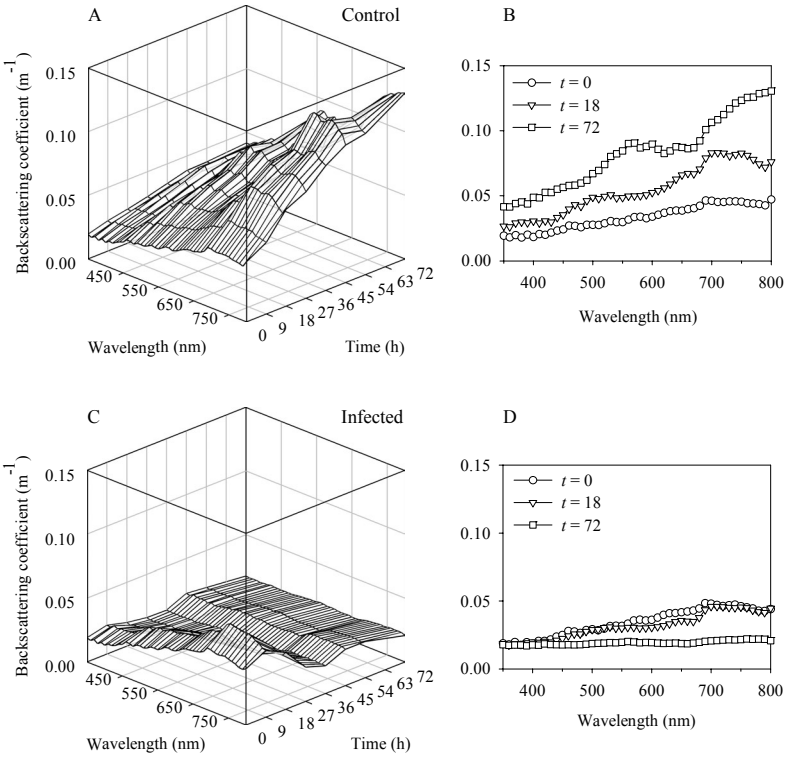

Figure 3.7. (**A**, **C**) Calculated $b_{bp}(\lambda)$ spectra for uninfected and (**C**, **D**) infected cultures. Panels B and D give the spectra at t = 0, 18 and 72 h. The data is plotted at 10-nm intervals in all panels.

PSD of volume-equivalent spheres representing whole trichomes rather than individual cells. Additionally, calculations with the non-adjusted PSDs did not always lead to convergence of modelled and measured data, especially at shorter wavelengths. Only for the infected cultures at $t \geq 18$ optimized $m(\lambda)$ values were approximately the same regardless of the treatment of the PSD. These infected cultures were dominated by smaller particles including short trichomes, cell debris, and heterotrophic bacteria, so adjustment of the PSD did not have a large effect on its shape.

The calculated $b_{bp}(\lambda)$ spectra (Figure 3.7) all show a slight positive slope with wavelength, comparable to experimental and modelled results by Ahn *et al.* (1992). Between control (Figure 3.7A, B) and infected (Figure 3.7C, D) cultures, differences were largest around t = 18 h, marking also the first burst of free VLP and release of small cellular debris. At that time the $b_{bp}(\lambda)$ spectrum of infected cultures also showed slight depressions around the blue and red absorption peaks of Chl *a*. Beyond t = 18 h, the backscattering intensity of these samples decreased and spectrally flattened again,

simultaneous with $b_p(\lambda)$. In the control culture the $b_{bp}(\lambda)$ spectra were sloped and spectral features around the major absorption peaks became increasingly apparent. The backscattering ratio $B(\lambda)$ was higher for infected samples (Figure 3.8C, D) than for the control culture (Figure 3.8A, B) from t = 18 onwards. Intensity and spectral shape of $B(\lambda)$ were relatively stable for the control culture.

It was investigated how the calculated $b_{bp}(\lambda)$ and $B(\lambda)$ spectra were influenced by the representation of SMP in the PSD. For the infected cultures at t = 18, small particles < 0.7 µm which would not have been detected by the particle counter, were added to the PSD in the model. The 'enriched' PSD and the original measurements of $a_p(\lambda)$ and $b_p(\lambda)$ were used to optimize $m(\lambda)$ for an increasing amount of SMP added to the PSD input of the model. The number of added SMP was proportional to the number of lysed *L. boryana* cells between t = 9 and t = 18 h. An enrichment factor was defined as the number of SMP added in the 0.2 – 0.7 µm range per lysed host cell. For enrichment factors of 0, 1, 10, 20, 30, and 50 SMP per lysed cell, Figure 3.9 shows the enriched PSDs and distribution of the shape factor S resulting from this approach. An enrichment factor of 0 represents the original PSD after the substitution of individual particles for cells in trichomes. Because S increased in proportion to the number of added small particles, $\overline{Q}_a(\lambda)$ and $\overline{Q}_b(\lambda)$ decreased (Eq. 3.2), forcing a lower value for both imaginary and real part of the $m(\lambda)$. The increased importance of small particles meanwhile raised $\overline{Q}_{bb}(\lambda)$ and consequentially (Eq. 3.2) $b_{bp}(\lambda)$ and $B(\lambda)$, as shown in Figure 3.10. At the highest enrichment factor of 50 added particles per lost cell of *L. boryana*, $b_{bp}(\lambda)$ and $B(\lambda)$ were approximately 2 times higher than with the enrichment set to zero. An enrichment factor of 50 implied for this sample that the number of added SMP was one order of magnitude higher than the total number of particles > 0.7 µm.

In spectra of the backscattering albedo $\omega_b(\lambda)$ modelled for infected cultures (Figure 3.11A) the feature of absorption by PC and Chl *a* around 620 nm largely disappeared as lysis took place. At t = 18 h, $\omega_b(\lambda)$ from 700 to 800 nm reached high values and it was particularly pronounced at 650 nm, the wavelength of the local absorption minimum between 620 nm (PC and Chl *a*) and 675 nm (Chl *a*). Until t = 36 h, $\omega_b(\lambda)$ decreased in the red and near-infrared, followed by an increase in the 550 to 650 nm range until the end of the experiment, while the value of $\omega_b(\lambda)$ between 750 and 800 nm dropped below the starting value. The red peak around 705 nm was very high at t = 18 and t = 54. In the spectral range 350 to 500 nm little change was observed throughout the experiment. In the latter region decline of $a_p(\lambda)$ was least while $b_p(\lambda)$ remained relatively high and $b_{bp}(\lambda)$ was lowest during the experiment. With increasing representation of SMP at t = 18 h, $\omega_b(\lambda)$ of the infected cultures increased and eventually doubled at an enrichment factor of 50. The virtual addition of SMP to the PSD did not change the shape of the $\omega_b(\lambda)$ spectrum (SD < 0.05 for $\omega_b(\lambda)$ spectra normalized to their maximum).

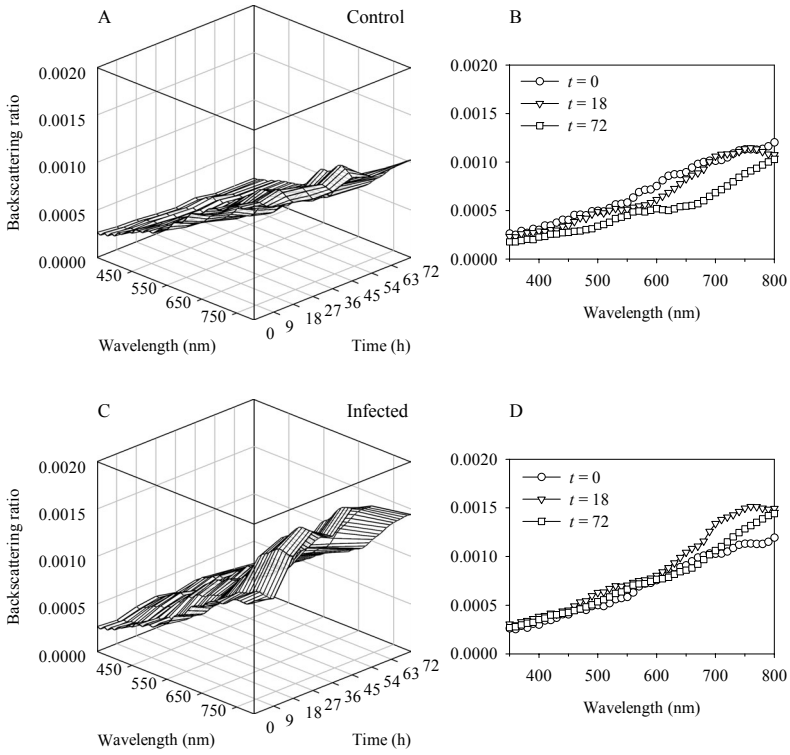

Figure 3.8. Backscattering ratios $B(\lambda)$ derived from measured $b_p(\lambda)$ (Figure 3.4C-D) and modelled $b_{bp}(\lambda)$ (Figure 3.7) data, for (**A**, **B**) uninfected and (**C**, **D**) infected cultures. Panels B and D give the spectra at t = 0, 18, and 72 h. The data is plotted at 10-nm intervals in all panels.

The shape of $\omega_b(\lambda)$ spectra changed markedly if $a_p(\lambda)$ and $b_{bp}(\lambda)$ were lowered relative to the absorption of water $a_w(\lambda)$. Spectra of $\omega_b(\lambda)$ are given for t = 18 h at various such 'dilutions', for the cases excluding and including high representation (enrichment factor 50) of SMP in the PSD (Figure 3.11 C and D, respectively). Dilution to 10 % of the original values of $a_p(\lambda)$ and $b_{bp}(\lambda)$ yielded spectra that are representative of well-mixed eutrophic lakes, whereas the undiluted spectra (indicated with 100 %) would probably only be encountered with hypertrophic systems or surfacing blooms (Rijkeboer *et al.* 1998).

It is noted that effects of optically active substances that were not present in our cultures such as suspended minerals, most organic detritus, CDOM, and also of bottom reflectance on $\omega_b(\lambda)$ were not considered. Due to the strong absorption by water, diluting the culture suspensions would primarily cause decrease of $\omega_b(\lambda) > 700$ nm. Dilutions from 50 % to 10 % also lowered $\omega_b(\lambda)$ between 550 and 675 nm. Only at the

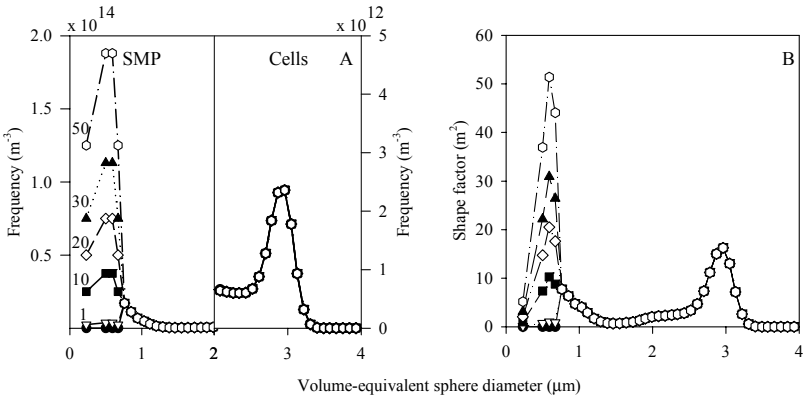

Figure 3.9. PSDs used to test the effect of increasing representation of SMP (< 0.7 µm) in the PSD on the amplitude of $b_{bp}(\lambda)$, for the infected cultures at t = 18. (**A**) PSD for the case of 0 (no change), 1, 10, 20, 30, and 50 small particles for every cell that was lysed in the 9 – 18 h interval. (**B**) Geometric shape S of the PSDs in panel A (Eq. 3.1).

strongest dilution considered (1 %) a decrease of $\omega_b(\lambda)$ down to 450 nm would be expected. With increasing dilution, the peaks in the $\omega_b(\lambda)$ spectra shifted to shorter wavelengths. At 10 % dilutions, changes in $\omega_b(\lambda)$ following infection of the cultures were insignificant below 450 nm and above 750 (Figure 3.11E), but the green peak around 550 nm became more pronounced. At the 10 % dilution it is easy to follow the dynamics of waveband ratios that are used for remote sensing of the photosynthetic pigments Chl *a* and PC. The ratio of reflectance bands recorded by the Medium Resolution Imaging Spectrometer (MERIS) on the ENVISAT satellite is 709 : 665 nm for Chl *a* (Gons *et al.* 2005). The retrieval of PC is mainly based on the ratio of bands 709 : 620 nm (Simis *et al.* 2005*a*).

In accordance with previously published results on the pigment ratio PC : Chl *a* during lysis of cyanobacteria in enclosed lake water (Simis *et al.* 2005*b*), it was observed (Figure 3.11F) that the band ratio indicative for PC declines more rapidly than the band ratio for Chl *a* retrieval.

3.4. Discussion

Previous studies have pointed out that live cells of most phytoplankton species, and cyanobacteria in particular, have a weak influence on the backscattered light signal whereas detritus particles and bacteria may contribute most to particulate backscattering (Morel and Ahn 1991, Stramski and Kiefer 1991, Ahn *et al.* 1992, Stramski and Mobley 1997). During a cyanobacterial bloom, mass viral lysis can dramatically alter the nature of the dominant scattering particles, and backscattering

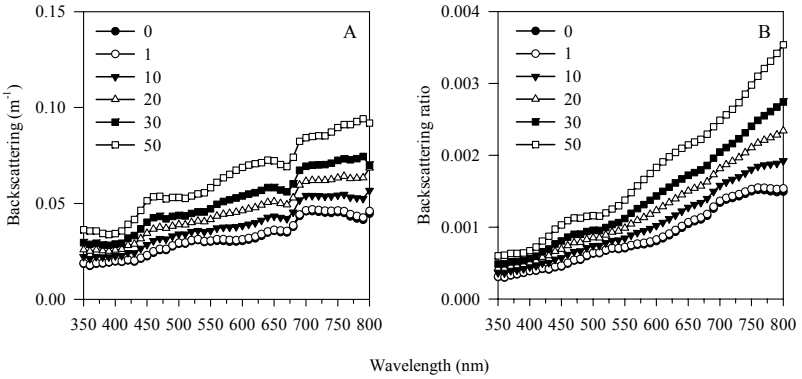

Figure 3.10. Modelled spectra of (**A**) $b_{bp}(\lambda)$ and (**B**) $B(\lambda)$ as a function of SMP representation in the PSD for t = 18 h (Figure 3.9). The data is plotted at 10-nm intervals.

may become more important as a result of a shift of the particle size distribution towards smaller particles, including heterotrophic bacteria degrading the lytic material. It was shown in this work that under the assumption of homogeneous spheres representing cells organized in cyanobacterial trichomes, the backscattering ratio remained low throughout an experimental mass lysis event. A more significant increase of the backscattering ratio was found when the presence of a very large release of sub-micron cell debris, not visible to the particle sizer, was accounted for. In all cases, however, the increased importance of small particulate matter did not markedly alter the spectral shape of modelled backscattering. The optimized values of the refractive index remained low throughout lysis and also following the enrichment of the PSD for the model with small particles, suggesting that the dominant particles were indeed weak scatterers. It was previously shown that $m(\lambda)$ is largely dependent on cell material and relative water content (Aas 1996). The cellular structure and biochemical composition of *L. boryana* is not expected to be essentially different from previously studied cyanobacterial species, and indeed the optimized values of $m(\lambda)$ compared reasonably well with expectations raised from earlier reports (Ahn *et al.* 1992, Volten *et al.* 1998).

Absence of strong absorption in the CDOM fraction upon lysis was likely the result of the presence of heterotrophic bacteria. They existed in the cultures to prevent released water-soluble phycobilin pigments from discolouring the medium, in order to retain relevance to earlier findings with enclosed lake water (Simis *et al.* 2005*b*). A positive response of the heterotrophic bacterial community exists upon lysis of the dominant cyanobacterial host in such enclosures (Van Hannen *et al.* 1999, Tijdens *et al.* unpubl.). In the cultures of *L. boryana*, heterotrophic bacteria normally grow at low densities on exudates and cellular debris. The influence of the bacteria on the bulk

optical properties could be significant towards the end of the lysis experiment as lysis induced an increase in their numbers, but these observations lack sufficient detail to be certain. It is likely that the release of lytic products was, at least in part, countered by heterotrophic bacterial activity, as can also be expected during lysis of natural blooms. In nature the exact scenario will depend largely on the food quality of the released organic matter for the heterotrophic bacterial community and higher trophic levels.

Changes in the colour (hue and brightness) of a water body can be recorded using current remote sensors, whether placed on ships, aircraft, or satellites. Bio-optical models relate the contribution of the various water constituents to the spectral reflectance of the water body. The optical behaviour of phytoplankton blooms is still insufficiently known to correctly interpret remotely sensed signals in terms of bloom dynamics. It was previously found that drastic changes in the inherent optical properties $a_p(\lambda)$ and $b_p(\lambda)$ occurred upon mass lytic activity in nutrient-induced blooms of a filamentous cyanobacterial community (Gons *et al.* 2002*a*, Simis *et al.* 2005*b*). Due to the magnitude of these changes it was postulated they could be recorded from satellite-born remote sensors. However, from $a_p(\lambda)$ and $b_p(\lambda)$ alone it is not possible to predict the appearance of a water body. The backscattering albedo $\omega_b(\lambda)$ was obtained by combining modelled and measured results, and allows evaluation of spectral changes in the upwelling light as a result of mass lysis.

Because of the generally low values that were found for the refractive index and the absence of marked spectral changes of $b_{bp}(\lambda)$ as a result of lysis, changes in $\omega_b(\lambda)$ were dominated by changes in the absorption of the water constituents, and by the importance of their absorption relative to water. The intensity of the $\omega_b(\lambda)$ spectra did show a positive linear response to inclusion of SMP in the PSD, i.e. particles that could have been present below the detection limit of the particle sizer. The spectral shape of $b_{bp}(\lambda)$ was not markedly affected by these theoretical experiments, and $\omega_b(\lambda)$ was only significantly elevated when very high population densities were considered, or when many SMP were included. Still, the amount of released SMP as well as the rate of degradation of this material and thus the time of observation, can have a significant effect on the amplitude of the reflected light signal. The intensity of reflectance is therefore not considered a consistent indicator of mass lysis events.

Spectral changes in $\omega_b(\lambda)$ revealed a more pronounced 'green peak' of reflectance at λ = 560 to 600 nm, as also observed earlier with enclosed lake water using a generic VSF (Petzold 1977) to calculate reflectance spectra (Simis *et al.* 2005*b*). This spectral change is explained jointly by relatively small changes of $a_p(\lambda)$ and $b_p(\lambda)$ in the blue spectral domain, an increase in $b_{bp}(\lambda)$ towards longer wavelengths, and the disappearance of absorption by photosynthetic pigments in the red spectral domain.

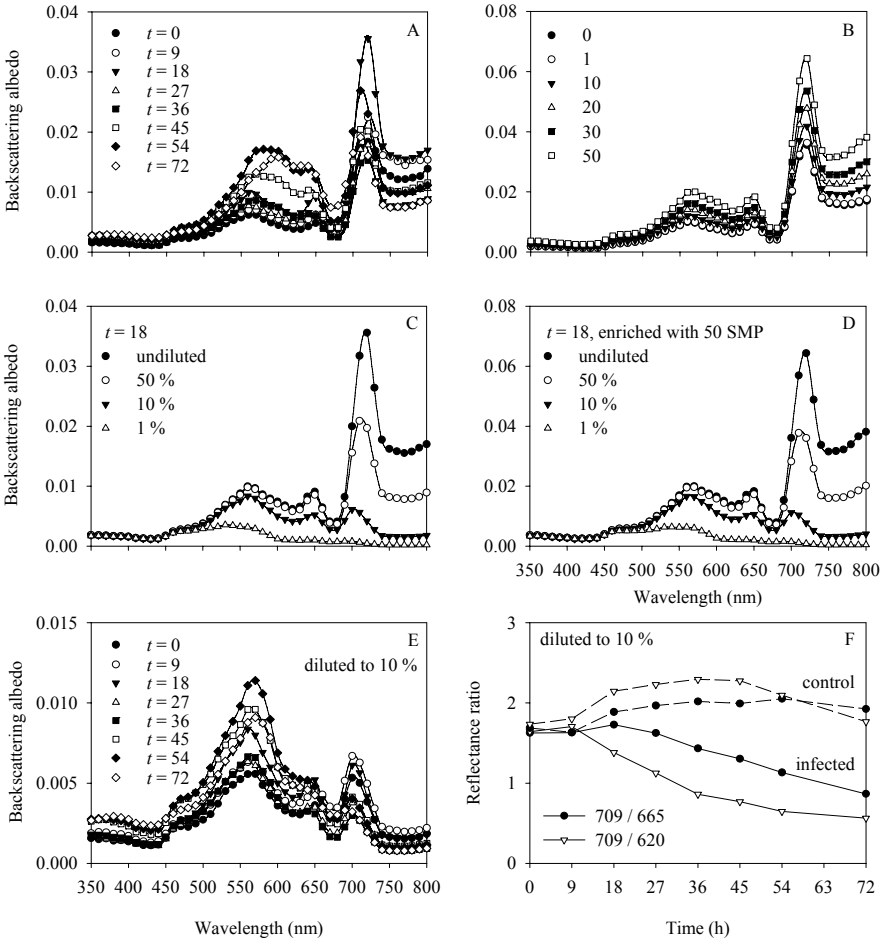

Figure 3.11. Modelled reflectance $\omega_b(\lambda)$ (see Method) for infected cultures using (**A**) $b_{bp}(\lambda)$ from Figure 3.7C and (**B**) $b_{bp}(\lambda)$ from Figure 3.10A (t = 18 h, varying representation of SMP in the PSD). Reflectances of panel A at t = 18 h and panel B at enrichment factor 50 are shown in (**C**, **D**) for various dilutions (as indicated) of the optical properties $a_p(\lambda)$ and $b_{bp}(\lambda)$ relative to the absorption by pure water $a_w(\lambda)$. (**E**) Dilutions to 10 % of the time series displayed in panel A. (**F**) Ratios of bands 709 : 665 nm and 709 : 620 nm, used for respectively chlorophyll *a* and phycocyanin retrieval from remotely sensed imagery, based on the 10 % dilution series (panel E).

The typical absorption features of PC and Chl *a* underwent significant changes which may be retrieved by reflectance band ratios operated on turbid water bodies (Gons *et al.* 2005, Simis *et al.* 2005*a*, Chapter 5). It was observed that ratios of 709 : 665 nm for Chl *a* and 709 : 620 nm for PC retrieval increased briefly in the growth phase before the lysis event. This increase was probably due to the first release of small particles and the growth of yet uninfected cells. Subsequently the band ratios dropped, as released pigments and small particles degraded. The band ratio indicating PC absorption dropped more rapidly than the band ratio for Chl *a* as explained above. This observation is in agreement with measurements of the concentrations of these pigments in lysis studies of enclosed lake water (Gons *et al.* 2002*a*, Simis *et al.* 2005*b*). It appears that irrespective of the dynamics in the amplitude of the reflected light signal which cause the $\omega_b(\lambda)$ spectra to shift up and down in a less predictable manner, the ratio of PC to Chl *a* may be used to indicate mass lysis of cyanobacteria (Simis *et al.* 2005*b*).

In conclusion, the present work contains the first optical modelling of the scattering behaviour during mass viral lysis of phototrophs. It was possible to show temporal trends in the modelled backscattering behaviour of a population of cyanobacteria undergoing mass viral lysis. Although the use of the Mie-scattering model is widespread in hydrological modelling, giving insight in the scattering behaviour of polydisperse populations of nonspherical particles, the modelled results at backward scattering angles should always be treated with scrutiny (Stramski *et al.* 2004 and references therein). Scattering models for irregularly shaped particles exist (Mishchenko *et al.* 2000), but the added complexity brings higher computational needs, and no scattering model can be expected to precisely describe the optical behaviour of complex biological particles. For example, the internal structure of cyanobacterial cells is relatively simple compared to eukaryotic phytoplankton, but inhomogeneous distribution of the absorbing photosynthetic pigments may be observed in filamentous species like *L. boryana*. Fluorescence has also not been taken into in these scattering models, but can be a significant component of the upwelling light in clear water systems as well as in measurements of $b_{bp}(\lambda)$ of cultured species (Ahn *et al.* 1992). Above all, it is encouraged that (1) optical modelling of mass lysis of phytoplankton is carried out for other cultured species, and (2) such studies are validated with actual measurements of the VSF, preferably at several wavelengths. Despite these considerations, it is believed that the optical characteristics of lysis of a phytoplankton bloom, a situation where the light field is dominated first by a dense host and then by lytic products, bacteria, and viruses, may be approximated by applying these simplifying scattering models, especially where temporal trends in the scattering data are considered.

The present results can be implemented in bio-optical models that also incorporate other optically active water constituents: plankton species unaffected by the ongoing viral lysis, CDOM, and suspended sediments. Remote sensing studies may thus focus on bloom dynamics both as blooms first appear on imagery, and as they fade or disappear. This information may lead to better understanding of the conditions in which mass lytic events occur. Hypoxia following release of organic matter, and the possible release of harmful substances produced by algal and cyanobacterial species warrant special attention for the causes of mass viral lysis and general bloom dynamics.

3.5. Acknowledgments

We thank Hans van der Woerd, Hester Volten and two anonymous reviewers for their comments that helped to improve this manuscript. Part of the work was carried out at the Institute for Environmental Studies, Vrije Universiteit, Amsterdam.

4. REMOTE SENSING OF THE CYANOBACTERIAL PIGMENT PHYCOCYANIN IN TURBID INLAND WATER

Stefan G. H. Simis, Steef W. M. Peters[1] & Herman J. Gons
[1]Institute for Environmental Studies (IVM), Vrije Universiteit, Amsterdam, The Netherlands.

Limnology and Oceanography (2005) 50: 237-245

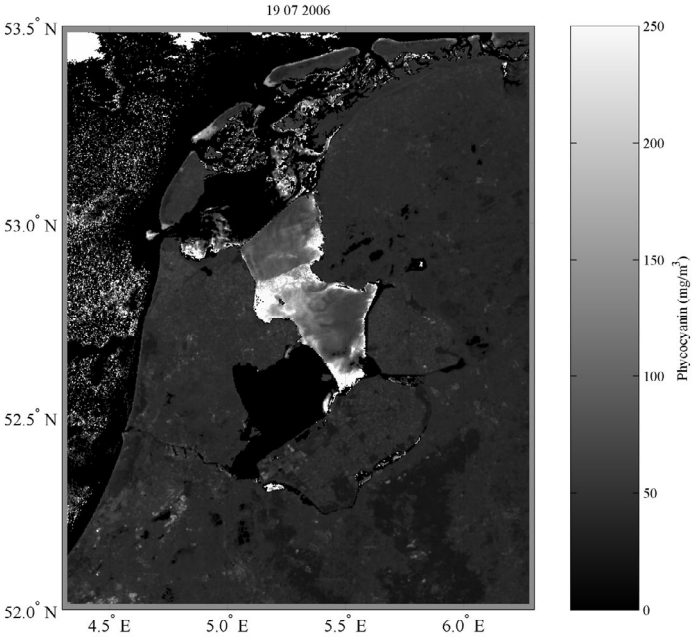

Abstract

The pigment phycocyanin (PC) is a marker for cyanobacterial presence in eutrophic inland water. We present a reflectance band ratio algorithm for retrieval of cyanobacterial PC. The model conforms to the band settings of the Medium Resolution Imaging Spectrometer (MERIS). The parameters of the algorithm were optimized using reflectance and absorption data from two highly eutrophic lakes. Using measured specific absorption coefficients for PC [$a^*_{pc}(620)$] for every sample, error in the predicted PC concentrations was 19.7 % ($r^2 = 0.94$, $n = 34$) for measured PC concentrations up to 80 mg m^{-3}. Applying a fixed value of $a^*_{pc}(620)$ caused an overestimation of the PC content that increased towards lower PC concentrations. The PC prediction best matched observed values during periods of high relative abundance of cyanobacteria in the plankton community. The results suggest strong seasonal variation in $a^*_{pc}(620)$. The presence of pigments other than PC and Chl *a*, and a variable influence of Chl *a* on retrieved absorption at 620 nm, are potential causes of error in PC retrieval. The algorithm in its current form is considered suitable for detection of the PC concentration in turbid cyanobacteria-dominated waters.

4.1. Introduction

Eutrophic inland waters often exhibit blooms of cyanobacteria. Notorious for their negative impact on water quality, cyanobacterial blooms have been increasingly subject of water management and scientific studies. Hazards of toxic cyanobacterial blooms call for frequent and rapid monitoring of water bodies. Remote sensing provides insights in the distribution of blooms for a large number of lakes or reservoirs simultaneously. The concentration of chlorophyll *a* (Chl *a*) as a general indicator for plankton biomass can be assessed using imagery from a wide range of air- and spaceborn sensors (Vos *et al.* 2003). Recent advances in spaceborn remote sensing technology broaden the perspectives of monitoring towards identification and quantification of plankton groups. Algorithms for the retrieval of Chl *a* from turbid water reflectance were already being developed (cf. Gons *et al.* 2002*b*). Now, it is attempted to retrieve the pigment phycocyanin (PC), which is characteristic of the presence of cyanobacteria. It is known that the presence of PC can be detected from spectral reflectance (Dekker *et al.* 1991, Gons *et al.* 1992, Jupp *et al.* 1994). However, empirical relationships that have been devised to quantify cyanobacterial PC from spectral reflectance of turbid water (Dekker 1993, Schalles and Yacobi 2000) required more spectral information than is provided by satellite sensors with global coverage. In the current work, band settings of the Medium Resolution Imaging Spectrometer (MERIS) were adopted for two reasons: first, a band located at 620 nm includes the maximum absorption of a number of modifications of the PC pigment (Bryant 1994),

and second, the 300-m spatial resolution suffices to monitor moderately sized lakes and reservoirs.

We describe a simple optical model that retrieves the PC concentration from turbid water reflectance. Aiming primarily at the quantification of PC in waters where cyanobacteria dominate, the pigments Chl *a* and PC are incorporated into the model as the major absorbing water constituents in the red and near-IR spectral range. As a major simplification, absorption by coloured dissolved organic matter (CDOM) and tripton are neglected, which reduces the number of optically active components that are taken into account. A second simplification is the assumption that the backscattering coefficient, b_b, can be retrieved from a single band in the near infra-red and that it is spectrally neutral (Gons 1999). The parameters of the semi-empirical model were optimized using optical data and pigment measurements of two turbid lakes.

Algorithm development

The spectral reflectance just below the water surface, $R(0^-, \lambda)$, is related to the inherent optical properties of the water column, absorption a and backscattering b_b, through a factor f that is dependent on the light field (Morel and Gentili 1991, 1993). The following relationship between inherent and apparent optical properties of a water body, established by Gordon *et al.* (1975), has become widely accepted (see Table 4.1 for a list of symbols):

$$R(0^-, \lambda) = f \frac{b_b(\lambda)}{a(\lambda) + b_b(\lambda)} \tag{4.1}$$

For spectral neutrality of f and b_b, the absorption by water and its constituents at wavelength λ_1 [$a(\lambda_1)$] can be solved from the reflectance ratio $R(\lambda_2) : R(\lambda_1)$, known b_b, and known absorption in band λ_2:

$$a(\lambda_1) = \frac{R(\lambda_2) \times \left(a(\lambda_2) + b_b\right)}{R(\lambda_1)} - b_b \tag{4.2}$$

A reflectance band ratio for λ_2 = 709 and λ_1 = 665 nm (ratio 1) is effective to retrieve the absorption by Chl *a* in eutrophic inland water (Mittenzwey *et al.* 1992, Dekker 1993, Gons *et al.* 2002*b*), while a ratio for λ_2 = 709 and λ_1 = 620 nm (ratio 2) is introduced to retrieve the PC absorption. For both ratios, a simplified model is obtained when $a(\lambda_2)$ is attributed solely to the absorption by water [$a_w(\lambda_2)$], and $a(\lambda_1)$ to the absorption by water [$a_w(\lambda_1)$] and phytoplankton pigments [$a_{ph}(\lambda_1)$]. By these simplifications it is assumed that pigment absorption is negligible at 709 nm, which may lead to an underestimation of $a(\lambda_1)$, increasing with pigment concentration. In addition, the absorption by coloured dissolved organic matter (CDOM) and tripton is considered negligible, which can cause an overestimation of $a(\lambda_1)$ that is not necessarily correlated with pigment concentration. It is attempted to correct for these

simplifications by the introduction of a correction factor γ that reflects the ratio of retrieved absorption vs. measured absorption by pigments at wavelength λ_1. Thus, substituting the optically active components according to the mentioned simplifications, the following relationship is obtained:

$$a_{chl}(665) = \left[\frac{R(709) \times \left(a_w(709) + b_b\right)}{R(665)} - b_b - a_w(665) \right] \times \gamma^{-1} \tag{4.3}$$

A variation of Eq. 4.3 was successfully applied to a range of eutrophic, turbid lakes, where b_b was retrieved from a single band in the near-infra red (Gons 1999). In the present work, b_b was retrieved from a 778.75-nm, 15 nm-wide band following Gons (1999). In brief, this involves solving Eq. 4.1 for $a(778.75) = a_w(778.75)$ and a value for f that is realistic for turbid waters.

For ratio 2, it is expected that the pigments PC and Chl *a* compose the absorption envelope around 620 nm that is apparent from reflectance spectra of cyanobacteria-rich waters. This reflectance feature is captured within the 620-nm band. Rewriting Eq. 4.3. for band ratio 2 and introducing correction factor δ for the correction of $a(620)$, similar to γ for the correction of $a(665)$, yields:

$$a_{chl}(620) + a_{pc}(620) = \left[\frac{R(709) \times \left(a_w(709) + b_b\right)}{R(620)} - b_b - a_w(620) \right] \times \delta^{-1} \tag{4.4}$$

Next, to unravel the absorption by Chl *a* and PC at 620 nm, first $a_{chl}(620)$ is derived from $a_{chl}(665)$ that was obtained from Eq. 4.3. The conversion factor ε is introduced to relate the *in vivo* absorption by Chl *a* at 665 nm to its absorption at 620 nm. Subsequently, Eq. 4.4 is solved for $a_{pc}(620)$:

$$a_{pc}(620) = \left[\frac{R(709) \times \left(a_w(709) + b_b\right)}{R(620)} - b_b - a_w(620) \right] \times \delta^{-1} - \left[\varepsilon \times a_{chl}(665)\right] \tag{4.5}$$

Finally, dividing $a_{pc}(620)$ by the specific absorption coefficient of PC $[a^*_{pc}(620)]$, results in the PC concentration:

$$[\mathrm{PC}] = \frac{a_{pc}(620)}{a^*_{pc}(620)} \tag{4.6}$$

Table 4.1. List of recurrent symbols.

Symbol	Description	Units
$a_i(\lambda)$	absorption coefficient of compound 'i' at waveband λ used subscripts: w – water; chl – chlorophyll *a;* PC – phycocyanin; TSM – total suspended matter; tripton – pigment-bleached TSM	m^{-1}
$a^*_i(\lambda)$	specific absorption coefficient of pigment i at waveband λ	$m^2(mg\ pigment)^{-1}$
b_b	backscattering coefficient	m^{-1}
$R(0^-,\lambda)$	subsurface irradiance reflectance at wavelength λ and depth 0	dimensionless

4.2. Methods

Lake sampling

The algorithm parameters were optimized using *in situ* reflectance data and optical properties from Lake Loosdrecht (52°11.7'N; 5°3.1'E) and Lake IJsselmeer (52°45'N; 5°20'E), The Netherlands. Lake Loosdrecht (A = 9.8 km^2; $\bar{z}$ = 1.9 m) originated from peat excavation and is well-mixed, eutrophic and turbid, with an average annual Secchi disk depth of 0.6 m and average Chl *a* concentration of 66 mg m^{-3} (sd = 20 mg m^{-3}, n = 20 in 2002-2003). Wind resuspension of the phosphorus-rich sediment occurs frequently (Gons *et al.* 1991). An important part of the vertical attenuation of light is caused by detritus. The dominant cyanobacterial species belong to the filamentous *Limnothrix/Pseudanabaena* group (Pel *et al.* 2003, Zwart *et al.* 2005). The Chl *a* and *b* but no PC-containing prochlorophyte *Prochlorothrix hollandica* occurs in lower abundances. Physical and biological characteristics of Lake Loosdrecht and other shallow Dutch lakes have been described in detail in Van Liere and Gulati (1992). Sampling at Lake Loosdrecht took place every 2 weeks in the period March-November 2003.

Lake IJsselmeer (A = 1190 km^2; $\bar{z}$ = 4.4 m) is the largest lake in the Netherlands, exhibits a Secchi disk depth around 0.8 m and Chl *a* concentrations up to 200 mg m^{-3} in summer. The vertical light attenuation is mainly due to microalgae and cyanobacteria. Surface scums of cyanobacteria occur, but the water column is usually fully mixed. Colonies of *Microcystis* sp. and *Aphanizomenon* sp. filaments represent most of the cyanobacterial biomass. The distribution of cyanobacteria and green algae in summer is inhomogeneous, with locations of relatively high cyanobacterial to green algal biomass and vice versa. From midsummer onward, cyanobacteria dominate the plankton community. Surveys of Lake IJsselmeer were made on r/v *Luctor* (NIOO, Yerseke) on 10 April, 24 June, 5 August, and 9 September in 2003.

Reflectance measurements

Reflectance measurements were made using a portable spectroradiometer, model PR-650 (Photo Research, Chatsworth, CA, USA), that measures radiance at a small (1°) acceptance angle, 8-nm full width – half maximum bandwidth, and at 4-nm increments within the spectral range 380-780 nm. Details on the measurement procedure and computation of $R(0^-, \lambda)$ are given in Gons (1999). Measured reflectance was recalculated for the adopted bandwidths by weighted averaging. The 15-nm wide band at 778.75 nm was partly outside the range of the instrument, so the available 771.25 – 780 nm range was used.

Pigment extraction and quantification

Samples for Chl *a* analysis were concentrated on glass fibre filters (Schleicher & Schuell GF 6, 1 µm pore size) and stored at –20°C for a maximum of 3 weeks. Chl *a* and phaeopigments were measured in duplicate using hot ethanol extraction (NEN 1981). All Chl *a* concentrations refer to 'uncorrected Chl *a*', the sum of Chl *a* and 1.7 times the phaeopigment concentration, to account for absorption by phaeopigments as well as Chl *a*. For the determination of PC concentration, a method was devised based on the freeze-thaw procedure as explored by Sarada *et al.* (1999). Samples of 200 ml were concentrated in two centrifugation runs on a Sorvall RC5C centrifuge that was cooled to < 10°C. The first centrifugation was at 15000 *g* for 25 min, then pellets were transferred to 35 ml of pH 7.4 phosphate buffer, whereafter the suspension was centrifuged again at 27000 *g* for 20 min. Finally, the pellet was transferred to a 15 ml falcon tube that was filled up to 6 ml with buffer solution and then frozen at -20°C. The concentrates were frozen within 2 h after sampling, except during cruises on Lake IJsselmeer when samples for PC analysis were kept on ice and processed within the next 24 h. By photospectrometrical analysis of the supernatant after concentration of the samples by centrifugation, it was confirmed that cells were not disrupted by centrifugation. Thus, no phycocyanin was lost before starting the extraction procedure. Within 4 weeks of storage, samples were subjected to nine cycles of freezing (–20°C) and thawing (at room temperature). Purification of the samples was carried out by centrifugation at 13000 *g* for 90 min. PC concentrations were spectrophotometrically derived following the equations given by Bennett and Bogorad (1973). Where replicate samples were collected, average pigment concentrations were used for subsequent analyses.

Optical properties

All spectrophotometric measurements were carried out on a Lambda 800 UV/Vis spectrophotometer (PerkinElmer, Wellesley, MA, USA) in the 350 to 800 nm range, using a 150-mm integrating sphere (Labsphere Inc, North Sutton, NH, USA) for filterpad measurements (Maske and Haardt 1987). Absorption values were averaged

over the width of the used bands. The absorption by pure water, $a_w(\lambda)$, was taken from Buiteveld *et al.* (1994). Whatman GF/F filters, Ø 25 mm, for absorption measurements of particulate matter were placed in the centre of the sphere, at a 100° angle from the light beam. For each sample, blank and sample filters were wetted in the filtrate of the sample before measurements. Path length amplification was corrected by a factor 2 (Roesler 1998) while the absorbance of the material concentrated on the filters was kept > 0.1 (at λ = 550 nm). Known sample volumes were concentrated on the filters to obtain the absorption by total suspended matter [$a_{TSM}(\lambda)$]. Pigments were bleached from the filters with 80% ethanol at 75°C in two steps, to obtain the tripton absorption ($a_{tripton}(\lambda)$). No residual phycobilipigment absorption was apparent from the tripton absorption spectra. Phytoplankton pigment absorption [$a_{ph}(\lambda)$] was derived as $a_{TSM}(\lambda)$ - $a_{tripton}(\lambda)$. When the bleaching procedure did not completely remove absorption by chlorophyllous pigments, an exponential function was fitted through the $a_{tripton}(\lambda)$ spectra at 350 and 750 nm, which was then substituted for the $a_{\text{tripton}}(\lambda)$ spectrum. The presence of remnant chlorophyllous absorption around 350 nm caused the exponential slope to be slightly overestimated, resulting in a small correction of remnant absorption in the blue region, an overcorrection in the green region, and an acceptable correction in the red region of the spectrum where an error in the exponential slope has only a small effect. Thus, the fitted curve could be used in the present work, where only the 600-710 nm spectral region was used. Absorption by CDOM was measured as the beam attenuation of sample filtrates (0.2 µm pore size, cellulose acetate, Schleicher & Schuell) using a 5-cm glass cuvette with distilled water as a reference. The integrating sphere accessory was not used to measure CDOM absorption.

Using ε, and $a_{ph}(\lambda)$ at λ = 665 and λ = 620 nm, the absorption by PC ($a_{pc}(620)$) could be derived from the absorption measurements as $a_{ph}(620) - (\varepsilon \times a_{ph}(665))$. Subsequently, $a^*_{pc}(620)$ was determined as $a_{pc}(620)$ divided by the measured PC concentration. The specific absorption coefficient for Chl *a* at 665 nm, $a^*_{chl}(665)$, was determined from $a_{ph}(665)$ divided by the measured Chl *a* concentration.

Parameter optimization

Factors γ and δ in Eqs. 4.3 and 4.4 were retrieved from a dataset of $R(0^-, \lambda)$ and $a(\lambda)_{ph}$ spectra, of which 37 pairs were available from the field campaigns at Lake Loosdrecht and Lake IJsselmeer. The linear least squares fit of 'uncorrected' retrieved absorption (Eqs. 3 and 4 with γ, δ = 1) against $a(\lambda)_{ph}$ for λ = 665 and 620 nm, yielded two slopes that were adopted for γ and δ.

Conversion factor ε (Eq. 4.5) was used to define the absorption by Chl *a* at 620 nm relative to 665 nm. It was iteratively retrieved from the best fit of computed versus observed PC concentration for the samples from Lake Loosdrecht where $R(0^-,\lambda)$, $a(\lambda)_{ph}$, and PC concentration data were collected (one outlying measurement of PC was

omitted, n = 18). The data from Lake IJsselmeer was not used in this analysis because the presence of pigments other than PC and Chl *a*, a situation common in Lake IJsselmeer but not in Lake Loosdrecht, would prevent ε to converge to an optimal value. It was not possible to derive ε directly from *in vivo* absorption measurements because no phytoplankton samples were present that contained only Chl *a* and no accessory pigments absorbing in the 600-700 nm region (all samples of cyanobacteria-rich water had a PC : Chl *a* ratio > 0.38). The optimal value of ε was defined as the value where the slope of the linear least-squares fit of modelled against observed PC concentration approximated 1.

4.3. Results

Table 4.2 lists the partial absorption coefficients at 620, 665 and 709 nm for pigments, tripton and CDOM, for the sampling series of the two lake sites. From the filterpad absorption measurements it becomes clear that CDOM generally contributes little (< 12%) to the total absorption at $\lambda \geq 620$ nm (with the exception of 22% in Lake IJsselmeer, April 2003). The slope of the exponential curve describing CDOM absorption between 620 and 709 nm (cf. Bricaud *et al.* 1981) varied between 0.006-0.011 nm^{-1}, and one higher average slope of 0.020 measured in June 2003 in Lake IJsselmeer. Relative absorption by tripton is generally high in these lakes (up to 50% of the water constituents' absorption at 620 nm, and 57% - 75% at 709 nm). However, tripton absorption can be considered flat in the region of interest, with an exponential slope not exceeding 0.006 nm^{-1}.

Optimization of γ, δ, and ε

Figure 4.1 shows the relation between uncorrected retrieval of absorption (Eqs. 3 and 4 with γ, δ = 1) and filterpad measurements of $a(\lambda)_{ph}$, that was used to find the optimal values for γ and δ. Eq. 4.3 with γ = 1 related to $a(665)_{ph}$ with a regression slope = 0.68 and offset = 0.019 (r^2 = 0.87). Eq. 4.4 with δ = 1 resulted in slope = 0.84 and offset = 0.080 (r^2 = 0.89). All results presented hereafter were obtained with the adopted values for γ (0.68) and δ (0.84). The offset values, resulting mainly from ignoring absorption by tripton and CDOM in the model (results not shown), were considered negligible in the current case and were not incorporated as an extra term to be subtracted from the computed absorption in Eqs. 3 – 5.

For the optimization of ε it can be seen from figure 4.2 that the optimal fit (see *Methods*) of predicted to observed PC concentrations (Eq. 4.5) was reached at ε = 0.24 (slope = 0.99, offset = 0.23, r^2 = 0.81). Fixing ε at 0.24, yielded a mean $a^*_{pc}(620)$ for these samples of 0.0095 $m^2(mg\ PC)^{-1}$.

Table 4.2. Absorption properties (m^{-1}), pigment concentrations (mg m^{-3}), and pigment-specific absorption values (m^2(mg pigment)$^{-1}$) at Lake Loosdrecht (averaged over 19 samplings during the period March-November 2003) and Lake IJsselmeer (number of sampling stations indicated for each cruise). The last section lists the averaged values for all Lake IJsselmeer cruises.

	620 nm				665 nm				709 nm			
	avg.	SD	min	max	avg.	SD	min	max	avg.	SD	min	max
Lake Loosdrecht (March-November 2003)												
CDOM	0.19	0.08	0.10	0.38	0.12	0.07	0.03	0.27	0.07	0.05	0.00	0.16
Tripton	0.80	0.35	0.37	1.64	0.65	0.30	0.29	1.41	0.53	0.26	0.22	1.20
Pigments	0.59	0.09	0.48	0.80	1.07	0.17	0.81	1.40	0.11	0.05	0.05	0.20
Chl *a*	70.9	14.1	48.1	97.5								
PC	50.8	16.8	21.7	79.8								
PC : Chl *a*	0.83	0.35	0.39	1.55								
$a^*_{pc}(620)$	0.0095	0.0033	0.0059	0.0174								
$a^*_{chl}(665)$	0.0153	0.0016	0.0130	0.0189								
Lake IJsselmeer, 10 April 2003 (3 locations)												
CDOM	0.14	0.04	0.11	0.19	0.10	0.04	0.06	0.14	0.07	0.03	0.03	0.10
Tripton	0.33	0.15	0.18	0.47	0.25	0.12	0.13	0.37	0.19	0.10	0.09	0.28
Pigments	0.18	0.02	0.17	0.20	0.49	0.02	0.47	0.51	0.07	0.03	0.05	0.10
Chl *a*	24.07	1.90	22.55	26.20								
PC	1.85	0.95	0.80	2.63								
PC : Chl *a*	0.07	0.04	0.03	0.10								
$a^*_{pc}(620)$	0.1084	0.0679	0.0680	0.1868								
$a^*_{chl}(665)$	0.0203	0.0022	0.0180	0.0225								
Lake IJsselmeer, 24 June 2003 (12 locations)												
CDOM	0.06	0.02	0.04	0.09	0.03	0.01	0.02	0.05	0.01	0.00	0.00	0.01
Tripton	0.56	0.14	0.40	0.67	0.43	0.11	0.31	0.51	0.32	0.08	0.23	0.39
Pigments	0.86	0.33	0.49	1.09	1.12	0.30	0.79	1.34	0.15	0.07	0.09	0.23
Chl *a*	64.77	15.22	34.85	85.32								
PC	14.38	8.02	2.06	26.42								
PC : Chl *a*	0.19	0.09	0.03	0.36								
$a^*_{pc}(620)$	0.0706	0.0317	0.0468	0.1066								
$a^*_{chl}(665)$	0.0181	0.0010	0.0170	0.0188								
Lake IJsselmeer, 5 August 2003 (12 locations)												
CDOM	0.13	0.02	0.10	0.16	0.11	0.02	0.07	0.13	0.06	0.02	0.02	0.08
Tripton	0.67	0.14	0.52	0.80	0.51	0.11	0.39	0.62	0.39	0.09	0.29	0.47
Pigments	0.64	0.18	0.43	0.76	0.93	0.27	0.62	1.15	0.17	0.11	0.06	0.27
Chl *a*	61.29	19.01	31.23	91.67								
PC	7.19	2.35	2.30	11.94								
PC : Chl *a*	0.12	0.05	0.06	0.23								
$a^*_{pc}(620)$	0.0931	0.0587	0.0461	0.1589								
$a^*_{chl}(665)$	0.0165	0.0030	0.0146	0.0199								
Lake IJsselmeer, 9 September 2003 (12 locations)												
CDOM	0.07	0.02	0.04	0.10	0.05	0.02	0.01	0.08	0.04	0.01	0.01	0.05
Tripton	0.74	0.08	0.65	0.79	0.57	0.05	0.51	0.61	0.44	0.03	0.40	0.47
Pigments	0.60	0.09	0.49	0.66	0.84	0.09	0.74	0.92	0.14	0.05	0.09	0.18
Chl *a*	60.50	10.13	43.80	75.03								
PC	36.92	17.73	14.30	64.80								
PC : Chl *a*	0.54	0.20	0.28	0.85								
$a^*_{pc}(620)$	0.0162	0.0093	0.0088	0.0266								
$a^*_{chl}(665)$	0.0138	0.0017	0.0119	0.0150								
Lake IJsselmeer total (39 samples)												
CDOM	0.10	0.04	0.04	0.19	0.08	0.04	0.01	0.14	0.05	0.02	0.00	0.10
Tripton	0.57	0.19	0.18	0.80	0.44	0.15	0.13	0.62	0.34	0.12	0.09	0.47
Pigments	0.57	0.31	0.17	1.09	0.85	0.30	0.47	1.34	0.13	0.07	0.05	0.27
Chl *a*	59.11	17.66	22.55	91.67								
PC	18.24	17.07	0.80	64.80								
PC : Chl *a*	0.27	0.23	0.03	0.85								
$a^*_{pc}(620)$	0.0721	0.0547	0.0088	0.1868								
$a^*_{chl}(665)$	0.0172	0.0030	0.0119	0.0225								

Retrieval of PC with sample-by-sample calculation of $a^*_{pc}(620)$

The PC concentration obtained through Eq. 4.6 was calculated for the subset of samples from Lake IJsselmeer (n = 15) and Lake Loosdrecht (n = 18) for which $R(0^-, \lambda)$, $a_{ph}(\lambda)$, and PC concentration data were collected. For every sample, $a^*_{pc}(620)$ was calculated from the measured absorption, ε = 0.24, and PC concentration. Estimated PC compared well to measured PC (Figure 4.3). The root mean square error (RMSE) of the PC estimate, compared to measured PC, was 6.5 mg PC m^{-3} or 19.7% ($r^2 = 0.94$). Because a substantial part of the data was used to optimize the model parameters, the slope of the regression for this dataset, unsurprisingly, approximated 1.

Variability of $a^*_{pc}(620)$ and $a^*_{chl}(665)$

For Lake Loosdrecht, it was investigated how strongly $a^*_{pc}(620)$ and $a^*_{chl}(665)$ fluctuated over the period March-November 2003 (Figure 4.4). The average value of $a^*_{pc}(620)$ was 0.0095 $m^2(\text{mg PC})^{-1}$. Variability was high, with standard deviation of 0.0033 $m^2(\text{mg PC})^{-1}$. The period of greatest stability was found in late summer. High values occurred from mid May until mid July, and lower values in early spring. A three-fold increase of $a^*_{pc}(620)$ occurred in May, and could be associated with strong fluctuations in the cellular pigment ratio (Figure 4.4, upper plot) for which the cause remained unknown. The $a^*_{chl}(665)$ values displayed a higher stability than $a^*_{pc}(620)$, with a yearly average of 0.0153 (± 0.0016) $m^2(\text{mg Chl } a)^{-1}$.

From the samples collected on Lake IJsselmeer, $a^*_{pc}(620)$ was also calculated. A non-linear inverse relationship between $a^*_{pc}(620)$ and the ratio of PC to Chl *a* was observed for both lakes (Figure 4.5). Lower relative abundance of cyanobacteria (lower PC : Chl *a*) resulted in elevated $a^*_{pc}(620)$ values, which only occurred during the first three cruises on Lake IJsselmeer. The $a^*_{chl}(665)$ values, averaged for all sampling stations, decreased steadily from April to September (Table 4.2).

Applying a fixed $a^*_{pc}(620)$ value

To illustrate the effect of a fixed $a^*_{pc}(620)$ value for remote sensing, the average $a^*_{pc}(620)$ of Lake Loosdrecht (0.0095 $m^2(\text{mg PC})^{-1}$) was used to calculate the PC concentration from $R(0^-, \lambda)$ spectra from Lake IJsselmeer (Figure 4.6). The 15 $R(0^-, \lambda)$ spectra that were used to plot figure 4.3 were used in addition to 34 $R(0^-, \lambda)$ spectra for which no absorption data was collected. For every sample in this set, PC concentration data was available. Overestimation of PC was strong during the first cruises, while the best match with the measured PC concentrations was found during the September 2003 cruise. A linear least-squares fit through the latter subset, resulted in a vertical intercept of 29 mg PC m^{-3} ($r^2 = 0.77$).

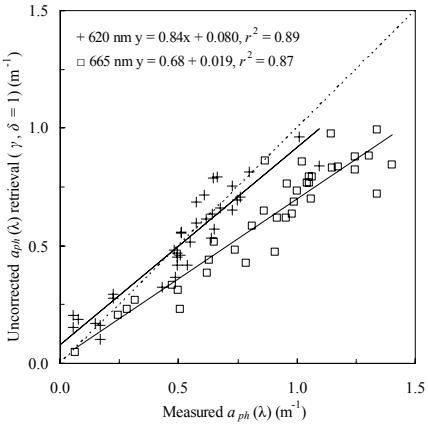

Figure 4.1. Uncorrected $a_{ph}(\lambda)$ retrieval at 620 and 665 nm versus measured $a_{ph}(\lambda)$. The plotted values conform to Eqs. 4.3 and 4.4, with δ, $\gamma = 1$. Dashed line indicates unity.

4.4. Discussion

Optimization of model parameters

It was demonstrated that the retrieval of PC is possible for water bodies that are dominated by cyanobacteria, using a simple optical model. The introduction of model parameters γ and δ was adequate to fit the retrieved absorption to pigment absorption for a dataset from two different lakes at different times. The value of ε was also fitted from these data, to define the spectral behaviour of Chl *a* absorption in cyanobacteria-dominated waters. In cases where the phytoplankton community consisted primarily of cyanobacteria, this approach was sufficient to derive the absorption by pigments at 620 and 665 nm that was needed to obtain the PC concentration. When compared to literature values on $a^*_{chl}(\lambda)$, $\varepsilon = 0.24$ is relatively low, and values around 0.4 – 0.5 fit expectations better (cf. Hoeppfner and Sathyendranath 1993). However, to our knowledge there exists no literature that deals with *in vivo* $a^*_{chl}(\lambda)$ values connected to cyanobacterial species and pigments, while reports on the $a^*_{chl}(\lambda)$ values beyond the main absorption peaks, i.e. at 675 and 623 nm, are rare. Further, *in vivo* specific absorption by phycobilisomal pigments can not be measured independent of Chl *a* with currently available methods. At present, it must therefore be concluded that the empirical value $\varepsilon = 0.24$ explains the absorption by PC and Chl *a* at 620 nm reasonably well for cyanobacteria. For other phytoplankton groups differing in the ratio $a^*_{chl}(620)$: $a^*_{chl}(665)$, for instance because of the package effect, a different value for ε may be needed.

The data for parameter optimization was obtained throughout different seasons for two lakes that differ markedly in their plankton species and abiotic environment.

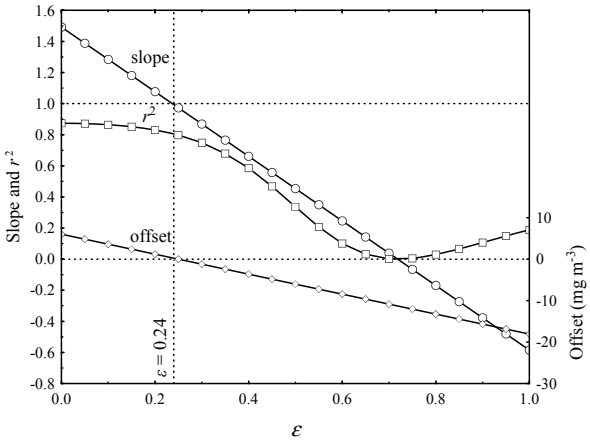

Figure 4.2. Results of the linear regression (slope, offset and r^2) between modelled and measured PC concentration as a function of ε, for Lake Loosdrecht in the period March-November 2003. The optimal value (regression slope = 1) of $\varepsilon = 0.24$ is highlighted by the vertical line.

Nonetheless, one set of parameters could be applied for the whole dataset where cyanobacteria-dominated waters were concerned. It is therefore likely that the parameters γ, δ, and ε are equally fitting for other turbid, eutrophic lakes and reservoirs, provided that they exhibit a eutrophic state with predominance of cyanobacteria. However, the contribution of CDOM to total absorption can be considered low (< 10%) for both studied lakes, and band ratio algorithms are generally insensitive to low background absorption. The relative contribution of tripton to total absorption was consistent throughout most samples, and the offset in retrieved absorption relative to measured absorption was in this case not significant (Figure 4.1). Application of the algorithm to lakes that differ in these characteristics may require local optimization of the model parameters.

Errors

Variability of $a^*_{pc}(620)$

A cyanobacterial species' response to changing environmental conditions can result in variable values of $a^*_{pc}(620)$, as visible from figure 4.4. It has been shown before that $a^*_{chl}(\lambda)$ varies with cell morphology and photoadaptive responses (Sathyendranath *et al.* 1987, Bricaud *et al.* 1995, Staehr *et al.* 2002). PC is an accessory pigment that can efficiently increase the light harvesting capacity in the 'green gap' of Chl *a* (Britton 1983, Raven 1984). The cellular pigment concentration of PC can be expected to fluctuate more than Chl *a* does, for changing nutrient and light environments (Tandeau de Marsac 1977, Bryant 1981). It has been proposed that phycobiliproteins might be broken down during nitrogen shortage, in order to recycle amino-acids (Bogorad 1975,

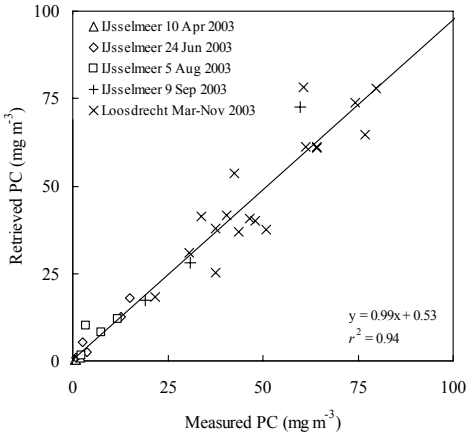

Figure 4.3. PC concentrations predicted by the algorithm (Eqs. 4.5, 4.6) versus measured PC concentrations, with $a^*_{pc}(620)$ calculated independently from absorption measurements, ε, and measured PC, for every sample.

Grossman *et al.* 1993). Such mechanisms imply high variability in cellular PC content, with corresponding effects on $a^*_{pc}(620)$.

Estimation of $a_{pc}(620)$

Methodological errors in the retrieval of $a_{pc}(620)$ occur when $a_{ph}(620)$, after correction for Chl *a* absorption, is not fully attributable to absorption by PC. This can be the case when other substances than the mentioned pigments contribute to the retrieved absorption signal. Some pigments exhibit absorption in or closely around the 620 nm waveband. For the application of the present model in waters with a mixed phytoplankton composition rather than a dominating cyanobacterial population, the effect of specific pigments on the prediction of PC deserves further exploration. A second possibility for an erroneously high estimate of PC absorption is expected when the correction for Chl *a* absorption (following from $a_{chl}(665) \times \varepsilon$) insufficiently cancels out Chl *a* absorption at 620 nm. This would be the case if ε was chosen too low to fit the Chl *a*-specific absorption properties of a sample. It was shown that $a^*_{chl}(665)$ decreased gradually with time in Lake IJsselmeer throughout the period April – September (Table 2), a trend that was accompanied by change from green algal to cyanobacterial dominance. Figure 4.5 also shows a clear inverse relationship between $a^*_{pc}(620)$ and the PC : Chl *a* ratio which is indicative of cyanobacterial presence. Since ε was retrieved from data from a cyanobacteria-dominated lake, the value might be too low to correct for absorption by Chl *a* when plankton species with a higher $a^*_{chl}(620)$: $a^*_{chl}(665)$ ratio are abundant. Such species would be characterized by a strong package effect. Both errors result in incorrect $a_{pc}(620)$ values, leading to elevated $a^*_{pc}(620)$, and thus overestimated PC concentrations. It is likely that this type of error caused

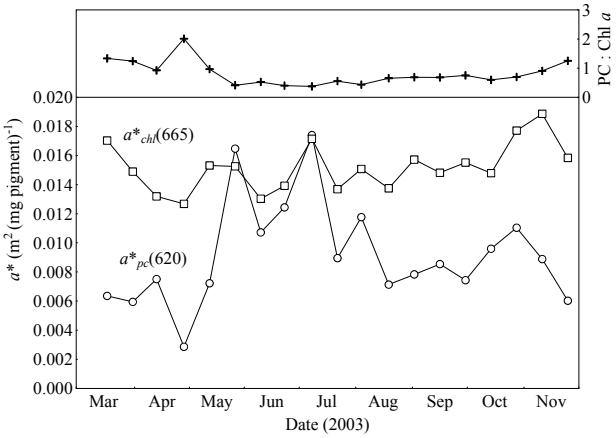

Figure 4.4. Values of $a^*_{pc}(620)$, $a^*_{chl}(665)$ and PC : Chl *a* ratio measured every two weeks for Lake Loosdrecht during the period March – November 2003.

overestimation of PC in the case of Lake IJsselmeer samples with a low PC : Chl *a* ratio. As a rule of thumb, with a PC : Chl *a* ratio < 0.4, error in the PC prediction will rise steeply (Figure 4.5).

PC extraction and quantification

The assessment of PC concentration is a cumbersome procedure. Various methods have been proposed to release the pigment from cells, using freeze-thaw cycles (Sarada *et al.* 1999), osmotic shock, grinding, enzymatic disruption (Stewart and Farmer 1984), sonication (Bennett and Bogorad 1973), or disruption by French press (Schalles and Yacobi 2000). Unfortunately, comparative studies on the effects of such methods on the stability of the phycobiliprotein structure and its absorption properties are lacking. The different methods also present problems of selectivity on size or on robustness of the cell material. If the extraction efficiency is lower than assumed, overestimation of $a^*_{pc}(620)$ and thus underestimation of PC results. The low average of PC values in this study is likely the result of low extraction efficiency. For progress of remote sensing of PC beyond the limits of one laboratory's methodology, intercomparison of the efficiency of extraction methods will be a priority. Methods that are less selective on the nature of sample material should be preferred. In this light it is noted that recently, Viskari and Colyer (2002, 2003) claimed a 90% extraction efficiency using nitrogen cell disruption of cultured material. Using this method, nitrogen gas is dissolved into sample solutions. Upon sudden return to normal air pressure, cells into which nitrogen dissolved burst and water-soluble pigments are released.

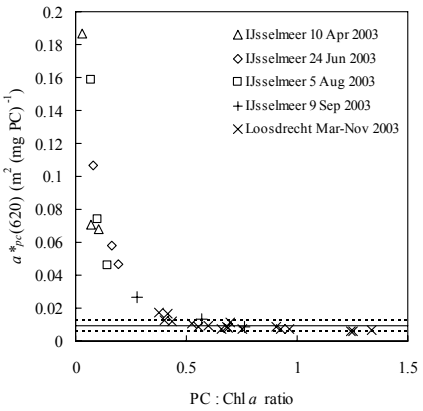

Figure 4.5. Coefficient $a^*_{pc}(620)$ versus PC : Chl *a* ratio. Horizontal lines indicate the average (solid line) and standard deviation (dashed lines) of $a^*_{pc}(620)$ for L.Loosdrecht.

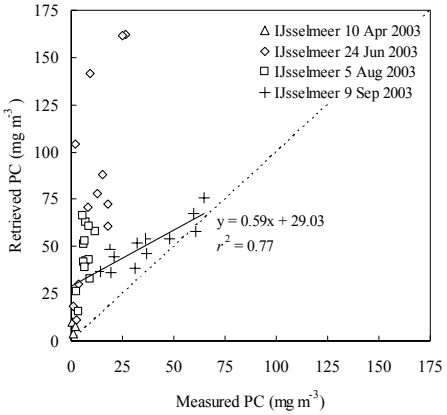

Figure 4.6. PC estimate (Eqs. 4.5, 4.6) vs. measured PC for L. IJsselmeer, using $a^*_{pc}(620)$ = 0.0095 m^2 (mg PC)$^{-1}$ and ε = 0.24. All samples for which reflectance and pigments were measured, were plotted. The linear fit was plotted for samples of 9 Sep 2003.

Applicability of the PC retrieval algorithm

Remotely sensed Chl *a* products have greatly benefited estimations of global oceanic productivity, and provide a useful tool to fisheries. Remote sensing of Chl *a* greatly enhances the efficiency of water quality monitoring. One might similarly expect validated PC products to contribute to monitoring of cyanobacterial blooms, and to yield insights into spatially heterogeneous population dynamics and plankton group-specific production estimates.

The semi-empirical band ratio model (Eq. 4.5) can be used to detect absorption in the 620 nm band for eutrophic, turbid lakes. To relate this absorption to cyanobacterial biomass, information on the composition of phytoplankton in the water body is still needed. Without adaptations of the algorithm, it can be used to monitor the PC status of water bodies that are known to be dominated by cyanobacteria at the time of observation. For lakes where blooms are known to occur, monitoring the PC concentration or PC to Chl *a* ratio can be useful to identify critical cyanobacterial population densities (in terms of PC) for bloom formation, and advanced predictions on bloom formation may follow with the aid of hydrological models. Other applications can be found in the study of bloom termination events as caused by intensive grazing or viral attacks when the cyanobacterial population reaches high densities. Such events would be characterized by sudden drops in the PC to Chl *a* ratio of the water body which could be identified using the current model.

The present algorithm accommodates the band specifications of the MERIS instrument, but essentially it could be tailored to any sensor that can record reflectance in bands that include wavelengths of PC absorption (around 615 nm), Chl *a* absorption (around 675 nm), and at a far red (>705 nm) and near-infrared location (between 760-800, cf. Gons 1999).

The current model falls short in situations where the phytoplankton community does not primarily consist of cyanobacteria. However, some possibilities for these erroneous results were identified (see *Errors*) and could well lead to further improvement of the algorithm, in turn leading to a wider applicability.

It is concluded that the present algorithm can aid in the monitoring of cyanobacterial populations in turbid, eutrophic lakes and reservoirs. Optimization of the algorithm parameters based on data from two different lakes was possible. A sensitivity analysis of the algorithm and comparison of the performance of this and other proposed approaches to phycocyanin detection (Dekker 1993, Schalles and Yacobi 2000, Vincent *et al.* 2004) is now desirable. The influence of other pigments than PC and Chl *a* on the absorption at 620 nm, and the effect of phytoplankton composition on the model parameters, deserve further study. For known environmental conditions, it should be possible to estimate $a^*_{pc}(620)$ allowing the monitoring of PC in cyanobacteria-rich water bodies.

4.5. Acknowledgments

The authors thank the captain and crew of r/v *Luctor*, and Hans Hoogveld for technical assistance. Comments by Dr. S. Sathyendranath and an anonymous reviewer helped to improve this manuscript.

5. INFLUENCE OF PHYTOPLANKTON PIGMENT COMPOSITION ON REMOTE SENSING OF CYANOBACTERIAL BIOMASS

Stefan G. H. Simis, Antonio Ruiz-Verdú[1], Jose Antonio Domínguez-Gómez[1], Ramón Peña-Martinez[1], Steef W.M. Peters[2] & Herman J. Gons

[1]Centre for Hydrographic Studies (CEDEX), Madrid, Spain.
[2]Institute for Environmental Studies (IVM), Vrije Universiteit, Amsterdam, The Netherlands.

Remote Sensing of Environment, in press

Lake IJsselmeer, the Netherlands, while sampling from R/V *Luctor*.

Abstract

An extensive field campaign was carried out for the validation of a previously published reflectance band ratio algorithm for quantification of the cyanobacterial pigment phycocyanin (PC). The algorithm uses band settings of the Medium Resolution Imaging Spectrometer (MERIS) onboard ENVISAT, and should accurately retrieve the PC concentration in turbid, cyanobacteria-dominated waters. As algae and cyanobacteria often co-occur, the algorithm response to varying phytoplankton composition was explored, using empirical data. Remote-sensing reflectance and reference pigment measurements were obtained in the period 2001-2005 in Spain and the Netherlands. For intercalibration of methods, field data was collected in Spain in May 2005. Methods for the extraction of PC from concentrated water samples, as well as measurement of *in situ* PC fluorescence were compared. Reflectance and PC measurements with different instrumentation used in Spain and the Netherlands during the sampling campaigns gave nearly identical results. Residual analysis of PC prediction by the algorithm suggested that overestimation of PC occurred mainly at low PC : Chlorophyll *a* ratios and in the presence of chlorophyllous pigments that are not accounted for by the algorithm. The error was mainly associated with the presence of green algae for the current dataset, and a correction applied for absorption by Chl *b* markedly improved the prediction. Without compensation for absorption by pigments other than Chl *a*, the quality of the PC prediction still increased rapidly with predicted PC concentrations > 50 mg m^{-3}. This limit may be lowered when a high intracellular PC : Chl *a* ratio or cyanobacterial dominance is expected. Below this limit, predicted PC concentrations should be considered as the highest estimate.

5.1. Introduction

The management of inland water quality is a growing concern wherever anthropogenic eutrophication affects water bodies. Potentially toxic cyanobacterial blooms pose a health threat, and are detrimental to the economic and environmental value of many lakes and reservoirs. Regular monitoring of water bodies is necessary to provide timely warnings in case of cyanobacterial bloom. Remotely sensed water quality products have the potential to provide high spatial and temporal coverage, while conventional sampling methods lack both. The Medium Resolution Imaging Spectrometer (MERIS) onboard the ENVISAT mission is the first sensor to offer the combination of several narrow wavebands to target both Chl *a* and accessory pigment absorption in the red spectral region, at a spatial resolution (260 m across track) sufficient for medium-sized water bodies, and with acceptable signal-to-noise ratio. Reflectance band ratio algorithms utilizing wavebands in the red and near-infrared (NIR) spectral region can be used to retrieve photosynthetic pigment concentrations in

turbid inland water bodies, where often the most severe water quality problems are experienced.

For optical remote sensing of the concentration of the main photosynthetic pigment chlorophyll *a* [Chl *a*], the ratio of a near infra-red band (around 700 nm) over a band near the red absorption maximum of Chl *a* at 675 nm (Mittenzwey *et al.* 1992) has been validated for a wide range of turbid water bodies for > 10 mg Chl *a* m^{-3} (Gons 1999; Gons *et al.* 2000). The band ratio targeting Chl *a* absorption thus serves as an indicator for phytoplankton biomass (algae and cyanobacteria) in productive water bodies, and can be used with MERIS imagery (Gons *et al.* 2005). A semi-analytical, nested band-ratio algorithm for the retrieval of the pigment phycocyanin [PC] was recently proposed to specifically target cyanobacterial biomass (Simis *et al.* 2005*a*). PC is a water-soluble pigment common to freshwater cyanobacteria, and detectable from reflectance spectra (Jupp *et al.* 1994, Dekker 1993). The absorption signal of the most common modification of PC in eutrophic lakes is strongest at 615 nm, and overlaps with the 10-nm wide, 620-nm centred waveband of MERIS. The PC algorithm by Simis *et al.* (2005*a*) attributed the absorption signal in this band to PC and to the absorption shoulder of Chl *a* around 623. Absorption by dissolved substances, suspended sediments and detrital matter did not seem to significantly affect the retrieval of the pigment absorption around 620 nm and 665 nm in the turbid water bodies studied thus far. However, other phytoplankton pigments absorbing light in the same spectral region could interfere with PC prediction.

All chlorophyllous pigments and their degradation products absorb light in the red spectral region. For most pigments, absorption around 620 nm only amounts to a fraction of their absorption at longer wavelengths. However, the diatom pigments chlorophyll c_1 and c_2 [Chl *c*] have absorption maxima on both sides of the 620-nm band (Jeffrey *et al.* 1997, Ficek *et al.* 2004). Chl *c* is therefore likely to lead to overestimations of the PC concentration as it is not corrected for by the algorithm. The pigment chlorophyll *b* [Chl *b*] is another major accessory photosynthetic pigment in inland water bodies, present mainly in green algae and prochlorophytes. Chl *b* has a broad absorption maximum around 650 nm and a minor feature around 600 nm (Sathyendranath *et al.* 1987, Jeffrey *et al.* 1997, Ficek *et al.* 2004) and should lead to overestimates of the absorption in both the 665-nm and 620-nm wavebands. Degraded chlorophyll forms may also contribute to absorption in these bands. During development of the PC algorithm, overestimations of the PC concentration were indeed observed at mixed-phytoplankton sites.

Table 5.1*a*. Summary of sampled lakes and reservoirs. Depth refers to echo soundings at sampling stations. Symbols and abbreviations: n.a – no data; m.a.s.l. – metres above sea level; lat. – latitude; lon.- longitude; R. – reservoir; L. – Lake; Lgn. – Lagoon.

Location name	Position lat. *d.dd*	lon. *d.dd*	Depth m	Surface area km^2	Elevation m a.s.l.	Chl *a* $mg\ m^{-3}$	Secchi-depth m (avg.)
The Netherlands							
L. IJsselmeer	52.73	5.39	4.4	1190	0	43.9	0.8
L. Ketelmeer[a]	52.6	5.72	3.0	35	0	12.5	1.0
Spain							
Aguilar R.	42.81	-4.31	14.1	18	942	6.6	1.4
Alarcón R.	39.6	-2.16	17.4	69	806	3.5	2.4
L. L'Albufera	39.34	-0.35	0.9	24	1	304.9	0.2
Alcántara R.	39.73	-6.61	47.0	103	218	4.4	3.5
Alcorlo R.	41.02	-3.03	27.0	7	920	1.6	2.1
Almendra R.	41.24	-6.28	71.3	79	730	13.2	2.7
Los Arroyos R.	40.59	-4.05	n.a	<1	845	24.8	0.0
El Atazar R.	40.91	-3.49	49.5	10	870	4.5	7.2
Beniarrés R.	38.81	-0.36	14.0	2	318	57.0	1.0
Bornos R.	36.82	-5.72	13.1	22	104	6.2	0.9
Brovales R.	38.35	-6.7	n.a	1	303	53.8	0.6
Buendía R.	40.4	-2.77	40.0	80	712	0.5	9.6
Burguillo R.	40.43	-4.57	30.5	9	729	18.9	2.1
El Campillo Lgn.	40.32	-3.50	n.a	<1	538	37.2	0.7
Canelles R.	42.01	0.64	104.0	16	506	1.0	6.0
Castrejón R.	39.83	-4.3	n.a	5	425	144.8	0.5
Castro R.	39.81	-3.75	n.a	<1	559	48.2	0.3
Cernadilla R.	42.02	-6.47	38.0	13	889	3.1	3.3
Cijara R.	39.34	-4.93	28.5	74	428	1.4	5.2
Contreras R.	39.61	-1.53	27.0	27	669	1.6	2.6
Cortes R.	39.25	-0.93	15.0	4	326	1.5	4.0
Ebro R.	42.98	-4.04	4.9	62	838	52.8	0.9
Entrepeñas R.	40.51	-2.73	25.0	34	718	2.1	4.5
Finisterre R.	39.65	-3.65	n.a	5	686	14.7	0.7
Giribaile R.	38.09	-3.49	26.0	23	346	2.9	2.3
Guadalcacín R.	36.66	-5.73	29.5	11	102	1.0	3.6
Guadalén R.	38.17	-3.47	22.0	11	350	2.5	1.0
Guadalteba R.	36.96	-4.83	21.0	8	362	106.5	1.3
Guajaraz R.	39.8	-4.09	n.a	2	605	12.0	0.7
Iznájar R.	37.27	-4.34	44.3	25	421	32.2	2.5
Jándula R.	38.24	-3.95	56.0	10	360	2.9	5.5
Molino de la Hoz R.	40.53	-3.94	n.a	<1	632	53.6	0.0
Navalcán R.	40.04	-5.12	n.a	9	370	53.0	0.6
Negratín R.	37.57	-2.9	28.5	25	638	1.1	4.4
Pedrezuela R.	40.76	-3.62	n.a	4	828	21.6	0.0
Picadas R.	40.33	-4.25	n.a	<1	1040	9.0	2.8
Pinilla R.	40.94	-3.73	13.1	4	1089	24.3	1.6
El Porcal-1 Lgn.	40.30	-3.53	n.a	1	535	38.4	0.6
El Porcal-2 Lgn.	40.30	-3.52	n.a	<1	534	39.7	0.6
El Porcal-3 Lgn.	40.31	-3.52	n.a	<1	531	n.a	0.5
Rialb R.	41.96	1.22	14.2	18	430	8.7	2.0
Riaño R.	42.96	-5.05	31.5	21	1100	10.6	3.4
Ricobayo R.	41.61	-5.94	32.9	54	684	5.9	3.2
Rosarito R.	40.1	-5.3	7.9	13	307	61.9	0.7
San Juan R.	40.38	-4.33	43.5	6	580	13.1	5.0
L. Sanabria	42.12	-6.72	47.0	4	998	1.3	5.4
Santa Teresa R.	40.61	-5.61	34.0	24	886	3.5	3.0
Santillana R.	40.72	-3.84	11.0	11	894	41.3	1.0
La Serena R.	38.9	-5.19	31.8	40	352	2.9	4.3
Terradets R.	42.07	0.89	5.4	3	372	0.9	0.6
Tremp R.	42.21	0.95	22.3	8	501	2.4	4.6
Ullívarri R.	42.93	-2.59	13.7	15	547	3.3	4.0
Valdecañas R.	39.8	-5.5	29.6	62	315	15.8	2.7
Valmayor R.	40.55	-4.05	24.5	7	831	28.8	1.7
Valparaíso R.	41.98	-6.29	25.0	11	833	5.0	3.0
Valuengo R.	38.31	-6.66	n.a	2	297	37.3	0.6
Vega de Jabalón R.	38.76	-3.79	n.a	3	639	41.0	0.7

[a]Includes samples of lower River IJssel.

Table 5.1*b*. Number of visits and samples taken at the lakes and reservoirs. Symbols and abbreviations: FT – freeze/thaw cycles method; MG – mechanical grinding method; FL – *in situ* fluorescence; R. – reservoir; L. – Lake; Lgn. – Lagoon.

Location name	Visits[b]	Samples	Radiometry		Pigment samples			
		Total	PR-650	ASD-FR	HPLC	PC		
						FT	MG	FL
The Netherlands	**6**	**290**	**289**	**0**	**203**	**201**	**75**	**0**
L. IJsselmeer	6	256	256	0	187	186	68	0
L. Ketelmeer[a]	6	34	33	0	16	15	7	0
Spain	**89**	**193**	**23**	**170**	**169**	**16**	**122**	**168**
Aguilar R.	2	4	0	4	4	0	4	4
Alarcón R.	2	4	0	4	4	0	4	4
L. L'Albufera	4	20	7	19	16	0	14	15
Alcántara R.	1	2	0	2	2	0	2	2
Alcorlo R.	1	1	0	1	1	0	1	1
Almendra R.	2	3	0	3	3	0	3	3
Los Arroyos R.	1	1	1	0	1	1	1	0
El Atazar R.	3	4	0	4	4	0	4	3
Beniarrés R.	1	1	0	1	1	0	1	1
Bornos R.	1	2	0	2	2	0	2	2
Brovales R.	1	1	1	0	1	0	1	1
Buendía R.	1	1	0	1	1	0	1	1
Burguillo R.	2	4	0	4	4	0	3	4
El Campillo Lgn.	1	2	0	0	2	2	2	0
Canelles R.	1	4	0	4	4	0	0	4
Castrejón R.	1	1	0	0	1	1	1	0
Castro R.	1	1	0	0	1	1	1	0
Cernadilla R.	1	1	0	1	1	0	1	1
Cijara R.	1	2	0	2	2	0	2	2
Contreras R.	1	2	0	2	2	0	2	2
Cortes R.	1	1	0	1	1	0	1	1
Ebro R.	2	3	0	3	2	0	3	3
Entrepeñas R.	1	1	0	1	1	0	1	1
Finisterre R.	1	1	0	0	1	1	1	0
Giribaile R.	1	1	0	1	1	0	1	1
Guadalcacín R.	1	2	0	2	2	0	2	2
Guadalén R.	1	1	0	1	1	0	1	1
Guadalteba R.	1	2	0	2	2	0	2	2
Guajaraz R.	1	1	1	0	1	1	1	0
Iznájar R.	2	4	0	4	3	0	4	4
Jándula R.	1	2	0	2	2	0	2	2
Molino de la Hoz R.	1	1	1	0	1	1	1	0
Navalcán R.	1	3	3	3	3	0	3	3
Negratín R.	1	2	0	2	2	0	2	2
Pedrezuela R.	1	1	1	0	1	1	1	0
Picadas R.	1	1	1	0	1	1	1	0
Pinilla R.	3	4	0	4	4	0	4	4
El Porcal-1 Lgn.	1	1	0	0	1	1	1	0
El Porcal-2 Lgn.	1	1	0	0	1	1	1	0
El Porcal-3 Lgn.	1	1	0	0	0	1	0	0
Rialb R.	1	4	0	4	4	0	0	4
Riaño R.	1	2	0	2	2	0	2	2
Ricobayo R.	2	4	0	4	4	0	4	4
Rosarito R.	12	49	2	48	35	0	2	44
San Juan R.	1	2	0	2	2	0	2	2
L. Sanabria	1	2	0	2	2	0	2	2
Santa Teresa R.	1	2	0	2	2	0	2	2
Santillana R.	2	4	0	3	4	1	4	3
La Serena R.	2	4	0	4	4	0	4	4
Terradets R.	1	2	0	2	1	0	0	1
Tremp R.	1	4	0	3	4	0	0	4
Ullívarri R.	1	2	0	2	2	0	2	2
Valdecañas R.	3	5	0	4	4	0	4	5
Valmayor R.	3	6	2	4	6	2	6	4
Valparaíso R.	2	3	0	3	2	0	2	3
Valuengo R.	1	2	2	0	2	0	2	2
Vega de Jabalón R.	1	1	1	1	1	0	1	1

[a]Includes samples of lower River IJssel. [b]Visits spanning 2 days counted as 1.

This paper reports on the influence of the major phytoplankton groups on the retrieval of PC, using improved pigment quantification methods and a broad empirical dataset. Up to date, the retrieval of PC was not validated even for the simple case of cyanobacteria-dominated waters. Radiometric and pigment data were gathered from a wide range of water bodies in Spain and the Netherlands, with varying share of PC containing cyanobacteria in the phytoplankton. Errors in PC retrieval were regressed against the presence of marker pigments for different algal groups. It was aimed to distinguish between situations where the original PC algorithm for MERIS bands may be applied and situations where additional information is needed because of interference by algal pigments. The results of this exploration may be used in the spectral design of future sensors and to define the boundary conditions for operational monitoring of cyanobacteria using remote sensing.

5.2. Method

Study sites

An overview of sampling sites and instrumentation used is given in Table 5.1. The Spanish water bodies represented a range of oligotrophic to hypertrophic lakes and reservoirs located in various parts of the country, visited in the period 2001 – 2005. Monospecific blooms of algae or cyanobacteria are common in several water bodies from spring onward, but the dataset also includes several deep and clear lakes. In the Netherlands, Lake IJsselmeer was visited 6 times for 2-day cruises in 2004 and 2005. This turbid, eutrophic lake exhibits a seasonal phytoplankton distribution where cyanobacteria are more abundant towards the end of summer. Large horizontal differences in phytoplankton pigment composition are common.

Radiometric measurements

Remote-sensing reflectance $R_{RS}(\lambda)$ was defined as for the MERIS level-2 standard product 'normalized water-leaving reflectance' (Montagner 2001):

$$R_{RS}(\lambda) = [\rho_w]_N(0^+,\lambda) = \pi\, L_w(0^+,\lambda) / E_d(0^+,\lambda) \quad (5.1)$$

where $L_w(0^+,\lambda)$ is water-leaving radiance corrected for reflected sky light, $E_d(0^+,\lambda)$ is downward irradiance, depth 0^+ points to the situation just above the water surface and wavelength dependence is denoted λ. These quantities can all be obtained from shipboard measurements. In that case, $L_w(0^+,\lambda)$ is calculated from

$$L_w(0^+,\theta,\varphi,\lambda) = L_{wu}(0^+,\theta,\varphi,\lambda) - [r(\theta)\, L_{sky}(0^+,\theta,\varphi,\lambda)] \quad (5.2)$$

where $L_{wu}(0^+,\theta,\varphi,\lambda)$ is water-leaving radiance uncorrected for reflectance of downwelling light at the water surface; this correction is given by the bracketed term. Sky radiance is denoted $L_{sky}(0^+,\theta,\varphi,\lambda)$. For small instrument acceptance angle there is

negligible dependence of L_{wu} on viewing angle θ and azimuth angle φ as long as θ < 42° from zenith, and for φ ranges 90° - 135° (Tyler 1960, Morel and Gentili 1993). The measurement geometry was kept within these limits (details below), and sun zenith angles > 60° were avoided in all cases. The skylight correction factor $r(\theta)$ can be approached by a constant value for calm water surfaces, or obtained as a function of wind speed and cloud cover (Mobley 1999). The irradiance $E_d(0^+,\lambda)$ can be acquired with a cosine collector, or by measuring the radiance L_d from an intercalibrated spectrally neutral diffuse plate.

The radiometric measurements with the Analytical Spectral Devices Field Radiometer (ASD-FR, Boulder, CO, USA) were carried out with θ = 40° and φ = 135°, instrument acceptance angle 8°, and L_d from a 25% reflective (grey) Spectralon panel. The skylight reflectance $r(\theta = 40°)$ was obtained following Mobley (1999). Most measurements in this data subset were carried out under clear skies and at low wind speeds. The Photo Research model 650 colorimeter (PR-650) features a 1° acceptance angle. The PR-650 measurements were made according to Gons (1999), with θ = 42°, φ = 90°, and a 100% reflective (white) Spectralon panel. If the radiance from the Spectralon plate saturated the instrument, a 95% attenuation filter and matching conversion of L_d to E_d were applied. The PR-650 instrument was set to produce the average of 10 exposures for each radiance quantity. For direct skylight reflectance at θ = 42° the calibrated value of $r = 0.029$ was used and a correction for diffuse skylight reflectance was applied for Lake IJsselmeer samples, as described previously (Gons 1999). For both ASD-FR and PR-650 measurements, a minimum of 3 R_{RS} spectra were produced from the radiances L_{wu}, L_{sky}, and L_d, measured in repeated sequence. After removal of invalid R_{RS} spectra due to the capture of sun glint or variable cloud cover during the measurement cycle, remaining spectra were averaged.

Pigment analysis

Samples for pigment analysis were always taken from the surface water layer. For phycobilin pigments there is no standard method of extraction. Two different methods were used for cell disruption and extraction of PC and phycoerythrin (PE), and concurrent measurements are available in the current dataset for their intercalibration. In addition, for samples taken and analysed in Spain, PC fluorescence was measured *in situ*, providing a third PC reference for the radiometric approach. The freeze/thaw cycles method (PC_{FT}) was slightly adapted from earlier work (Simis *et al.* 2005*a* and references therein): the phosphate buffer pH was lowered to 6.7, increasing extraction yield from cultured *Limnothrix* sp. by approximately 28% (unpublished results). Because of increased extraction yield, the specific absorption coefficient of PC in the 620-nm band [$a^*_{PC}(620)$] that was previously published (Simis *et al.* 2005*a*) was lowered to 0.007 $m^2\ mg^{-1}$. The second method for phycobilin pigment extraction is based on mechanical grinding (PC_{MG}) of samples concentrated on glass fibre filters

(Whatman GF/F) and resuspended in glycerol (Quesada and Vincent 1993, Wyman and Fay 1986). After collection, filters were frozen in liquid nitrogen and later stored at -80°C. The filters were thawed, cut into small pieces, and one volume of glycerol was added to the filter remains placed in a centrifuge tube. A close-fitting Teflon pestle connected to an electric drill was used to homogenize the sample in the tube at 500 – 1000 rpm while avoiding the sample to heat up. The samples were kept in the dark for approximately 2 h after which 9 volumes of distilled water were added to induce osmotic shock. The samples were briefly subjected to another round of homogenization in the pestle-tube combination. The supernatant of centrifuged samples were spectrophotometrically analysed as with the PC_{FT} method, and the phycobilin pigment concentrations were computed according to Bennett and Bogorad (1973). The PC_{MG} extraction was repeated on the pelleted material and the results summed to give the final concentration, after correction for the initially filtered sample volume. The PC quantification *in situ* based on the pigment's fluorescence (PC_{FL}) was performed using a Mini^{tracka} II PA Fluorometer Model HB202 (Chelsea Instruments Ltd., Surrey, UK) with excitation centred at 590 nm (35 nm band width) and recorded emission around 645 nm (35 nm band width). The instrument was factory-calibrated to a PC standard in the 0.03 – 100 mg m^{-3} range.

HPLC pigments

Pigments that could be extracted with organic solvents were analysed using gradient HPLC based on the protocols in Jeffrey *et al.* (1997). Samples collected and analysed in the Netherlands were concentrated on Schleicher and Schuell GF6 filters, frozen in liquid nitrogen and stored in a -80°C freezer. The solvent was 90% acetone; filters and cells were disrupted in a bead beater. After centrifugation, the pigment content of the supernatant was separated using a reversed-phase column (Waters Nova-pak C18 column; Waters Millennium HPLC system) to which gradients mixing pumps delivered three mobile-phase solvents: methanol/ammonium acetate, 90% acetonitril and 100% ethyl acetate (Rijstenbil 2003 and refs therein). Pigments were identified against commercially available standards (DHI Water and Environment, Hørsholm, Denmark) using a fluorescence detector (Waters 474 Scanning Fluorescence Detector) and a photodiode array absorption detector (Waters 996 Photodiode Array Detector). The Spanish samples were concentrated on Whatman GF/F filters and kept in liquid nitrogen until analysis; cell disruption and pigment extraction was achieved by sonication followed by 24-h extraction at 4°C; the column was equipped with a Waters Spherisorb ODS-2 and HP Agilent 1050 diode array system. In addition, the Spanish samples were analyzed along with an external standard of canthaxanthin. The concentrations of the following pigments were acquired for all samples in both countries: Chl *a*, Chl *b*, phaeophytin, peridinin, neoxanthin, violaxanthin, alloxanthin, lutein, zeaxanthin, and fucoxanthin.

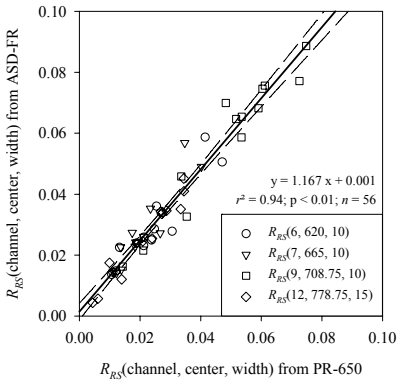

Figure 5.1. Comparison of remote-sensing reflectance [R_{RS}(MERIS channel, band center, band with)] derived from the instrumentations used in Spain (ASD-FR) and The Netherlands (PR-650). Results for the bands used in Eq. 5.4 and for the retrieval of the backscattering coefficient are plotted. The measurements were carried out on a number of Spanish water bodies, in May 2005. Regression results are shown by the solid line and dashed 95% confidence limits.

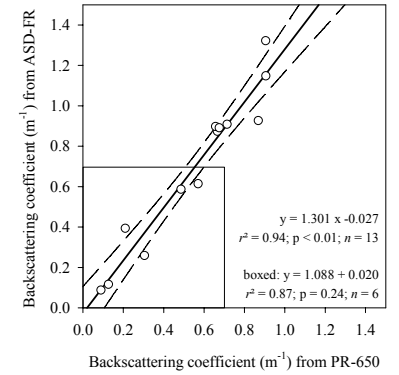

Figure 5.2. Comparison of backscattering values derived from the instrumentations used in Spain (ASD-FR) and The Netherlands (PR-650). The measurements were carried out on a number of Spanish water bodies in May 2005. The boxed area excludes points from L. l'Albufera where cyanobacterial biomass was exceptionally high. Solid regression line and dashed 95% confidence limits represent the regression results through all plotted points.

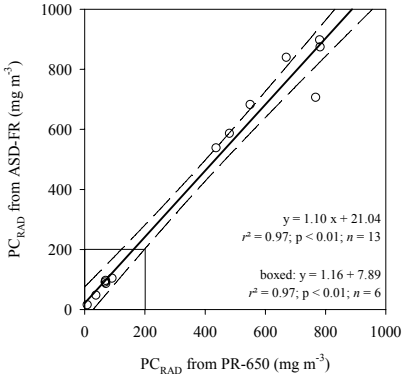

Figure 5.3. Comparison of PC values derived from the instrumentations used in Spain (ASD-FR) and The Netherlands (PR-650). The measurements were carried out on a number of Spanish water bodies in May 2005. The boxed area excludes points from L. l'Albufera where cyanobacterial biomass was exceptionally high. Solid regression line and dashed 95% confidence limits represent the regression results through all plotted points.

PC retrieval from radiometry

$R_{RS}(\lambda)$ data at either 1 or 4-nm intervals (from ASD-FR and PR-650, respectively) were transformed to MERIS band resolution. Current MERIS band settings are, denoted R_{RS}(MERIS channel, midpoint, band width): R_{RS}(6, 620, 10), R_{RS}(7, 665, 10), R_{RS}(9, 708.75, 10), and R_{RS}(12, 778.75, 15). Weighted averaging (weight depending on the overlap with the MERIS band) was used to derive the bands from the 4-nm resolution data. Band R_{RS}(778.75) derived from PR-650 data was based on the 771.25 – 780 nm range as 780 nm was the upper measurement limit of the instrument. For 1-nm data the wavelength ranges, rounded to the nearest nm, were averaged.

Calculation of the backscattering coefficient [b_b] from R_{RS}(778.75) has been described elsewhere (Gons *et al.* 2005). The PC algorithm (Simis *et al.* 2005*a*) assumes that b_b is spectrally neutral over the used wavelength range, that absorption in the 665-nm band can be attributed to Chl *a* and water [$a_w(\lambda)$], and absorption in band 6 to water, Chl *a*, and PC. Absorption by phytoplankton pigments [$a_{ph}(\lambda)$] is obtained from the ratio of two reflectance bands, in fact a ratio of the Gordon reflectance model for these bands (Gordon *et al.* 1975), which results for bands λ = 620 or 665 nm in:

$$a_{ph}(\lambda) = \left[\frac{R(709) \times \left(a_w(709) + b_b\right)}{R(\lambda)} - b_b - a_w(\lambda) \right] \times p(\lambda)^{-1} \qquad (5.3)$$

where $p(\lambda)$ is an empirical factor to compensate for a weaker absorption signal retrieved from radiometric data compared to absorption measurements with a spectrophotometer. Substitution of $a_w(620)$ = 0.281, $a_w(665)$ = 0.401, $a_w(708.75)$ = 0.727 from Buiteveld *et al.* (1994), $a^*_{PC}(620)$ = 0.007 m^2 mg^{-1}, $p(620)$ = 0.84, and $p(665)$ = 0.68 (Simis *et al.* 2005*a*) gives the PC algorithm adapted to remote sensing reflectance and with the revised a^*_{PC} value:

$$a_{ph}(665) = 1.47 \times \left[\frac{R(709) \times \left(0.727 + b_b\right)}{R(665)} - b_b - 0.401 \right] \qquad (5.4a)$$

$$\mathrm{PC_{RAD}} = 170 \times \left[\left[\frac{R(709) \times \left(0.727 + b_b\right)}{R(620)} - b_b - 0.281 \right] - \left[\varepsilon \times a(665) \right] \right] \qquad (5.4b)$$

where ε translates $a_{ph}(665)$, attributed to Chl *a*, to its contribution to $a_{ph}(620)$. From optimization of $\mathrm{PC_{RAD}}$ versus extracted PC, it was found that ε = 0.24 for cyanobacteria-dominated waters (Simis *et al.* 2005*a*).

Data screening and analysis

Concurrent radiometric measurements with ASD-FR and PR-650 instruments were available for 13 samples from 4 Spanish lakes, visited in May 2005. Paired *t*-tests showed the correlation between data subsets of the radiometric products R_{RS}, b_b, and

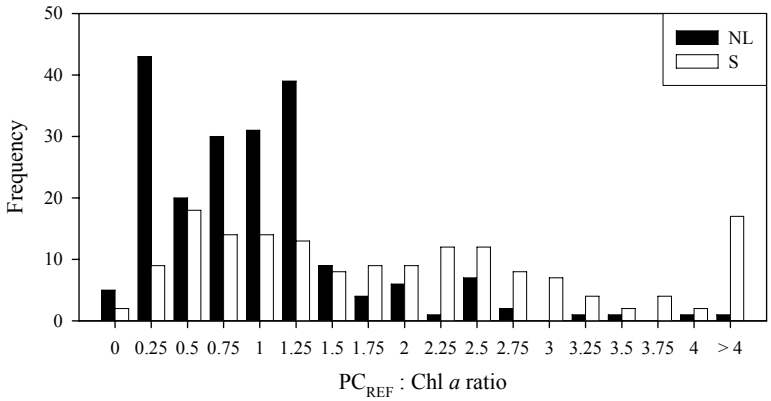

Figure 5.4. Histogram of the PC_{REF} : Chl *a* ratio measured in Spanish (S) and Dutch (NL) water bodies.

PC. The reference PC methods, i.e. PC extraction and *in situ* fluorescence, were also compared with paired *t*-tests for samples where more than one technique was used. The availability of the different data types for each of the water bodies is given in Table 5.1. For all paired *t*-tests presented in this study, results marked as significant passed Bonferroni's correction at 99 % confidence level unless stated otherwise.

HPLC pigment data were subjected to a principal component analysis to identify marker pigments for phytoplankton composition for later analyses. Two outliers from the Guadalteba reservoir, featuring a high-biomass dinoflagellate bloom, were omitted from PCA.

PC_{RAD} was compared with reference PC methods for the full data set and Dutch and Spanish samples separately. The correlation between the radiometric approach and the reference measurements was analysed using paired *t*-tests. PC_{RAD} was also compared to the average of the available reference PC measurements for each sample, denoted PC_{REF}. It is noted that averaging reference measurements is not optimal, as in several cases extraction of phycobilin pigments clearly failed (zero values for PC_{MG} discussed below) while cyanobacterial presence was evident. In those cases choosing the highest extraction value would eliminate part of the error caused by low extraction yield. In turn, the PC_{FL} method relies on the sensor sensitivity to PC among fluorescence of other substances (dissolved organic matter, algal pigments). In cases where PC_{MG} extraction failed, a concurrent PC_{FL} measurement would probably be closer to the 'real' PC concentration. However, since combinations of reference PC methods were not available for all samples, it was decided that averaging the results to yield PC_{REF} was the most straightforward approach.

To evaluate prediction errors by the PC algorithm, a regression with zero intercept was fitted through the plot of PC algorithm results against averaged PC reference measurements. The residuals of this regression were analysed in a multiple linear regression against chlorophyllous HPLC pigments including phaeophytin, and substituting fucoxanthin for Chl *c* as the latter was not measured for the whole dataset. The multiple regression was carried out separately for subsets of the data split at PC_{REF} = 50 mg m^{-3}. These analyses were made for the full dataset as well as separated by country.

5.3. Results

The $R_{RS}(\lambda)$ derived from ASD-FR and PR-650 measurements could be compared for a subset of 13 locations at 4 Spanish lakes where both instruments were used. Regression of the data in MERIS wavebands 6, 7, 9 and 12 yielded acceptable agreement between the used methods (Figure 5.1: $r^2 = 0.94$; $p < 0.01$; $n = 56$). The $R_{RS}(\lambda)$ values obtained with the ASD-FR setup were on average 17 % higher than PR-650 values in the 4 tested wavebands, but the limited number of observations did not warrant a calibration of one data set to the other. These different results for the used instrumentations lead to 30 % higher estimates of b_b (Figure 5.2; $r^2 = 0.94$; $p < 0.01$; $n = 13$), and 10 % higher PC_{RAD} (Figure 5.3; $r^2 = 0.97$; $p < 0.01$, significant at 95% confidence; $n = 13$) for ASD-FR compared to PR-650. The correlation coefficients for products b_b and PC_{RAD} remained high when 7 samples from the hypertrophic lake L'Albufera (see Table 5.1) were excluded from the regression ($r^2 = 0.87$ and 0.97 for b_b and PC respectively), but the relationship was no longer significant for b_b.

Considerable differences in pigment composition exist between the Dutch and Spanish samples as shown by a histogram of the ratio of PC_{REF} (the average of available PC extractions and PC fluorescence results) to Chl *a* (Figure 5.4). The PC_{REF} : Chl *a* ratio is a possible indicator of the cyanobacterial share in total phytoplankton biomass. Of the samples taken and analysed in the Netherlands, 84 % had a ratio PC_{REF} : Chl $a \leq 1.25$, suggesting lower intracellular PC : Chl *a* ratios, a lower share of cyanobacteria, or both. In contrast, 57 % of the samples collected and analysed in Spain had a ratio PC_{REF} : Chl $a \geq 1.25$.

PCA analysis based on pigment correlations showed good separation of cyanobacterial and green algal pigments in the full data set as well as subsets divided by country (Figure 5.5). The diatom pigment fucoxanthin grouped with cyanobacterial presence (phycobilin pigments and zeaxanthin) in Spanish samples while the influence of fucoxanthin on pigment variance was weak in the Dutch subset. Indeed, fucoxanthin concentrations were generally low in the Dutch samples. Fucoxanthin was always correlated with phaeophytin which could indicate samples influenced by resuspension of sedimented diatom cells. Cryptomonads in the phytoplankton community, indicated

Table 5.2. Results for linear regression between PC reference measurement methods, and between PC_{RAD} and (averaged and separate) PC reference methods. *n* = data points; regression equation parameters $y = ax + b$; NL = samples from The Netherlands, S = Spanish samples; bold-face p-values are significant at 99% confidence after applying Bonferroni's correction.

Figure	*y*-method	*x*-method	Country	*n*	*a*	*b*	r^2	p
6A	PC_{MG}	PC_{FT}	NL	73	1.18	1.55	0.96	**< 0.01**
			S	15	1.13	28.01	0.85	**< 0.01**
6B	PC_{MG}	PC_{FL}	S	106	0.89	17.82	0.59	0.489
7A	PC_{RAD}	PC_{FT}	NL	200	0.68	29.17	0.77	**< 0.001**
		PC_{FT}	S	8	0.34	241.93	0.00	0.034
		PC_{MG}	NL	75	0.58	29.37	0.74	0.450
		PC_{MG}	S	114	1.09	25.8	0.65	0.049
		PC_{FL}	S	162	0.99	15	0.53	0.164
7B	PC_{RAD}	PC_{REF}	NL	202	0.63	29.75	0.75	**< 0.001**
		PC_{REF}	S	171	1.18	-3.23	0.77	0.117
		PC_{REF}	NL + S	373	1.06	9.23	0.74	**< 0.001**
		PC_{REF}	NL + S	373	1.09	0[a]		**< 0.001**

[a] Intercept forced to zero.

by the alloxanthin pigment, were weakly represented regarding the full dataset, but prominent in the Dutch subset. Cryptomonad presence was not correlated to PC, even though cryptomonads are known to contain low concentrations of the latter pigment. Peridinin presence was restricted to some samples in the Spanish data and did not contribute much to total variance– however, two samples with a high-biomass dinoflagellate bloom were omitted for PCA and multiple regression analyses. The PCA analysis yielded the following marker pigments, to serve as proxies for the phytoplankton groups of which an influence on absorption in the red spectral area could be expected: fucoxanthin for diatoms, Chl *b* for green algae and prochlorophytes, alloxanthin for cryptomonads, and peridinin for dinoflagellates.

Reference measurements for PC were derived from extraction of the phycobilin pigments through cell disruption (PC_{FT} and PC_{MG}), or from *in situ* PC fluorescence (PC_{FL}). Figure 6 shows comparisons of these methods, which were available for subsets of the data (Table 5.1). Regression results are given in Table 5.2. For all comparisons of methods there was a high degree of scatter. Between PC_{MG} and PC_{FT} high correlation was found with on average slightly higher values of PC_{MG}, although the number of concurrent measurements was low for Spanish water bodies (Fig 6A). Between PC_{MG} and PC_{FL} methods (Figure 5.6B) the linear regression equation was not significant, which is primarily explained by a high number of zero PC_{MG} values (plotted at 0.11 mg m^{-3}). From the high degree of scatter between methods and the

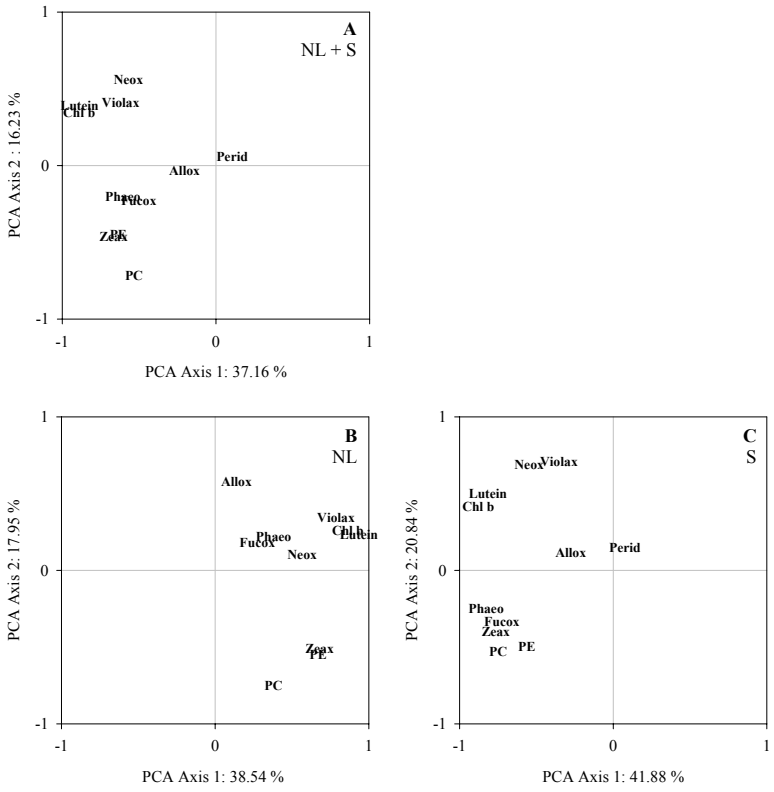

Figure 5.5. PCA factor scores based on pigment correlations for (**A**) the full dataset, (**B**) Dutch samples, and (**C**) Spanish samples. The following pigments were included to represent the indicated phytoplankton groups: alloxanthin – cryptomonads; phycocyanin, phycoerythrin, zeaxanthin – cyanobacteria; fucoxanthin – diatoms; peridinin – dinoflagellates; phaeophytin – not specified; chlorophyll *b*, neoxanthin, violaxanthin – green algae. Peridinin was not found in Dutch samples. Explained variance of the PCA axis is indicated at axis labels. Two samples taken during a high-biomass dinoflagellate bloom in Guadalteba reservoir were omitted from PCA.

absence of trends clearly deviating from unity, it was concluded that intercalibration of the used methods was neither required nor warranted.

Comparison of PC_{RAD} values with reference PC measurements (Figure 5.7A) only gave a significant correlation (regression results in Table 5.2) between PC_{RAD} and PC_{FT}. The regression slope of this comparison was low, caused by a substantial number of relatively high PC_{RAD} values in the lower PC_{FT} range. The correlation between PC_{RAD} and PC_{REF} (the average of available reference PC measurements) was significant for the full dataset and the Dutch subset, but not for Spanish samples alone. Positive errors of PC_{RAD} compared to PC_{REF} occurred most frequently at Dutch sites and were

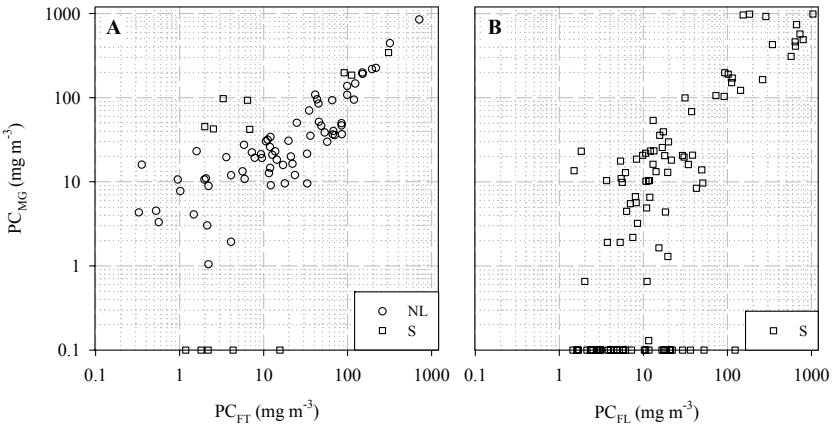

Figure 5.6. Log-log plot of reference PC measurements for samples where multiple methods were applied (**A**) Mechanical grinding (PC_{MG}) vs. Freeze/Thaw (PC_{FT}) method, separated by country. (**B**) PC_{MG} extraction method vs. PC_{FL} fluorescence method, for samples taken and analysed in Spain. Regression results are listed in Table 5.2.

again concentrated at the lower end of the PC_{REF} range. In general, the correlation between PC_{REF} and PC_{RAD} improved with $PC_{RAD} > 50$ mg m^{-3}. Negative differences of PC_{RAD} occurred mainly with PC_{FL} measurements.

An idealized regression (intercept forced through zero) of PC_{RAD} versus PC_{REF} reveals under- and overestimations of PC_{RAD}. Regression slope was 1.09 (Table 5.2). The deviation from unity of this slope is relatively low in comparison to the scatter that was found when comparing the reference methods for PC quantification, and is therefore interpreted as support for the PC algorithm's current parameterization. Similar to earlier findings (Simis *et al.* 2005*a*), relative residual errors in the algorithm prediction rose steeply with lower PC_{REF} : Chl *a* ratios, which in turn were mainly found in the Dutch dataset (Figure 8).

To identify the effects of phytoplankton pigment composition on estimation of PC by the reflectance algorithm (Eq. 5.4), multiple linear regression analyses were carried out on the residuals from the regression, with zeroed intercept, of PC_{RAD} against PC_{REF}. The multiple regression was carried out against the marker pigments for the main algal groups (identified from PCA) and phaeophytin. Table 5.3 lists the multiple regression results carried out for the full dataset and the Dutch and Spanish samples separately and split into parts with PC_{REF} higher or lower than 50 mg m^{-3}. Significant overestimations caused by Chl *b* and fucoxanthin were found in the lower concentration range. A positive effect of phaeophytin on PC_{RAD} was found to be significant only for the full dataset < 50 mg m^{-3}. Residual PC_{RAD} errors could not be explained by the regression model for the concentration range > 50 mg m^{-3}.

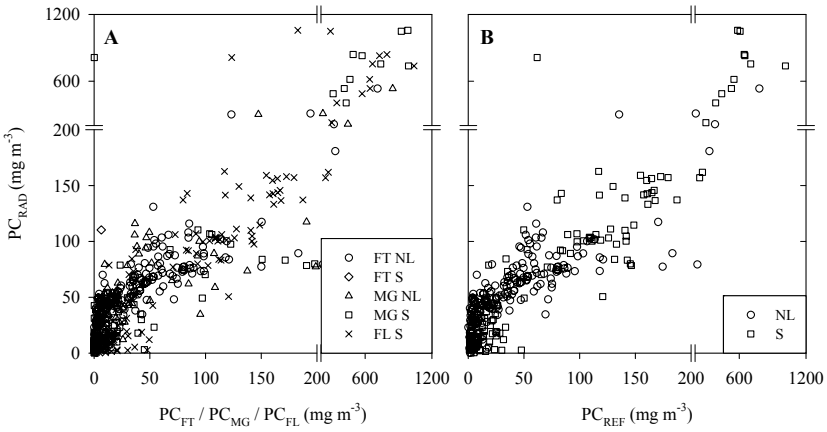

Figure 5.7. Comparison of PC assessment methods. (**A**) PC_{RAD} plotted against PC_{FT}, PC_{MG}, and PC_{FL}, samples separated by country. (**B**) PC_{RAD} plotted against PC_{REF} (the average of available reference methods), separated by country. Note the scale breaks at 200 mg m^{-3} in both panels. Regression results are listed in Table 5.2.

5.4. Discussion

The performance of a semi-analytical nested band ratio algorithm for the quantification of PC (Eq. 5.4) was tested with data of sampling campaigns in the Netherlands and Spain, in the period 2001-2005. The influence of phytoplankton pigment composition on the performance of the algorithm was explored using HPLC marker pigments for different phytoplankton groups. Analysis of PC : Chl *a* ratios and the HPLC pigment matrix suggested that co-occurrence of phytoplankton groups was common in Dutch samples while cyanobacterial predominance occurred in several Spanish water bodies. In general, the PC algorithm proved adequate over a wide range of PC concentrations. Closer investigation showed that PC_{RAD} errors were mainly overestimates, and occurred primarily in the low (< 50 mg m^{-3}) concentration range. The errors were most evident with Dutch samples and were primarily associated with the presence of Chl *b*, indicating the presence of green algae and prochlorophytes. Fucoxanthin, indicating diatom presence, and phaeophytin also appeared to cause overestimation of PC.

Comparisons of three methods for PC quantification showed similar values for concurrent measurements, but a high degree of scatter. Methodological problems resulting in low extraction yield could exaggerate the error of PC_{RAD}. Besides scatter and a number of samples for which the PC_{MG} method was ineffective, comparison with PC_{FL} suggest that there was no such methodological bias with the current dataset.

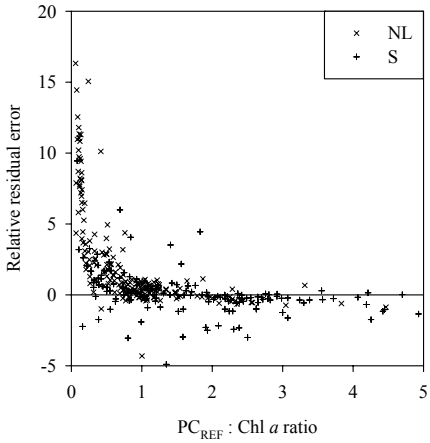

Figure 5.8. Residual error of the regression model $PC_{RAD} = 1.09 \times PC_{REF}$, plotted as a function of the PC_{REF} : Chl *a* ratio.

Nonetheless, PC_{FL} was not available for the Dutch dataset, so the comparison is incomplete. It is noted that the quality of PC extraction for Dutch sites has improved, thereby reducing the overestimation that was previously found (cf. Figure 6 of Simis *et al.* 2005*a*). In general, the results show that PC ground truth measurements should be used with scrutiny. *In vivo* PC fluorescence methods are perhaps most promising for routine measurement of PC, as sample preservation and pigment extraction are avoided (cf. Lee *et al.* 1994, 1995; Asai *et al.* 2001; Izydorczyk *et al.* 2005).

It was previously shown (Simis *et al.* 2005*a*) that bulk pigment absorption can be adequately retrieved from turbid water reflectance regardless of suspended sediments and coloured dissolved organic matter. Assuming this holds true for the current dataset (absorption spectra were not available for most of the data), the PC overestimation must be associated with phytoplankton pigments that are not accounted for by the algorithm. *In vivo* pigment absorption obtained from multiple regression and decomposed into multiple Gaussian curves for each pigment, shows that the main chlorophyllous pigments (Chl *a*, *b*, *c*, and phaeophytin) absorb light throughout the 600 – 675 nm region (Sathyendranath *et al.* 1987; Hoepffner and Sathyendranath 1993; Ficek *et al.* 2004). Indeed, the present study shows that Chl *b*, phaeophytin, and fucoxanthin as a proxy for Chl *c* caused overestimation of PC. Specifically at low PC concentrations, the absorption by these pigments could increase absorption in the 620-nm band significantly.

The only correction for chlorophyllous pigment absorption in the original PC algorithm was for Chl *a* absorption. The influence of this pigment in the 620-nm band

was derived from absorption in the 665-nm band, which was fully attributed to Chl *a*, using a fixed factor ε (Eq. 5.4). The optimized value of ε for cyanobacteria-dominated sites was set at $\varepsilon = 0.24$ (Simis *et al.* 2005*a*), i.e. lower than the value of 0.3 – 0.4 for Chl *a* in algal species, and much lower than for the specific *in vivo* absorption of Chl *b* with $\varepsilon = 0.5 – 0.6$ and Chl *c* with $\varepsilon = 1.7 – 3.7$ (Sathyendranath *et al.* 1987; Bidigare *et al.* 1990; Hoepffner and Sathyendranath 1993; Ficek *et al.* 2004). Obviously, with increasing concentrations of Chl *b* and *c*, the ε-correction of 0.24 is increasingly inadequate and the derived PC absorption will be too high. Unfortunately it is yet unknown whether additional spectral information could solve this problem. For further algorithm and sensor development, it is important to realize where more spectral information is required.

From the current dataset, a correction for Chl *b* absorption by using a specific Chl-*b* absorption value for the 620-nm band of 0.05 m^2 (mg Chl *b*)$^{-1}$ efficiently removed most of the overprediction in the whole data set ($PC_{RAD} = 0.83 \times PC_{REF} + 1.71$; $r^2 = 0.90$; p = 0.002; $n = 223$). This specific absorption value is, however, considerably higher than reported values for *in vivo* Chl *b* absorption in this waveband, which range 0.002 - 0.013 m^2 (mg Chl *b*)$^{-1}$. Additional corrections for Chl *c* or phaeophytin did not improve the PC prediction, as these pigments were only found in very low concentrations in most samples. Detection of the contribution of Chl *b* to the absorption envelope therefore appears to be the next step in algorithm development.

The present validation efforts showed that for PC concentrations *in situ* above 50 mg m^{-3}, PC_{RAD} was increasingly reliable. Furthermore, higher PC : Chl *a* ratios will contribute to the quality of PC retrieval. Below the 50 mg m^{-3} level, PC predictions should be considered as the high estimate, *i.e.* the concentration could be lower, but is unlikely to be higher. Monitoring an increase in cyanobacterial biomass is therefore limited by the sensitivity of the PC algorithm for PC among other pigments, which in the current dataset was mainly Chl *b*. Decline of cyanobacterial blooms, however, can be detected by routinely following the PC algorithm predictions. This conclusion allows monitoring for potentially hazardous events like the sudden lysis of toxic cyanobacterial blooms. The relatively high PC : Chl *a* ratios found in Spain also suggest that MERIS can be used to routinely monitor cyanobacterial blooms in these water bodies.

Table 5.3. Multiple regression results of residual errors of PC_{RAD} versus PC_{REF} with intercept forced to zero. The residuals were fitted against the marker pigments Chl *b* (green algae), peridinin (dinoflagellates), alloxanthin (cryptophytes), and fucoxanthin (diatoms), and degradation product phaeophytin. The analysis was performed for all samples and separated by country, and for the PC_{REF} ranges split at 50 mg m^{-3}. Significant (> 99% confidence) p and β values are printed in bold face. Prior to analysis outliers (residuals more than ± 2 times standard deviation) were removed. Symbols and abbreviations: NL – Samples from The Netherlands; S – Spanish samples; *n* – number of valid cases; SE – standard error; n.a – no data.

	PC_{REF} <50 mg m^{-3}			PC_{REF} > 50 mg m^{-3}		
Country	NL + S	NL	S	NL + S	NL	S
n	234	141	93	101	56	45
Multiple R^2	0.366	0.564	0.205	0.084	0.069	0.152
Adjusted R^2	0.352	0.551	0.160	0.046	-0.004	0.067
SE of estimate	14.90	9.37	15.00	45.50	41.69	49.43
whole-model p	**0.000**	**0.000**	**0.001**	0.073	0.442	0.150
β Chl *b*	**0.499**	**0.723**	**0.296**	0.219	-0.002	0.299
β Fucoxanthin	**0.210**	**0.202**	**0.304**	-0.057	-0.193	0.011
β Phaeophytin	**0.131**	0.065	-0.095	0.146	-0.006	0.130
β Alloxanthin	-0.026	-0.139	0.115	-0.093	-0.106	-0.087
β Peridinin	-0.041	n.a	0.020	n.a	n.a	n.a

5.5. Acknowledgments

The authors thank the drivers and field technicians at the Centre for Hydrographic Studies (CEDEX, Spain) and the crew of R/V *Luctor* (NIOO, The Netherlands). Antonio Quesada (Universidad Autonoma, Madrid, Spain) is thanked for advice and the use of lab facilities for PC extraction during data intercalibration efforts. Further thanks are due to Nicole Dijkman (NIOO) for advice on phytoplankton group representation in the pigment matrix, and to Ana Alonso and Covadonga Alonso (CEDEX) and Cobie Kleppe-van Zetten (NIOO) for HPLC pigment analysis. A one-month stay for SGHS at CEDEX was covered by a grant from the Schure-Beijerinck Popping fund (KNAW).

6. MERIS POTENTIAL FOR REMOTE SENSING OF WATER QUALITY PARAMETERS FOR TURBID INLAND WATER

Stefan G. H. Simis, Steef W. M. Peters[1] & Herman J. Gons
[1]Institute for Environmental Studies (IVM), Vrije Universiteit, Amsterdam, The Netherlands.

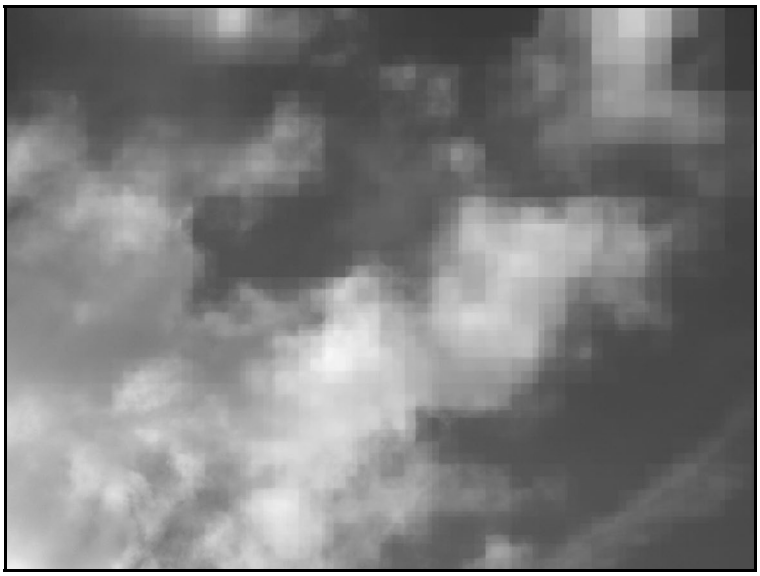

Abstract

This paper illustrates the use of level-2 (L2), geolocated and atmospherically corrected, imagery of the Medium Resolution Imaging Spectrometer (MERIS) for water quality monitoring of turbid inland water bodies. MERIS remote-sensing reflectance and derived water quality parameters were compared with field spectroradiometric data and laboratory measurements of light absorption and phytoplankton pigment concentrations. Generic problems with overcorrection for atmospheric path radiance were associated with high reflectance values in the near-infrared (NIR). High NIR reflectance was associated with accumulation of phytoplankton biomass near the surface, or with atmospheric path radiance originating from adjacent land. For a large inland lake, the L2 MERIS reflectance was generally correct, but the adjacency effect caused poor erroneous values for smaller water bodies. Overcorrected reflectance spectra lead to poor performance by NIR-red band ratio models for the retrieval of water quality parameters such as chlorophyll *a* and phycocyanin. By comparison of non-atmospherically corrected (L1B) imagery with L2 data, and subsequent adoption of the atmospheric correction scheme from a region with generally good results, the mixed water/land reflectance for a problematic region was reconstructed. The land adjacency effect prevented the use of NIR-red band ratio algorithms due to raised NIR values. Additional filtering of the data based on product confidence flags and MERIS estimations of the aerosol optical thickness at 865 nm improved the quality of band ratio products for the large inland lake, but caused strongly reduced data density over the smaller lakes. It was concluded that L2 MERIS products for turbid inland water could greatly benefit from improved, possibly locally fine-tuned, atmospheric correction schemes. Also, strategies for the unmixing of land and water signals could improve the value of MERIS and its successors for water quality monitoring of smaller lakes.

6.1. Introduction

The water quality of freshwater lakes and reservoirs is of growing concern. The occurrence of potentially toxic cyanobacterial blooms in many eutrophicated water bodies requires frequent updates on their phytoplankton status. Conventional monitoring efforts are costly and therefore not carried out at optimal time intervals. Remote sensing may assist the monitoring of water quality parameters that indicate the suitability of a water body for drinking water supply or recreation. Moreover, remote sensing methods may provide simultaneous data on many water bodies, and information on the spatial heterogeneity of water quality parameters in larger water bodies. Over recent years several algorithms have been developed to allow mapping of algae and cyanobacteria in turbid, eutrophic water, but up to date no satellite sensor has provided data at the required spectral, spatial, and temporal resolution required for

operational inland water quality monitoring, while airborne missions are too laborious. The European Space Agency's ENVISAT mission, carrying the Medium Resolution Imaging Spectrometer (MERIS), provided new opportunities for monitoring turbid coastal waters, due to the implementation of narrow bands in the red part of the spectrum, suitable for the detection of phytoplankton pigments in turbid water. The instrument was not designed specifically for inland waters (Rast 1999), but MERIS' 260-m across and 290-m along track ground resolution should allow water colour measurements over medium-sized lakes. The recent availability of atmospherically corrected and geolocated (level-2, L2) MERIS imagery for a set of small to medium-sized inland water bodies allows to evaluate the use of MERIS for monitoring lakes and reservoirs. On the other hand, over small water bodies the influence of adjacent land pixels can be considerable. Elevated NIR reflectance over water bodies that are already bright scatterers due to suspended sediments, may defy the atmospheric correction process. It is therefore desirable to test a set of imagery and field data match-ups in the early stage of MERIS use, to define whether the L2 imagery may be used as is, or whether additional processing of the radiometric data for use with inland waters is required.

This paper illustrates the quality of L2 processed MERIS imagery for water quality monitoring of turbid inland water bodies of varying size. The upper levels of turbidity and trophic state of these water bodies are well above the range of standard Case 2 water quality algorithms (Schiller and Doerffer 1999). Instead, the products that may be obtained from MERIS reflectance over such water bodies are derived from near-infrared (NIR) over red reflectance ratios, yielding the absorption by water constituents which in turn may be attributed to phytoplankton photosynthetic pigments. For phytoplankton in general, retrieval of the concentration of chlorophyll *a* (Chl *a*) has been validated for turbid water bodies with MERIS bands simulated from field spectroradiometer data (Gons *et al.* 2002*b*). For cyanobacteria, the pigment phycocyanin (PC) and the ratio PC : Chl *a* are indicative of the cyanobacterial state of turbid water bodies and these products may also be obtained from MERIS reflectance bands (Simis *et al.* 2005*a*, Chapter 5). Near-real time updates of these proxies for phytoplankton biomass could complement traditional monitoring efforts. However, operational use of these products derived from satellite imagery requires a straightforward quality control scheme. This paper therefore also discusses the effect of data filtering procedures on the quality of band ratio algorithm output.

6.2. Method

MERIS imagery

Full resolution geolocated and atmospherically corrected (L2) MERIS images were obtained from the European Space Agency (ESA) for a period matching several

Table 6.1. Details on acquired MERIS imagery.

Record Date	Sensing start	Track	Cycle	Orbit	(near) Matchup
13 Apr 2003	10:21:22	280	15	5845	L. Loosdrecht[a] +1d
28 May 2003	10:07:02	423	16	6489	L. Loosdrecht[a] -1d
09 Jun 2003	10:29:47	94	17	6661	L. Loosdrecht[a] +1d
15 Oct 2003	10:07:12	423	20	8493	L. Loosdrecht[a] -1d
3 Aug 2004	9:52:21	108	29	12687	L. IJsselmeer system[b]
07 Sep 2004	9:56:09	108	30	13188	L. IJsselmeer system[b]
16 Aug 2005	10:13:22	8	40	18098	L. IJsselmeer system[b]
20 Sep 2005	10:14:27	8	41	18599	L. IJsselmeer system[b]

[a] The indicated time difference refers to field sampling either 1 day before (-1d) or 1 day after (+1d) the MERIS overpass. [b] Includes a sampling station on the connected L. Ketelmeer.

monitoring campaigns. The processor version for L2 imagery was 4.10 for all images. Table 1 lists the scenes selected for the present work. Matchups of MERIS imagery and sampling cruises were defined as the availability of both a MERIS image (acquired between 10.00 – 11.00 UTC) and field truth collected on the same day (8.00 – 15.00 UTC). Matchups with limited or no cloud cover were available during four days in 2004 – 2005, corresponding with sampling cruises on the large (1190 km^2), shallow (mean depth 4.5 m), and eutrophic Lake IJsselmeer (The Netherlands) and the connected L. Ketelmeer (37 km^2; mean depth 4 m), from which River IJssel water flows into L. IJsselmeer. Near-matchups were available with samples obtained from the small (9.8 km^2), very shallow (2 m) and eutrophic Lake Loosdrecht (The Netherlands). Near-matchups were defined as satellite overpass within 24 h before or after sampling time. Near-matching data were only compared for the horizontally and vertically well-mixed L. Loosdrecht, under weather conditions that were stable between sampling and satellite overpass.

Water surface retrieval

For a set of 14 lakes listed in Table 2 (excluding L. IJsselmeer), the number of water-classified pixels that could be extracted from L2 MERIS scenes was compared to the lake surface area. L2 data can only be used to extract water quality parameters if the L2 processing chain for water surfaces was followed. This exercise allows to evaluate the minimum lakes size required to obtain L2 water pixel data. Note that the classification of pixels as either land, water, or cloud was based on radiometric criteria since MERIS processing software version 4.10, while older versions relied on a shoreline database (ESA 2004).

Validation of MERIS R_{RS}

For comparisons of four MERIS scenes with field data of L. IJsselmeer and L. Ketelmeer, pixel data matching the geographic coordinates of field sampling stations were extracted from MERIS scenes. The pixel locations were selected from linearly interpolated tie point grids included with the MERIS scenes. All data in a 3 × 3 pixel

Table 6.2. Location and surface area of lakes included in this study.

Lake	Latitude (d.ddd)	Longitude (d.ddd)	Surface area (km^2)
De Leijen	53.156	6.060	2.6
Wijde Blik	52.221	5.057	3.5
Bergumermeer	53.191	6.036	4.5
Braassemermeer	52.191	4.652	4.5
Zuidlaardermeer	53.125	6.694	6.0
Amstelmeer	52.789	4.910	6.0
Westeinder Lakes	52.240	4.729	8.5
Sneekermeer	53.030	5.747	9.7
Loosdrecht Lakes	52.182	5.067	9.8
Slotermeer	52.914	5.631	11.1
Fluessen	52.936	5.541	11.9
Beulakerwijde	52.693	6.055	9.6
+ Belterwijde			5.3
Tjeukemeer	52.890	5.801	20.9
Volkerak	51.642	4.280	45.7
IJsselmeer lake system[a]			1227.3
Ketelmeer	52.580	5.875	37.3
IJsselmeer	52.800	5.300	1190.0
station 'Urk'	52.599	5.722	n.a
station 'Lemmer'	52.626	5.538	n.a
station 'Enkhuizen'	52.780	5.543	n.a
station 'Medemblik'	52.735	5.395	n.a
station 'Den Oever'	52.828	5.213	n.a
station 'Stavoren'	52.966	5.169	n.a

[a] For L. Ketelmeer and L. IJsselmeer stations the surface area included in the sampled 3 x 3 pixel frame was 0.7 km^2 based on 260-m across track and 290-m along track resolution.

frame surrounding the pixel corresponding to each field station were extracted. Land (only L. Ketelmeer) and cloud-classified pixels were filtered from the extracted data, as well as pixels which contained zero-values in any of bands 6, 7, 9 or 12 (see Table 3 for a list of current MERIS band settings), which were used to calculate water quality parameters (discussed below).

Near-matchups of four MERIS scenes with Lake Loosdrecht sampling events were obtained in a slightly different manner. Field sampling was carried out at one station near the lake shore. All pixels included in the lake boundaries were included in the dataset for analysis, as long as these passed the filter criteria explained above. From data of the Royal Netherlands Meteorological Institute (KNMI) it was verified that weather conditions were stable between image acquisition and sampling: other than minor differences in regional cloud cover, no significant rainfall or strong wind occurred during the 1-d intervals. It may be assumed that L. Loosdrecht, because of its shallowness, is usually well-mixed.

Table 6.3. MERIS band settings valid throughout the study period (source: MERIS user guide issue 2.1, Table 1.1, http://envisat.esa.int/envisat/dataproducts/meris/).

Band number	Band centre (nm)	Band width (nm)	Application
1	412.5	10	Yellow substance and detrital pigments
2	442.5	10	Chlorophyll absorption maximum
3	490	10	Chlorophyll and other pigments
4	510	10	Suspended sediment, red tides
5	560	10	Chlorophyll absorption minimum
6	620	10	Suspended sediment
7	665	10	Chlorophyll absorption & fluorescence reference
8	681.25	7.5	Chlorophyll fluorescence peak
9	708.75	10	Fluorescence peak reference, atmosphere corrections
10	753.75	7.5	Vegetation, cloud
11	760.625	3.75	O_2 R- branch absorption band
12	778.75	15	Atmosphere corrections
13	865	20	Vegetation, water vapour reference
14	885	10	Atmosphere corrections
15	900	10	Water vapour, land

Retrieval of water quality products from L2 imagery

Reflectance in the bands centred at 665, 708.75, and 778.75 nm (MERIS bands 7, 9, and 12) were used to obtain the absorption by all water constituents at 665 nm [$a_{TOT}(665)$]. The absorption was obtained through inversion of the Gordon reflectance model (Gordon 1975), using the ratio $R_{RS}(708.75/665)$, the absorption of pure water (Buiteveld *et al.* 1994), and the backscattering coefficient obtained from $R_{RS}(778.75)$ and considered spectrally neutral (Gons 1999, Gons *et al.* 2005). The Chl *a* concentration in the surface water may be derived from $a_{TOT}(665)$ and the specific absorption of Chl *a*, estimated at 0.014 m^2 (mg Chl *a*)$^{-1}$ at this wavelength, referring to 'uncorrected' Chl *a* which includes absorption by degraded Chl *a* (Gons *et al.* 2005).

Through a nested band ratio and addition of a waveband centred at 620 nm (MERIS band 6) to the set described above, it is possible to also estimate absorption by water constituents around 620 nm [$a_{TOT}(620)$]. This absorption can in turbid waters be attributed to absorption by accessory photosynthetic pigments such as the cyanobacterial PC, assuming negligible influence of absorption by other water constituents (Simis *et al.* 2005*a*, Chapter 5). For estimation of PC over supposedly cyanobacteria-dominated water bodies, a specific absorption of PC of 0.007 m^2 (mg PC)$^{-1}$ was used.

MERIS and PR-650 derived values of $a_{TOT}(620)$ and $a_{TOT}(665)$ were compared with spectrophotometric measurements of these parameters. Similarly, the Chl *a* and PC products obtained from the radiometric measurements were compared with

concentrations of the pigments obtained from pigment extractions carried out on water samples in the lab. The procedures for the lab measurements are outlined further below.

Atmospheric correction evaluation

During the atmospheric correction process of MERIS scenes, the aerosol optical thickness at 865 nm [AOT(865)] is calculated for every pixel (Moore *et al.* 1999, Antoine and Morel 1999). Overestimates of AOT(865) are likely over surfaces with high NIR reflectance such as bright scattering water or water near land. The latter occurs as an effect of atmospheric path radiance and its effect is strongest with poor atmospheric visibility and high reflectance contrasts at the land / water boundary. Overestimated AOT(865) results in a too high atmospheric correction factor, and an underrepresentation of the water-leaving reflectance. This 'overcorrected' R_{RS} subsequently causes band ratio algorithms to perform poorly, when certain bands are affected. To illustrate this error, a MERIS scene was obtained at both L2 and L1B processing, the latter excluding atmospheric correction, for 15 October 2003, which was the image with the clearest atmosphere of the series. Top-of-atmosphere reflectances were calculated from L1 radiances using the radiance-to-reflectance processor included in the Basic ERS & Envisat (A)ATSR and Meris Toolbox (BEAM, Brockmann Consult, Germany). The L1B spectra of L. Loosdrecht were manually corrected for the influence of the atmosphere, the new product here designated as L2'. First, it was established that atmospheric correction over the large L. IJsselmeer did not cause many erroneous spectra. Therefore the averaged difference of approximately 6000 pixel pairs of an L1B and L2-processed image was taken as a 'correction spectrum' and applied to L. Loosdrecht L1B data. The difference spectrum was scaled so that the value at 412.5 nm was equal to the averaged L1B spectrum of L. Loosdrecht, so that L2' R_{RS}(412.5) was zeroed.

Additional data filtering

Filtering of the L2 data was based on the raised state of the water surface flag and the absence of zero values in bands 6, 7, 9, or 12, as discussed above. It was explored whether additional data filtering based on existing L2 product confidence and science flags would reduce the error found in the water quality parameters produced from L2 MERIS reflectance. The state of MERIS L2 product confidence and science flags was first checked for the (near-)matchup data set. The effects of filtering with any of these flags on the density of input data and the quality of output parameters $a_{\mathrm{TOT}}(665)$ and $a_{\mathrm{TOT}}(620)$ was subsequently explored for L. Loosdrecht and L. Ketelmeer.

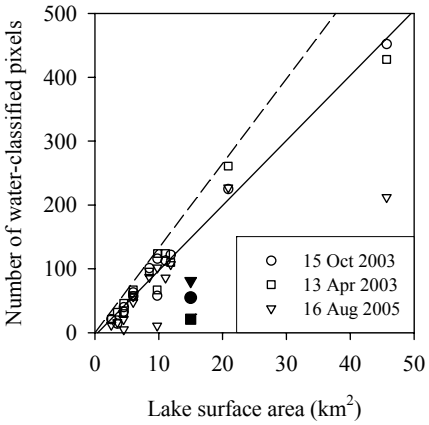

Figure 6.1. The number of water-classified pixels as a function of lake surface area for 14 lakes in the Netherlands on two days with good visibility (13 April and 15 October 2003) and one day with hazy atmosphere (16 August 2005). The filled symbols represent a lake area composed of two water bodies separated by a stretch of land that was not visible in every image, and was not used for regression (solid line). Regression results for the comparison on 15 October 2003: $y = 10.19x - 4.50$, $p = 0.006$, $r^2 = 0.98$, $n = 13$). Based on a pixel size of 260 m across track and 290 m along track, 13.26 pixels are ideally visible per 1 km^2, as indicated by the dashed line.

Field sampling

Absorption measurements

Spectral absorption measurements of coloured dissolved organic matter [$a_{CDOM}(\lambda)$], total suspended matter [$a_p(\lambda)$], bleached total suspended matter including detritus [$a_d(\lambda)$], and phytoplankton pigments [$a_{ph}(\lambda)$] obtained from the difference of $a_p(\lambda)$ and $a_d(\lambda)$, were obtained for every sampling site. In the case of L. IJsselmeer the samples were stored at 0°C for up to 40 h. Samples of L. Loosdrecht were processed within several hours after sampling. The suspended matter absorption spectra were obtained using a PerkinElmer lambda800 (PerkinElmer, Wellesley, MA, USA) spectrophotometer equipped with a 150-mm integrating sphere (Labsphere Inc, North Sutton, NH, USA). Samples concentrated on Whatman GF/F glass fibre filters were placed inside the sphere allowing precise measurement of the absorption coefficient (Maske and Haardt 1987, Babin and Stramski 2002, 2004). Details on protocol, optical geometry, and correction for path length amplification can be found elsewhere (Simis *et al.* 2005*b*). Spectra of $a_{CDOM}(\lambda)$ were obtained from the sample filtrate over a Schleicher & Schuell 0.2 µm cellulose acetate filter, measured in optical grade glass cuvettes of 0.05 m path length in dual beam mode of the standard configuration of the spectrophotometer, *i.e.*, without integrating sphere accessory. The absorption of all

water constituents [$a_{TOT}(\lambda)$] was obtained from the sum of $a_p(\lambda)$ and $a_{CDOM}(\lambda)$. All absorption coefficients were obtained at 1-nm intervals and subsequently integrated over the MERIS band widths (Table 3).

Spectroradiometric measurements

Spectroradiometric measurements were carried out at the sampling sites following protocol described elsewhere (Gons 1999). In short, measurements were made with a PhotoResearch model PR-650 spectroradiometer (Photo Research, Chatsworth, CA, USA), radiometric data was available in the 380-780 nm range at 4-nm intervals and full-width half maximum of 8 nm. Measurements of the water-leaving radiance (L_{wu}), skylight (L_{sky}), and of downwelling irradiance estimated from the radiance reflected by a Spectralon diffuser plate (E_d), were obtained to compute the above-water remote sensing reflectance (R_{RS}), equivalent to $[\rho_w]_N$, the MERIS product 'normalized water-leaving reflectance' (Montagner 2001):

$$R_{RS}(\lambda) = [\rho_w]_N(0^+,\lambda) = \pi \frac{L_{wu}(0^+,\theta,\varphi,\lambda) - r[(\theta)L_{sky}(0^+,\theta,\varphi,\lambda)]}{E_d(0^+,\lambda)} \quad (6.1)$$

where $r(\theta)$ is fraction of skylight reflected at the water surface, assumed to be a constant value 0.029 for the current viewing geometry (Gons 1999). The viewing angles θ for L_{wu} and L_{sky} were 42° from the nadir plane in the downward and upward direction, respectively. The azimuth angle φ for L_{wu}, L_{sky}, and E_d was 90° away from the sun. The factor π is used to convert radiance to irradiance units assuming an isotropic distribution of the water-leaving reflectance, and renders R_{RS} dimensionless. The handheld R_{RS} measurements were always based on repeated observations, eliminating spectra that were clearly influenced by measurement errors such as variable cloud cover. Compared to the MERIS spectra, variance between the spectra obtained with the PR-650 method was very low, hence no error bars are presented in this paper. To simulate MERIS bands from the 4-nm resolution PR-650 data, the weighted average was used. For the 15-nm wide $R_{RS}(778.75)$ of MERIS, the PR-650 data was limited to 780 nm, but this is not expected to significantly change the presented results.

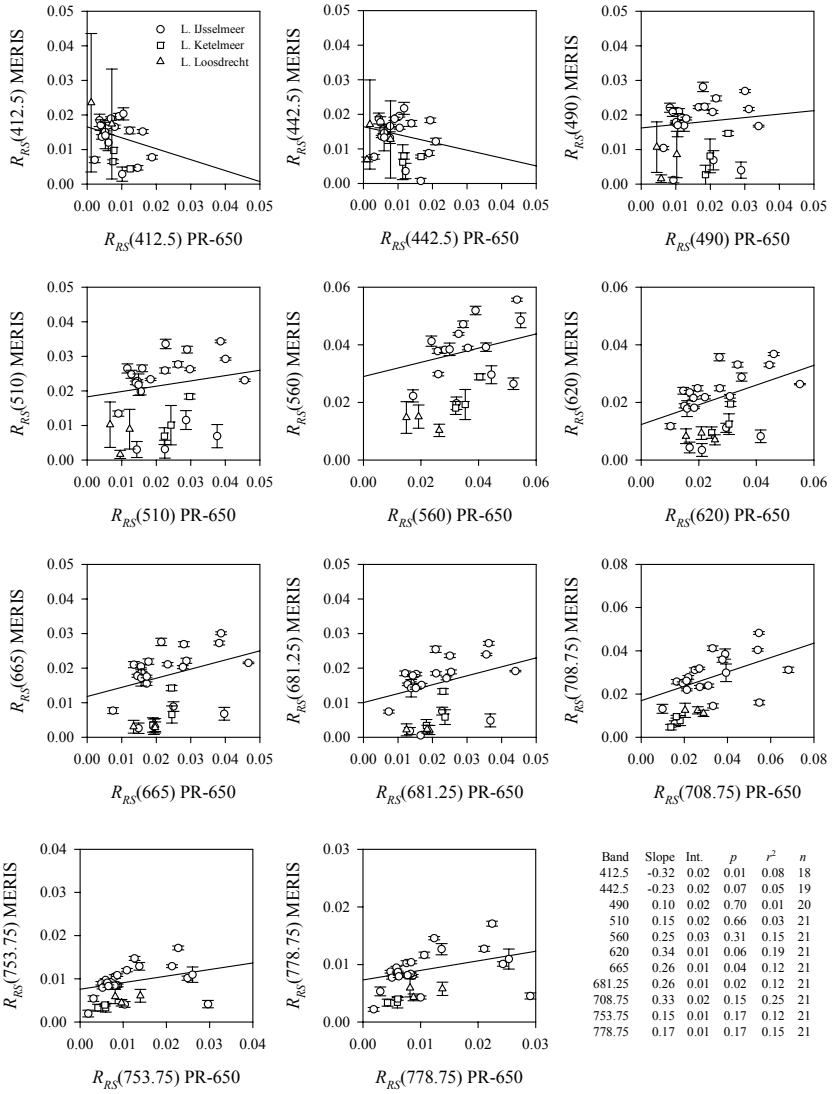

Band	Slope	Int.	p	r^2	n
412.5	-0.32	0.02	0.01	0.08	18
442.5	-0.23	0.02	0.07	0.05	19
490	0.10	0.02	0.70	0.01	20
510	0.15	0.02	0.66	0.03	21
560	0.25	0.03	0.31	0.15	21
620	0.34	0.01	0.06	0.19	21
665	0.26	0.01	0.04	0.12	21
681.25	0.26	0.01	0.02	0.12	21
708.75	0.33	0.02	0.15	0.25	21
753.75	0.15	0.01	0.17	0.12	21
778.75	0.17	0.01	0.17	0.15	21

Figure 6.2. R_{RS} from MERIS versus PR-650 plotted for bands 1 – 10 and 12. For MERIS data of L. IJsselmeer and L. Ketelmeer the average and SD (error bars) were plotted, each symbol representing up to nine pixels centered around the sampling location. MERIS data of L. Loosdrecht represent the lake-wide average and SD for all pixels passing the initial filtering criteria (see text). Regression lines have been drawn based on the L. IJsselmeer data only, and regression parameters can be found in the table inset.

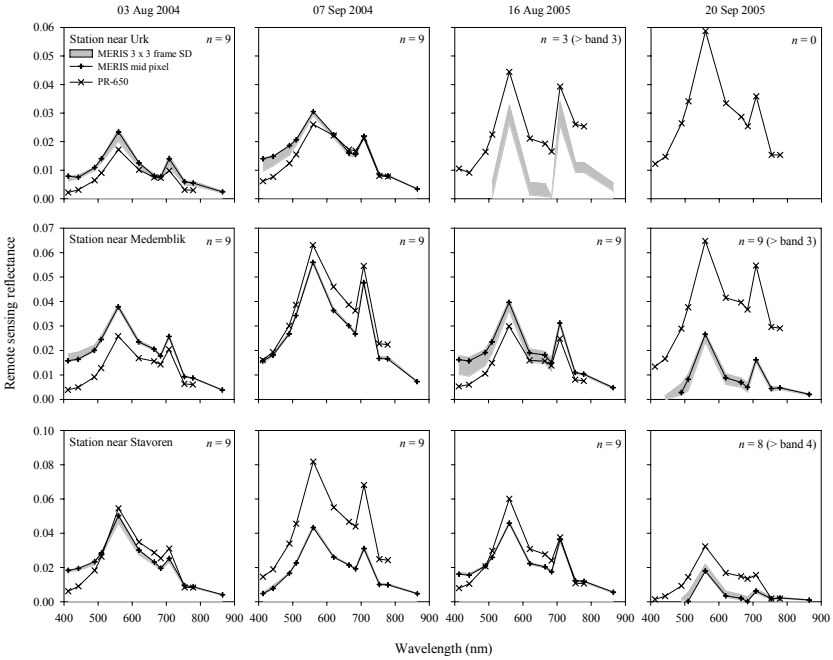

Figure 6.3. Matchup R_{RS} spectra of MERIS and PR-650 for L. IJsselmeer, derived from 4 scenes obtained during field sampling campaigns. Legend: n – number of MERIS spectra available from 3 × 3 cell grid around the sampling location. The grey area indicates the standard deviation of the MERIS spectra in this grid, while the drawn spectrum represents the pixel spanning the sampling location. For cases where values in the blue part of the spectrum were missing, the range to which n applies has been indicated.

Pigment analysis

Protocols for the extraction and quantification of photosynthetic pigments Chl *a* and PC have been described in detail elsewhere (Simis *et al.* 2005*a*, 2005*b*, Chapter 5). In short, PC was extracted by subjecting concentrated water samples to nine cycles of freezing at -20°C and thawing at room temperature based on Sarada *et al.* (1999). Supernatants were spectrophotometrically analysed to obtain phycobilipigment concentrations using published equations (Bennett and Bogorad 1973). Chl *a* was extracted from samples concentrated on glass fibre filters, in 80% hot (70°C) ethanol. The filtrate was spectrophotometrically analysed to yield concentrations of Chl *a* and phaeopigments (Moed and Hallegraeff 1987, NEN 1981). Chl *a* data are presented here as 'uncorrected' Chl *a*, i.e. the result of [Chl *a*] + 0.59 × [phaeopigments].

6.3. Results

Water surface retrieval

For lakes listed in Table 2 except L. IJsselmeer, the relation between lake surface area and the number of water-classified pixels that could be retrieved from several scenes was explored (Figure 6.1). The selected scenes differed in atmospheric visibility: AOT(865) over the lakes was on average (± SD) 0.55 ± 0.17, 0.21 ± 0.13, and 0.28 ± 0.17 for scenes on 13 April 2003, 15 October 2003, and 16 Aug 2005, respectively. Between the first scenes few differences were found in the number of water pixels that could be retrieved over the lake sites, despite the different AOT(865). The third scene had a relatively heterogeneous AOT(865) and gave poor pixel density over some lakes. Extrapolating from linear regression results of 15 October 2003, the retrieval of water pixels experienced a cut-off at 0.54 km^2 or 7.2 pixels (one pixel is 0.075 km^2 based on 260-m across and 290-m along track resolution).

Validation of MERIS R_{RS}

Reflectance obtained from L2 MERIS imagery was compared with PR-650 field radiometric measurements for all (near-)matchup data (Figure 6.2). The comparison was poor for all bands when considering L. Loosdrecht and L. Ketelmeer. Comparisons of reflectances (paired t-tests) at L. IJsselmeer stations were poor in bands 1 – 4 and improved somewhat towards the red and NIR bands; only at 665 and 681.25 nm a significant relation was found (see table inset in Figure 6.2). MERIS R_{RS} usually compared best with PR-650 R_{RS} in the lower range of reflectance values. All considered images showed a value of the ratio R_{RS}(778.75/865) of approximately 2.3, which is well above the value of 1.8 which was validated for turbid waters (Ruddick *et al.* 2005, 2006). This high NIR ratio may indicate a shortcoming in atmospheric correction, as also indicated by overestimated R_{RS} values in the blue region.

L. IJsselmeer matchups

Figure 6.3 shows MERIS and PR-650 R_{RS} spectra at three sampling stations on L. IJsselmeer. Several matchups included in the first three scenes were good, although MERIS R_{RS} often increased towards the blue. Several sites showed MERIS spectra that were considerably lower than their PR-650 equivalent. In these situations phytoplankton biomass had accumulated near the water surface, and high NIR reflectance was measured in the field. High NIR values could have been misinterpreted as an atmospheric influence on the radiance arriving at the MERIS sensor, resulting in overcorrected MERIS R_{RS}. Not all sites with high PR-650 reflectances in the NIR had a poor match-up, however. Generally, the performance was better on days and locations with better atmospheric conditions.

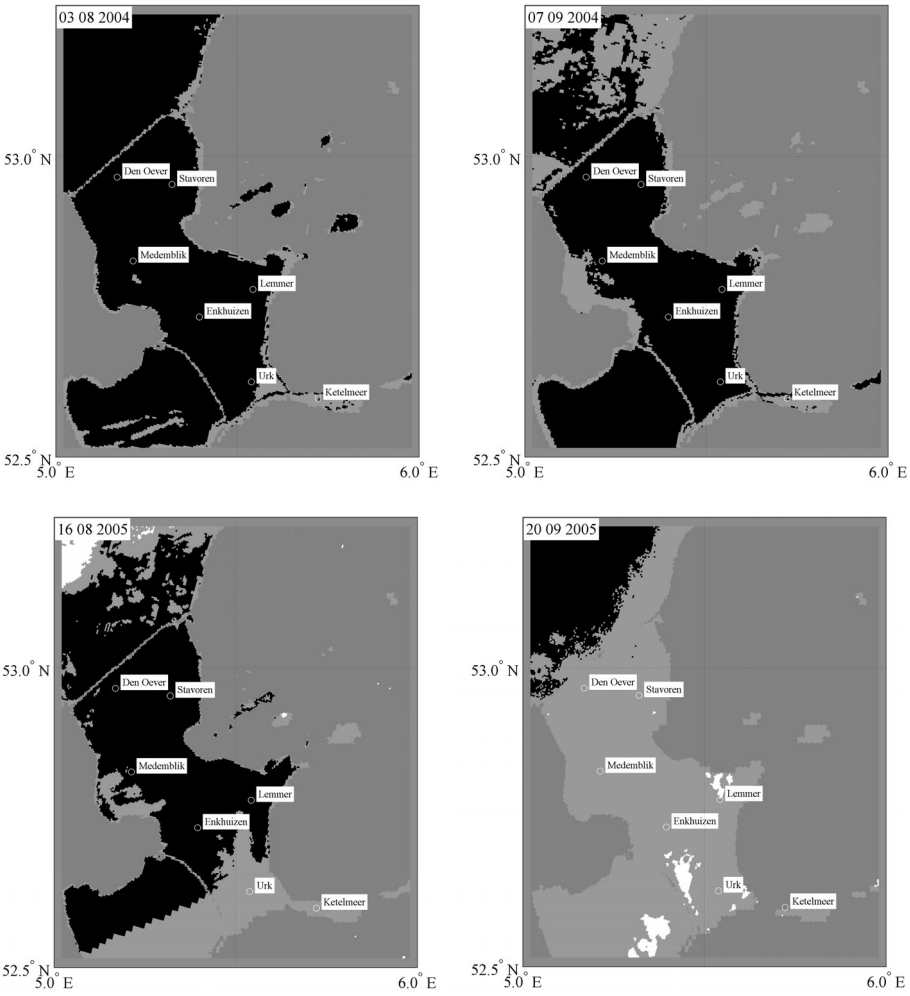

Figure 6.4. MERIS scenes over the Netherlands for the L. IJsselmeer and L. Ketelmeer matchup dates as shown in Figure 6.3. Legend: water, land, and cloud-classified surfaces were masked black, dark grey and white, respectively. Light grey areas are pixels where the PCD1_13 confidence flag was raised, indicating uncertain R_{RS} values. The sampling stations locations have been indicated.

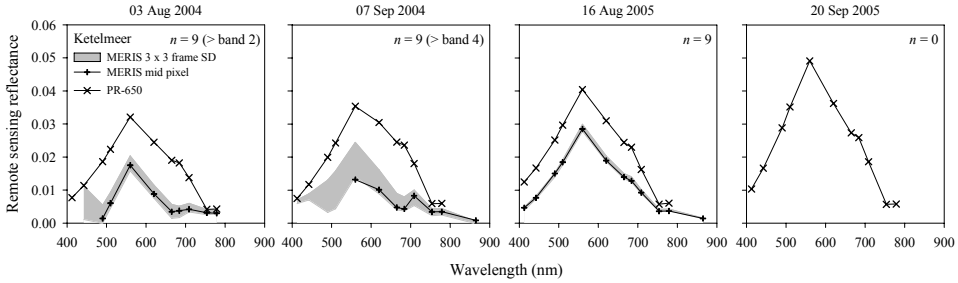

Figure 6.5. Same as Figure 6.3 but for the L. Ketelmeer sampling station.

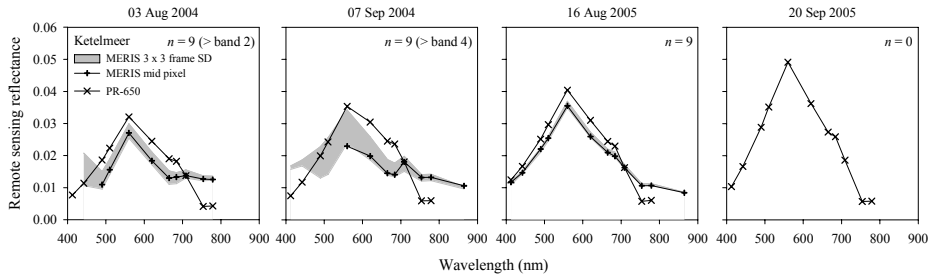

Figure 6.6. Same as Figure 6.5, but with MERIS R_{RS} spectra aligned to PR-650 spectra using the offset at 709 nm.

The quality of the MERIS scenes for each matchup was illustrated in figure 6.4 which shows the distribution of cloud cover and the product confidence flag PCD1_13 over the area. This composite flag represents a wide range of issues that reduce the confidence in the surface reflectance values and is often raised over inland water bodies. During the last two matchups extensive cloud cover occurred near the study sites, and unclassified cirrus clouds covered part of the image during the last matchup. The PCD1_13 flag was raised over large parts of the last two images, but not so in the first two scenes. These differences could explain why comparable PR-650 spectra, e.g. measured in the field station Medemblik, on 7 Sep 2004 and 20 Sep 2005, resulted in good and poor matchups, respectively.

L. Ketelmeer matchups

L. Ketelmeer is the main inlet for river water into L. IJsselmeer and characterized by high sediment loading and relatively low phytoplankton biomass. An island has been constructed near the center of the lake and close (< 0.5 km) to the sampling station. NIR reflectance of the field spectra were much lower than at the L. IJsselmeer sites where matchups were poor, yet the matchups at L. Ketelmeer were poor even under the favourable weather conditions of the first two matchup dates (Figure 6.5). Possibly

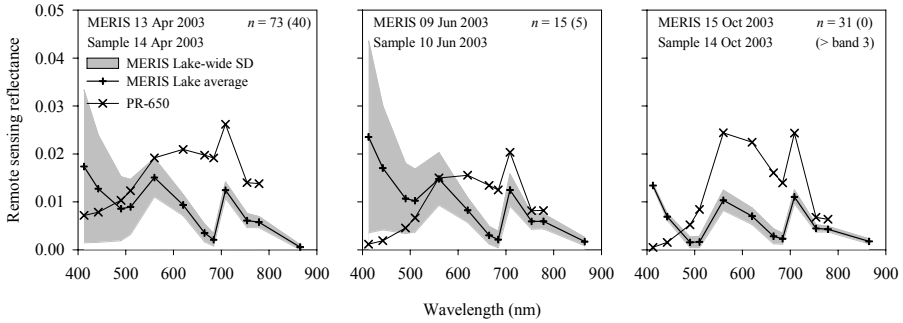

Figure 6.7. Near-matchup R_{RS} data of MERIS and PR-650 at L. Loosdrecht. Legend: *n* is the number of pixels in the lake for which the average (plus symbol) and standard deviation (grey area) of MERIS spectra were drawn.

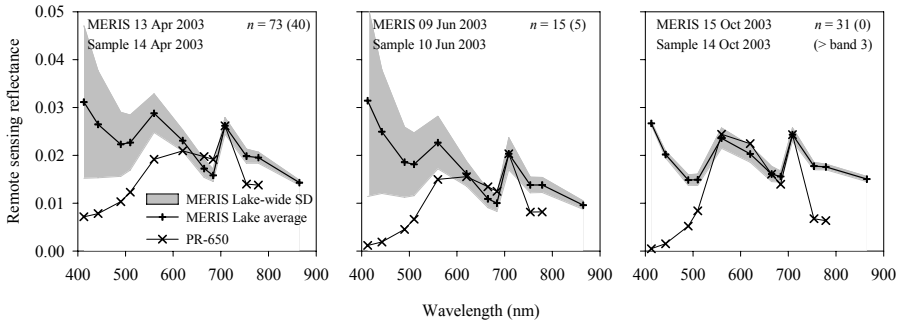

Figure 6.8. Same as Figure 6.7, but with MERIS R_{RS} spectra aligned with PR-650 spectra at 709 nm.

land reflectance 'contaminated' the signal NIR signal at the sensor, thus causing overcorrected MERIS R_{RS} spectra. This could also explain why R_{RS} in all of L. Ketelmeer was flagged as uncertain (PCD1_13) in the first two matchup scenes. Indeed, removal of the offset between MERIS and PR-650 spectra at 709 nm revealed relatively high NIR reflectances for the first two scenes while maintaining high similarity at the visible wavelengths (Figure 6.6).

L. Loosdrecht (near-matchups)

If there is an effect of adjacent land on the quality of the L2 MERIS imagery, this should be most clearly visible from matchups of the small and heterogeneously shaped L. Loosdrecht. Indeed, the near-matchup data gave poor results for all scenes. Some problems were related to the presence of clouds: cirrus clouds were visible but not classified as clouds in the L2 scene of 13 April 2003; scattered clouds obscured part of the lake on 9 June 2003 and cast shadows over other parts of the lake. Further, the scene obtained for 28 May 2003 did not yield any pixels with non-zero values in any

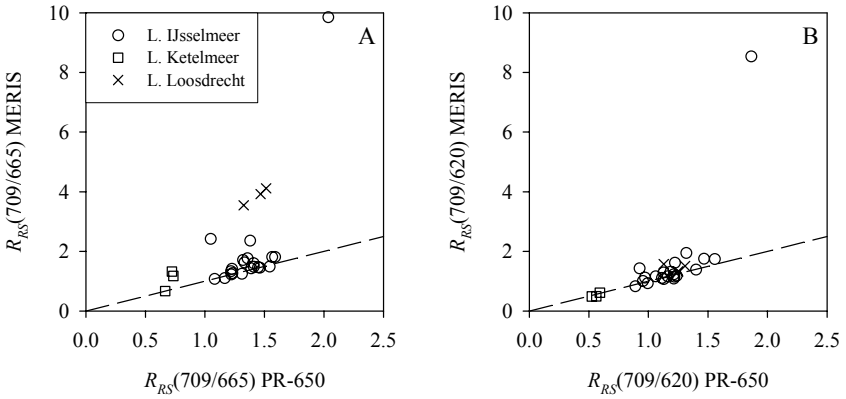

Figure 6.9. Comparison of the band ratios (**A**) R_{RS}(708.75/665) and (**B**) R_{RS}(708.75/620), obtained from L2 MERIS scenes and with the PR-650 field spectroradiometer. The obvious outlier, with both ratios > 8, was a situation with surfacing cyanobacterial bloom on 16 August 2005 at the L. IJsselmeer station near Urk. Two additional outliers of L. IJsselmeer with R_{RS}(708.75/665) > 2 were omitted from further analysis, both from the matchup at 20 September 2005, at stations Medemblik and Stavoren. For regression results based on the L. IJsselmeer data, refer to Table 6.4.

waveband, although atmospheric visibility was good. The image of 15 October 2003 was the clearest image of all images considered in this paper.

MERIS and field spectra differed significantly in shape and amplitude for all scenes (Figure 6.7). The offset between field and MERIS spectra at 709 nm was added to the MERIS spectra in the same way as described for L. Ketelmeer. A positive error in the blue region and the NIR was maintained after correcting the offset (Figure 6.8). These differences may again be explained in terms of poor atmospheric correction. First, the signal at the sensor would have been 'contaminated' by reflectance from adjacent land because L. Loosdrecht is very heterogeneously shaped and contains several small islands. Second, through elevated NIR reflectance, AOT(865) was overestimated, so that slight changes in the aerosol model (particularly the slope of attenuation towards the blue) could cause highly scattered blue reflectance values. This behaviour is indeed observed for the first two scenes plotted in figure 6.7 and 6.8. The aerosol epsilon parameter given with the L2 MERIS scene of 13 April 2003 was 1.063 ± 0.014 for central L. IJsselmeer pixels but as low as 1.00 ± 0.016 over L. Loosdrecht. This parameter describes the slope of the aerosol model and if chosen too low, reflectance may rise steeply towards the blue. Especially where AOT(865) was overestimated because of high NIR reflectance, an underestimate of the aerosol epsilon parameter may have caused the R_{RS} spectrum to be biased towards the blue.

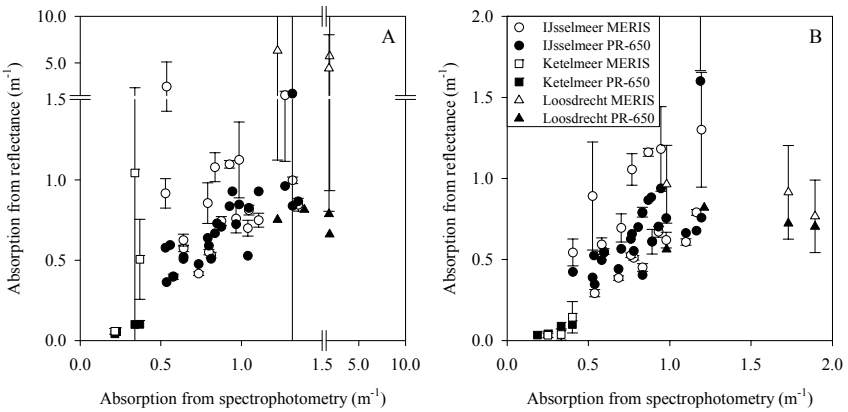

Figure 6.10. Comparison of the total absorption excluding water [$a_{TOT}(\lambda)$], retrieved from R_{RS} spectra of MERIS and PR-650 with spectrophotometric results, at (**A**) 665 nm and (**B**) 620 nm. Outliers of L. IJsselmeer data identified in figure 6.9 were omitted from the MERIS data set. Regression results for L. IJsselmeer data are given in Table 6.4.

Retrieval of water quality products from L2 imagery

The retrieval of phytoplankton biomass indicators such as the concentration of pigments Chl *a* and PC from turbid water bodies requires only a subset of the available MERIS bands. For Chl *a* estimation following Gons (1999) it is important to have a reasonable estimate of R_{RS}(778.75) and good retrieval of the ratio R_{RS}(708.75/665). PC retrieval (Simis *et al.* 2005*a*, Chapter 5) requires the same products and additionally the band ratio R_{RS}(708.75/620). Errors in specific bands are thus permitted as long as the ratios in which they participate are not affected. An example can be found in Figure 6.3 where MERIS and PR-650 data were matched at the station near Stavoren on 7 Sep 2004. The MERIS spectrum had an amplitude that was approximately half the amplitude of the field data. Despite the offset of the two spectra, the band ratios were equal within 4%. Figure 6.9 and regression results in Table 4 show that the band ratios described above were well retained through MERIS processing, as they compared well with PR-650 field measurements. Exceptions were cases of phytoplankton bloom in L. IJsselmeer which were mentioned above, and most matchups with L. Ketelmeer and L. Loosdrecht. These cases were omitted from further comparisons of MERIS R_{RS} band-ratio derived water quality parameters.

The PR-650 and MERIS-derived $a_{TOT}(665)$, $a_{TOT}(620)$, Chl *a*, and PC products were compared to their lab-measured equivalents. The absorption and pigment products are compared in figures 6.10 and 6.11, respectively. Regression results of absorption and pigment comparisons are given in Table 4. Both absorption and pigment products showed a higher positive trend when derived from MERIS then from PR650 data, but otherwise correspondence was fair. MERIS products were more scattered against the

laboratory measurements than PR-650 measurements were. From MERIS data, the retrieval of $a_{TOT}(620)$ and PC were least problematic.

Adopting atmospheric correction from L. IJsselmeer to L. Loosdrecht

A simplified local atmospherical correction (L2') was carried out for L. Loosdrecht on 15 October 2003. AOT(865) values given in the L2 product confirmed that the atmosphere was quite homogeneous over the area spanning the two lakes, which are separated by approximately 70 km of land and water. The average L2' spectrum (Figure 6.12) showed much stronger resemblance to the PR-650 spectrum for bands < 700 nm while the influence of land was now clear at longer wavelengths. The difference between L2' and PR-650 spectra in bands 6 – 8 could be explained by the 1-day difference between the field measurement and the MERIS observation, but it is possible that the atmospheric correction for L. Loosdrecht should have risen steeper towards the blue over L. Loosdrecht. The elevated $R_{RS}(708.75)$ in the L2' spectra compared to the PR-650 spectrum suggests the influence of adjacent land on the radiance at the sensor. Due to this elevated $R_{RS}(708.75)$ it was not possible to obtain an improved estimate of $a_{TOT}(665)$ and $a_{TOT}(620)$ compared to the L2 processing stage. In both cases, the PR-650 spectrum yielded Chl a = 51 mg m^{-3}, against 180 and 183 mg m^{-3} for the average L2 and L2' spectra, respectively. In this case, overcorrection of the MERIS R_{RS} spectrum did thus not solely contribute to the observed error. Unmixing of land and water influence on the signal measured at the sensors is therefore a definite requirement before useful water quality parameters can be derived from band ratio algorithms in this part of the spectrum, at least for lakes as small and heterogeneous as L. Loosdrecht.

Data filtering

Several product confidence and science flags included in the MERIS L2 product were raised for nearly all pixels that were included in the (near-)matchup dataset (Figure 6.13). For some flags this is expected behaviour: CASE2_S – indicating turbid water, CASE2_ANOM – bright water surface, CS2 | C2An – including either or both of the previous flags, and finally PCD_15 – flagging pixels not suitable for Case1 water processing (refer to Table 5 for a description of all mentioned MERIS flags). Other flags, when raised, may indicate fundamental problems associated with the image processing, such as a high percentage of pixels flagged with Dust-like absorbing aerosols (ABSOA_DUST) and a high percentage of pixels with uncertain AOT or aerosol type (PCD_19), only found over the smaller lakes. Finally, flag PCD_17 is raised when confidence for Case 2 water quality products is low, and would filter out 97 % of L. IJsselmeer pixels even though it was demonstrated here that acceptable products may be generated from these data.

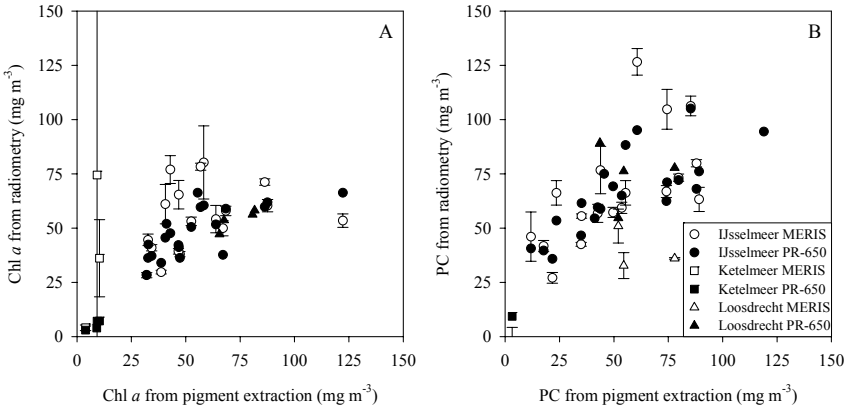

Figure 6.11. Pigment concentrations predicted from MERIS and PR-650 radiometry. (**A**) Chlorophyll *a*. Outliers of L. IJsselmeer (see figure 6.9) omitted from figures. Predictions for L. Loosdrecht from MERIS imagery exceeded 300 mg m^{-3} while pigment extraction yielded values ranging 50-70 mg m^{-3}. (**B**) Phycocyanin.

Table 6.4. Regression results for comparisons of L. IJsselmeer matchup data plotted in Figures 9-11 (outliers mentioned in figure 9 were omitted). Legend: regression coefficients $y = ax + b$, r^2 = coefficient of determination, n = number of pairs in t-test, p = probability resulting from paired t-test.

Regression	*a*	*b*	r^2	*n*	*p*
R_{RS}(709/665) MERIS vs. PR650	1.22	-0.18	0.58	18	< 0.01
a_{TOT}(665) MERIS vs. spectrophotometer	0.42	0.39	0.19	18	0.05
a_{TOT}(665) PR650 vs. spectrophotometer	0.53	0.22	0.55	21	< 0.001
[Chl *a*] MERIS vs. extraction	0.23	42.14	0.11	18	0.73
[Chl *a*] PR-650 vs. extraction	0.37	28.53	0.50	21	0.10
R_{RS}(709/620) MERIS vs. PR650	1.26	-0.24	0.74	18	0.09
a_{TOT}(620) MERIS vs. spectrophotometer	0.51	0.26	0.16	18	0.04
a_{TOT}(620) PR650 vs. spectrophotometer	0.55	0.19	0.41	21	< 0.001
[PC] MERIS vs. extraction	0.84	38.66	0.38	18	< 0.001
[PC] PR-650 vs. extraction	0.61	45.41	0.59	21	< 0.001

It may be possible to reduce the error in the retrieval of water quality parameters from MERIS imagery by applying a more restrictive data filter, heeding one or more of the product confidence flags provided with the L2 product. The filter criteria set up so far passed only pixels classified as water surface, thus not land or cloud, and pixels without zero values in bands 6, 7, 9 or 12. The results shown thus far indicate that further filtering of the data should focus on error in the atmospheric correction process, especially over areas with adjacent land, with phytoplankton bloom, or hazy atmosphere. PCD_19 is a composite flag made up of several indicators for poor atmospheric correction, but does not exclude pixels based on the Case 2 water algorithms input and output limitations like PCD_17 does. PCD_19 is also raised when the used aerosol model is not the aerosol model that would be expected from climatology, but not when AOT(865) values are just high; the PCD1_13 flag behaves exactly opposite.

To test whether adding any additional filter criteria could improve the quality of output of water quality parameters, without overly reducing data density, new filter combinations were tested for the number of output pixels and validity of the band ratio products for absorption in the 665 and 620-nm bands. Figure 6.14 shows the evolution of the root-mean-square error (RMSE) of these products as well as the number of valid pixels that resulted from different filter combinations, averaged per site over all (near-)matchup scenes. Only results for L. Ketelmeer and L. Loosdrecht are given; L. IJsselmeer had low per-site variance of the reflectance spectra, so additional filtering would not improved product quality. Like shown before, errors in the $a_{TOT}(620)$ product were far smaller than the error in $a_{TOT}(665)$. Filtering out all pixels with an AOT(865) value > 0.4 reduced the RMSE of $a_{TOT}(665)$ for L. Loosdrecht from 4.75 to 3.27, which is not sufficient. Further filters either increased RMSE or allowed very few pixels to remain. Additional filtering of L. Ketelmeer with PCD1_13 or PCD19 included in the filter markedly reduced the number of pixels (Fig. 14B), but not the $a_{TOT}(665)$ RMSE. Moreover, when filter PCD1_13 was used without PCD19, some anomalous pixels passed the filters while pixels with lower errors did not, which markedly increased the RMSE of $a_{TOT}(665)$. This suggests that allowing only small number of pixels to pass the data filter may significantly harm output product quality. It can be concluded from these results that the large errors associated with the $a_{TOT}(665)$ product, based on the ratio of reflectance at 709 and 665 nm, can not be excluded from the L2 product by the use of flag products delivered with the scenes. The errors were also not simply associated with high AOT(865) estimates, as may have been expected from our earlier results. However, it is noted that the threshold of AOT(865) > 0.4 may be too high to include all errors caused by atmospheric influence. Lowering the threshold would, however, also eliminate too many pixels.

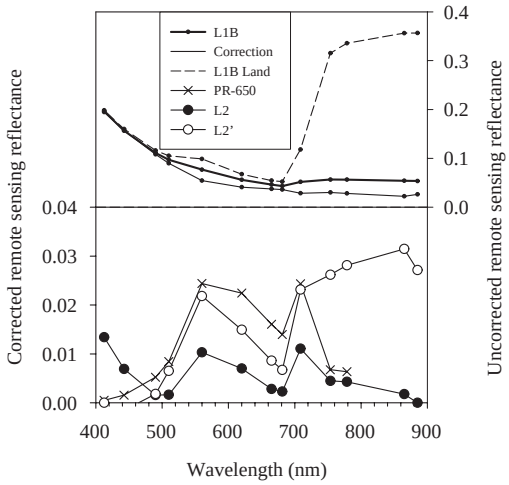

Figure 6.12. Different stages of atmospheric correction of L. Loosdrecht pixels for a scene of 15 October 2003. Error bars were omitted as spatial variation was low. For a description of the meaning of the various levels of processing, see text. A representative spectrum of land pixels around L. Loosdrecht was also included.

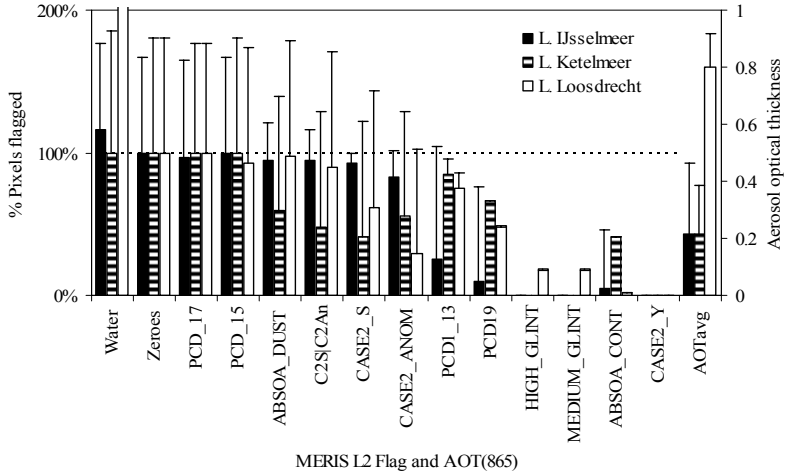

Figure 6.13. MERIS L2 product confidence (PCD) and science flags. AOT(865) plotted on the right axis as the lake-average for pixels passing the initial filter criteria, indicated as 'zeroes' and including water-classified pixels without zero-values in reflectance bands 6, 7, 9 or 12. The percentage of flagged pixels is given as the average for the 4 (near-)matchup dates of each lake, and error bars indicate standard deviation. For flag descriptions, see Table 6.5.

Table 6.5. Level 2 MERIS flag descriptions (source: BEAM software documentation).

Flag	Description
PCD_1_13	Uncertain R_{RS}
PCD_15	Uncertain Case-1 water products
PCD_17	Uncertain Case-2 water products
PCD_19	Uncertain aerosol type and AOT
ABSOA_CONT	Continental absorbing aerosol
ABSOA_DUST	Dust-like absorbing aerosol
CASE2_S	Turbid water
CASE2_ANOM	Anomalous scattering water
CASE2_Y	Yellow substance-loaded water
MEDIUM_GLINT	Pixel corrected for sun glint
HIGH_GLINT	Pixel uncorrected for high sun glint

6.4. Discussion

The current generation of satellite sensors can provide surface reflectance data at an unparalleled combination of temporal, spatial and spectral resolution. MERIS, designed to monitor the ocean, coastal, and land environment (Rast 1999), has thus far exceeded expectations concerning the quality of the raw data, although problems with overcorrected reflectance values for Case 2 waters have been identified (ESA 2004). The results presented here illustrate these problems for inland waters. Accurate reflectance spectra can be used to derive biomass indicators for phytoplankton and cyanobacteria in particular from a small set of NIR and red reflectance bands. However, overcorrection of R_{RS} spectra due to incorrect separation of NIR reflectance from the water and the atmosphere, may defy these algorithms. Unfortunately, additional data filtering does not guarantee reduced error of the water quality products, perhaps since none of the product confidence flags was dedicated to be used with the high-turbidity case 2 waters presented here.

High NIR reflectance measured at the sensor may derive from highly scattering water surfaces, or from atmospheric path radiance from adjacent land. By adopting the atmospheric correction parameters from unaffected areas, such as larger nearby water areas as shown here, or from patches of dense dark vegetation over land (Vidot and Santer 2005), the problem of bright scattering water may be dealt with adequately. Another approach is to predict the likely range of water-leaving reflectances from a bio-optical model and to set boundaries for atmospheric correction accordingly (Koponen *et al.* 2005).

Even if artefacts of poor atmospheric correction can be eliminated, the influence of adjacent land near the shoreline remains, and this poses a problem for satellite remote sensing over smaller inland water bodies. Typically, the adjacency effect wears off

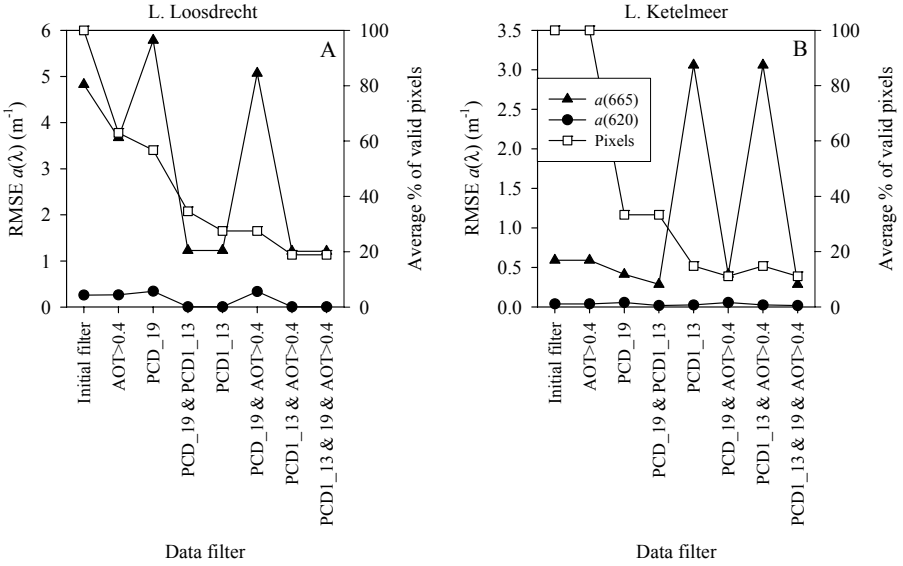

Figure 6.14. Root mean square error (RMSE) of the absorption products derived from MERIS spectra relative to lab spectrophotometry at 665 and 620 nm, plotted as a function of different data filter methods applied to the MERIS images. The RMSE values refer to the site-average of all error values in the (near-)matchup set, holding 4 scenes per site (panels). The number of valid pixels was plotted (right axis) relative to the total number available under the initial data filter (see text). The filter AOT>0.4 prevented pixels with an estimated aerosol optical thickness at 865 nm > 0.4 from passing. For a description of the product confidence flags (PCD) see Table 6.5. Combinations of filters indicated with the ampersand symbol were operated so that exclusion by any of the indicated filters caused exclusion of the pixel from the dataset.

within several pixels (approximately 1 km) from the shore, dependent on the extent of atmospheric scattering (Santer and Schmechtig 2000). In practice, all but the largest lakes presented in Table 2 will be influenced when dealing with imagery from a sensor with the viewing geometry of MERIS.

The lakes discussed here are highly turbid and eutrophic. Sediment, and CDOM absorption in the blue part of the spectrum are not coupled to phytoplankton biomass. Variable absorbance by the non-phytoplankton material prevents in these inland waters the use of blue-to-green reflectance ratio algorithms to estimate phytoplankton biomass. NIR/red band ratios to retrieve Chl *a* and derived products can be used, but land adjacency strongly influences the NIR reflectance signal of water-classified pixels. Thus, the combination of turbid water and small lake size is a definite problem. Adaptive schemes for the unmixing of land and water signatures over small lakes are therefore required before satellite sensors such as MERIS can be used for general inland water quality monitoring.

In conclusion, MERIS L2 products, claimed to suit land, ocean, and coastal water remote sensing applications, have potential for use with inland waters, but this is strongly limited by sensitivity of the atmospheric correction procedure to high NIR reflectance over turbid water pixels and near land. Water bodies with a surface area exceeding 0.54 km^2 (7.2 pixels) were correctly classified as water surfaces, but for most small lakes (< 100 pixels) additional strategies must be used to unmix land and water reflectance. It is advisable to apply locally valid parameters for atmospheric corrections to eliminate overcorrection of spectra, since near-zero reflectance values have the strongest effect on NIR/red band ratio algorithms. As long as such procedures are not implemented for operational use, MERIS cannot be routinely applied for water quality management.

6.5. Acknowledgments

The copyright of MERIS data lies with the European Space Agency. MERIS data was obtained through ESA/ENVISAT Category 1 project nr. 2729.

7. GENERAL DISCUSSION

The role of viruses in cyanobacterial population dynamics is poorly understood. Do viruses play a significant role in suppressing cyanobacterial bloom formation? Are viruses responsible for sudden clearing of cyanobacterial-dominated lakes? If so, which circumstances lead to these events, what is the physiological state of the hosts? Can viral activity be promoted to obtain a clear-water state in eutrophic lakes? Does epidemic infection and rapid decay of a large cyanobacterial biomass lead to yet unexplored ecological and health risks? These and many other questions will not be satisfactorily answered before the number of field studies of viral impact on bloom-forming cyanobacteria has increased. In most natural environments, populations of viruses and their hosts appear in balance, so catastrophic viral lysis is uncommon and may easily go by unnoticed. Optical detection methods can be used to frequently obtain up-to-date information on important lake water quality parameters. Knowledge of the optical characteristics of mass viral lysis of cyanobacteria may allow the use of optical remote sensing methods, to simultaneously search for mass lytic events in a large number of water bodies. Using remote sensing, the chances of identifying mass cyanobacterial lysis events in nature would be significantly increased, as long as the remote sensing instruments can provide qualitatively good data at regular intervals. This thesis provides an analysis of the potential of optical remote sensing methods to detect mass mortality of cyanobacteria by viruses. The main findings are discussed below.

7.1. Optical changes associated with cyanobacterial bloom termination

This thesis reports on experimental studies of mass mortality of cyanobacteria, associated with viral activity. For the lake water enclosure studies (**Chapter 2**) we used water from the turbid and eutrophic Lake Loosdrecht as an example of shallow peat lakes in Netherlands. The lake is perennially dominated by filamentous cyanobacteria, and after promoting their growth in the enclosures by nutrient addition—creating an environment of light-limited growth—their development halted within two weeks and mass lysis set in. Then, within several days, transparency increased markedly and the water changed from a green like pea soup to a pale yellow hue. It may be expected that such an event can be observed from space, when occurring lake-wide.

A marked decrease in both scattering and absorption of light was observed during the mass lysis in the enclosure experiments. Changes in the light absorption spectra indicated the disappearance of photosynthetic pigments—first the blue phycocyanin, then the green chlorophyll *a*. Yellow-coloured dissolved organic matter was released from the cells to be washed out of the system or slowly degraded by heterotrophic

bacteria. In contrast, the phycocyanin pigment disappeared rapidly, very likely because it provides a rich food source for the heterotrophic bacteria. Considerable amounts of chlorophyll *a* remained in the column, both in unaffected species and associated with cell debris. The results suggest that the ratio of phycocyanin to chlorophyll *a* is a sound indicator of the lytic event. After lysis, succession by various green algal species was observed.

To detect mass lytic events in nature, timing is crucial. Considering the cyanobacteria-rich, eutrophic lakes in the Netherlands, it is exceptional to obtain more than 1 cloud-free image of area per week, from most spaceborn sensors. Therefore it is most likely to catch only a glimpse of the situation before (during a bloom) and after mass lysis (clear water). It is as yet unknown whether mass lysis of cyanobacteria in nature will be immediately followed up by growth of other phytoplankton groups—like the green algae in the enclosures—or by other, unaffected cyanobacterial species. Alternatively, a clear state of the lake could persist for several days, weeks or even months as has been observed several times after unexplained mass mortality of cyanobacteria (Table 1.1).

The translation of bulk inherent optical properties of the water column to light reflectance was made in **Chapter 3**, as absorption and scattering properties of the water alone do not suffice to describe the appearance of a water body. The colour of water depends on (1) the quality and quantity of downwelling light that enters the water column, (2) the vertical attenuation of light in the water column by absorption and scattering, and (3) the quality and quantity of light scattered back towards the sensor. Backscattering is a weak signal compared to total scattering and absorption in the aquatic environment and is therefore difficult to assess, both in natural waters and in the laboratory. Measurements require dedicated equipment and are sensitive to instrumental error. We used an optical modelling approach to characterize the optical behaviour of a host-virus system from a culture collection. Drawbacks of this method are, as with any model, that the application to the natural situation may be awkward by simplifications in the experimental approach and in the model.

Two major conclusions could be drawn from the optical modelling approach. First, during mass lysis, a shift in the particle size distribution increased the intensity of particulate backscattering relative to total particulate scattering, although the backscattering probability remained low. The spectral shape of backscattered light did not change markedly. Second, the absorption signal did undergo dramatic changes in both intensity and shape. As was observed in the lake water enclosure experiments, the pigments contained in the cyanobacteria were quickly degraded when lysis occurred. This time, the release of coloured dissolved organic matter was not visible from absorption spectra, which was attributed to higher heterotrophic bacterial activity. As observed before, absorption of light by phycocyanin disappeared more rapidly than

absorption by chlorophyll *a*. Extrapolating these results to remote sensing, we find that the intensity of the recorded reflectance signal *may* increase during lysis, depending largely on the number of small particles released, and their persistence in the water column. The role of heterotrophic bacteria could be crucial here. An increase in the modelled reflectance was found around the maximum absorption of light by phycocyanin and chlorophyll *a* as a result of pigment degradation. These spectral changes proved indicative of the demise of the cyanobacterial population.

7.2. Remote sensing of cyanobacterial biomass

A remote sensing algorithm for the quantification of absorption by accessory photosynthetic pigments, focussing on the cyanobacterial pigment phycocyanin, was presented in **Chapter 4**. We found that a single parameterisation of the algorithm worked for two turbid, eutrophic lakes. However, errors in the algorithm prediction increased with decreasing phycocyanin : chlorophyll *a* ratios. Possibly, other optically active substances become more important light absorbers at low phycocyanin concentrations, most likely other photosynthetic pigments contained in green algae or diatoms.

To find out whether the algorithm would perform better with increasing cyanobacterial dominance and increasing phycocyanin : chlorophyll *a* ratios, a data set of pigment concentrations and spectroradiometry was compiled from water quality monitoring campaigns by the Centre for Hydrographic Studies of the CEDEX (Madrid, Spain) and new cruises at the Dutch Lake IJsselmeer. In **Chapter 5,** the algorithm was now validated for phycocyanin concentrations > 50 mg m^{-3}, allowing accurate monitoring of the pigment in eutrophic inland water. Higher phycocyanin : chlorophyll *a* ratios found in Spain appeared to reduce the problem of background absorption by other phytoplankton pigments. Overestimates by the algorithm were primarily linked to the presence of chlorophyll *b*, which is mainly present in green algae and prochlorophytes.

In terms of chlorophyll *a* content, green algae and cyanobacteria can be found in equal abundance during summer sampling cruises on L. IJsselmeer. The phycocyanin : chlorophyll *a* ratios found in this and similar lake environments are not as high as found in many Spanish lakes, likely a result of the mixed presence of phytoplankton groups and lower intracellular phycocyanin concentrations in the cyanobacteria. As a result, early development of cyanobacterial blooms may go unnoticed because the phycocyanin retrieval is hampered by the presence of green algal chlorophyll *b*. As soon as the cyanobacterial population starts to dominate the phytoplankton, or when light-limited growth promotes accessory pigment production, the algorithm estimate should improve. It is recommended to henceforth monitor the phycocyanin : chlorophyll *a* ratio wherever the phycocyanin estimate exceeds 50 mg m^{-3}.From the

bloom stage onward, cyanobacterial populations may thus be accurately monitored through their optical signature, including the situation where mass mortality occurs. Detection of the mass mortality event is, of course, only possible when the remote sensor is present around the transformation from the turbid to the clear-water situation. It is noted that in these studies no attention has yet been given to the increased influence of bottom reflectance on the water-leaving radiance, when transparency is improved as a result of mass lysis.

7.3. MERIS potential for inland water quality monitoring

The Medium Resolution Imaging Spectrometer is the only current spaceborn sensor to provide both global coverage and spectral bands suitable for the retrieval of the absorption signals of phycocyanin and chlorophyll in turbid water bodies. The sensitivity of the instrument is excellent, however in **Chapter 6** it was demonstrated that at least the atmospheric correction procedure applied to obtain the standard normalized surface reflectance is insufficient for brightly scattering water pixels. Such pixels are found where a high load of suspended sediment is present, or in case of phytoplankton bloom near or at the water surface. The errors seem to occur in the choice of the aerosol model and the estimation of aerosol optical thickness, which respectively cause an erroneous slope and amplitude of the water-leaving reflectance spectrum. A second problem was identified for the small lakes (< 10 km^2) that were studied. In these cases, the reflectance from adjacent land interfered with the signal measured at the sensor, causing elevated reflectance in the near-infrared. This so-called adjacency effect leads to misinterpretation of the contribution of the atmosphere to the signal at the sensor, and ultimately to reflectance values that are too low or even negative. The effect of these erroneous spectra on the predictions by the reflectance band ratio algorithms for chlorophyll *a* and phycocyanin were significant and no proper solution was found apart from reprocessing the imagery with a different configuration of the atmospheric correction processor. It is expected that the new version of this processor will give better performance and be less sensitive to elevated near-infrared reflectance. However, the differential signals derived from the water and from adjacent land would still need to be unmixed before the water quality parameters may be retrieved over small inland water bodies.

Unfortunately, specifically the small lakes are interesting in terms of cyanobacterial population dynamics. In lakes as large as L. IJsselmeer (1190 km^2) it would be difficult to assess whether disappearance of a patch of a dense cyanobacterial population was due to mortality, or to either horizontal or vertical redistribution of the cyanobacterial biomass. In small, shallow lakes that are generally well-mixed, and where species of cyanobacteria that control their buoyancy are not present, it is far

more likely that a drop in the observed phycocyanin : chlorophyll *a* ratio is related to cyanobacterial mortality.

In conclusion, current MERIS imagery did not appear useful for small (< 10 km^2) inland water bodies. However, we may still extrapolate from these results and consider future remote sensing approaches.

7.4. Outlook for remote sensing of cyanobacterial dynamics

Even in a 'wet' country such as the Netherlands, there are a limited number of recreational water bodies. Reasonable investments could thus be rewarding if up-to-date water quality can be communicated to the public. In addition, European governments are required by law to frequently provide information on water quality for all medium to large-sized lakes. Remote sensing can provide a significant contribution to standard monitoring programmes, and once potentially harmful cyanobacterial blooms are detected, conventional sampling can be efficiently directed to the site.

Satellite sensors with a broad viewing angle such as MERIS are not optimally suited to register the reflectance from the small water bodies which have important ecological and recreational functions. However, future instruments could work with smaller viewing angles, reducing the influence of reflectance signals that do not originate from the viewed water surface. Geostationary sensors can provide information whenever cloud cover permits and thus intensively monitor water colour. Closer to Earth, unmanned aircraft may be able to semi-continuously observe the water surface, depending on the balance between carrying an interesting payload and the capacity to generate sufficient power from solar cells. Finally, local optical sensors mounted on poles at lake sides, on ferries and oil rigs, can provide unparalleled data quality on water colour which, during the past decades, has proven to be a truly rich source of information on the ecological state of water bodies.

REFERENCES

Aas, E. 1996. Refractive index of phytoplankton derived from its metabolite composition. Journal of Plankton Research 18: 2223-2249.

Ahn, Y.H., A. Bricaud, and A. Morel. 1992. Light backscattering efficiency and related properties of some phytoplankters. Deep-Sea Research Part A-Oceanographic Research Papers 39: 1835-1855.

Anagnostidis, K., and J. Komárek. 1988. Modern approach to the classification system of cyanophytes. 3. Oscillatoriales. Archiv für Hydrobiologie. Supplementband. Algological Studies 80: 327-472.

Antoine, D., and A. Morel. 1999. A multiple scattering algorithm for atmospheric correction of remotely sensed ocean colour (MERIS instrument): principle and implementation for atmospheres carrying various aerosols including absorbing ones. International Journal of Remote Sensing 20: 1875-1916.

Asai, R., Y. Horiguchi, A. Yoshida, S. Mcniven, P. Tahira, K. Ikebukuro, S. Uchiyama, Y. Masuda, and I. Karube. 2001. Detection of phycobilin pigments and their seasonal change in lake kasumigaura using a sensitive in situ fluorometric sensor. Analytical Letters 34: 2521-2533.

Babin, M., and D. Stramski. 2002. Light absorption by aquatic particles in the near-infrared spectral region. Limnology and Oceanography 47: 911-915.

Babin, M., and D. Stramski. 2004. Variations in the mass-specific absorption coefficient of mineral particles suspended in water. Limnology and Oceanography 49: 756-767.

Balch, W.M., J.M. Vaughn, J.F. Novotny, D.T. Drapeau, R. Vaillancourt, J. Lapierre, and A. Ashe. 2000. Light scattering by viral suspensions. Limnology and Oceanography 45: 492-498.

Balch, W.M., J.M. Vaughn, J.F. Novotny, D.T. Drapeau, J.I. Goes, E. Booth, J.M. Lapierre, C.L. Vining, and A. Ashe. 2002. Fundamental changes in light scattering associated with infection of marine bacteria by bacteriophage. Limnology and Oceanography 47: 1554-1561.

Beltrami, E., and T.O. Carroll. 1994. Modeling the role of viral disease in recurrent phytoplankton blooms. Journal of Mathematical Biology 32: 857-863.

Bennett, A., and L. Bogorad. 1973. Complementary chromatic adaptation in a filamentous blue-green alga. The journal of cell biology 58: 419-435.

Bergh, Ø., K.Y. Børsheim, G. Bratbak, and M. Heldal. 1989. High abundance of viruses found in aquatic environments. Nature 340: 467-468.

Berman-Frank, I., K.D. Bidle, L. Haramaty, and P.G. Falkowski. 2004. The demise of the marine cyanobacterium, *Trichodesmium* spp., via an autocatalyzed cell death pathway. Limnology and Oceanography 49: 997-1005.

Bidigare, R.R., M.E. Ondrusek, J.H. Morrow, and D.A. Kiefer. 1990. In-vivo absorption properties of algal pigments. SPIE Proceedings on Ocean Optics X 1302: 290-302.

Bogorad, L. 1975. Phycobiliproteins and complementary chromatic adaptation. Annual review of plant physiology 26: 369-401.

Bohren, C.F., and D.R. Huffman. 1983. *Absorption and scattering of light by small particles*. New York: Wiley.

Bratbak, G., J.K. Egge, and M. Heldal. 1993. Viral mortality of the marine alga *Emiliania huxleyi* (Haptophyceae) and termination of algal blooms. Marine Ecology-Progress Series 93: 39-48.

Bricaud, A., A. Morel, and L. Prieur. 1981. Absorption by dissolved organic matter of the sea (yellow substance) in the UV and visible domains. Limnology and Oceanography 26: 43-53.

Bricaud, A., A. Morel, and L. Prieur. 1983. Optical efficiency factors of some phytoplankters. Limnology and Oceanography 28: 816-832.

Bricaud, A., A.L. Bedhomme, and A. Morel. 1988. Optical properties of diverse phytoplanktonic species - experimental results and theoretical interpretation. Journal of Plankton Research 10: 851-873.

Bricaud, A., M. Babin, A. Morel, and H. Claustre. 1995. Variability in the chlorophyll-specific absorption-coefficients of natural phytoplankton - analysis and parameterization. Journal of Geophysical Research-Oceans 100: 13321-13332.

Britton, G. 1983. *The biochemistry of natural pigments*. Cambridge University Press.

Brussaard, C.P.D., R.S. Kempers, A.J. Kop, R. Riegman, and M. Heldal. 1996. Virus-like particles in a summer bloom of *Emiliania huxleyi* in the North Sea. Aquatic Microbial Ecology 10: 105-113.

Brussaard, C.P.D. 2004. Viral control of phytoplankton populations - a review. Journal of Eukaryotic Microbiology 51: 125-138.

Bryant, D.A. 1981. The photoregulated expression of multiple phycocyanin species. European Journal of Biochemistry 119: 425-429.

Bryant, D.A. [ed.]. 1994. The molecular biology of cyanobacteria. Dordrecht: Kluwer Academic Publishers.

Buiteveld, H., J.H.M. Hakvoort, and M. Donze. 1994. The optical properties of pure water. SPIE Proceedings on Ocean Optics XII 2258: 174-183.

Butler, W.L. 1962. Absorption of light by turbid materials. Journal of the Optical Society of America 52: 292.

Campbell, J.B. 2002. *Introduction to remote sensing* (3rd ed.). The Guilford Press, New York.

Cartaxana, P., B. Jesus, and V. Brotas. 2003. Pheophorbide and pheophytin a-like pigments as useful markers for intertidal microphytobenthos grazing by *Hydrobia ulvae*. Estuarine Coastal and Shelf Science 58: 293-297.

Chorus, I., and Bartram, J. [Eds.]. 1999. Toxic Cyanobacteria in Water: a guide to their public health consequences, monitoring and management. World Health Organization, Geneva.

Cleveland, J.S., and A.D. Weidemann. 1993. Quantifying absorption by aquatic particles - a multiple-scattering correction for glass-fiber filters. Limnology and Oceanography 38: 1321-1327.

Dekker, A.G., T.J. Malthus, and E. Seyhan. 1991. Quantitative modeling of inland water-quality for high-resolution mss systems. IEEE Transactions on Geoscience and Remote Sensing 29: 89–95.

Dekker, A.G. 1993. Detection of optical water quality parameters for eutrophic waters by high resolution remote sensing. Phd Thesis. Vrije Universiteit Amsterdam.

Des Marais, D.J. 2000. When did photosynthesis emerge on Earth? Science 289: 1703-1705.

Dick, E. C., L.C. Jennings, K.A. Mink, C.D. Wartgow, and S.L. Inhorn. 1987. Aerosol transmission of rhinovirus colds. Journal of Infectious Diseases. 156: 442-448.

ESA. 2004. MERIS products quality status report. http://earth.esa.int/pcs/envisat/meris/documentation.

ESA. 2005. MERIS products and algorithms. *In* MERIS product handbook, pp. 222-226. http://envisat.esa.int/dataproducts/meris.

Ficek, D., S. Kaczmarek, J. Ston-Egiert, B. Wozniak, R. Majchrowski, and J. Dera. 2004. Spectra of light absorption by phytoplankton pigments in the baltic; conclusions to be drawn from a gaussian analysis of empirical data. Oceanologia 46: 533-555.

Francis, G. 1878. Poisonous austrialian lake. Nature 18: 11-12.

Gons, H.J., J.H. Otten, and M. Rijkeboer. 1991. The significance of wind resuspension for the predominance of filamentous cyanobacteria in a shallow, eutrophic lake. Memorie Dell' Istituto Italiano di Idrobiologia Dott. Marco De Marchi 48: 233-249.

Gons, H.J., J. Kromkamp, M. Rijkeboer, and O. Schofield. 1992. Characterization of the light-field in laboratory scale enclosures of eutrophic lake water (Lake Loosdrecht, the Netherlands). Hydrobiologia 238: 99-109.

Gons, H.J. 1999. Optical teledetection of chlorophyll a in turbid inland waters. Environmental Science & Technology 33: 1127-1132.

Gons, H.J., M. Rijkeboer, S. Bagheri, and K.G. Ruddick. 2000. Optical teledetection of chlorophyll *a* in estuarine and coastal waters. Environmental Science & Technology 34: 5189-5192.

Gons, H.J., J. Ebert, H.L. Hoogveld, L. van den Hove, R. Pel, W. Takkenberg, and C.J. Woldringh. 2002*a*. Observations on cyanobacterial population collapse in eutrophic lake water. Antonie Van Leeuwenhoek International Journal of General and Molecular Microbiology 81:319-326.

Gons, H.J., M. Rijkeboer, and K. G. Ruddick. 2002*b*. A chlorophyll-retrieval algorithm for satellite imagery (Medium Resolution Imaging Spectrometer) of inland and coastal waters. Journal of Plankton Research 24: 947-951.

Gons, H.J., M. Rijkeboer, and K.G. Ruddick. 2005. Effect of a waveband shift on chlorophyll retrieval from meris imagery of inland and coastal waters. Journal of Plankton Research 27: 125-127.

Gons, H.J., H.L. Hoogveld, S.G.H. Simis, and M. Tijdens. 2006. Dynamic modelling of viral impact on cyanobacterial populations in shallow lakes: implications of burst size. Journal of the Marine Biological Association of the United Kingdom 86: 537-542.

Gordon, H.R., O.B. Brown, and M.M. Jacobs. 1975. Computed relationships between the inherent and apparent optical properties of a flat homogeneous ocean. Applied Optics 14: 417-427.

Griffiths, B.M. 1939. Early references to water-blooms in British lakes. Proceedings of the Linnean Society of London 151: 12-19.

Grossman, A.R., M.R. Schaffer, G.G. Chiang, and J.L. Collier. 1993. Environmental-effects on the light-harvesting complex of cyanobacteria. Journal of Bacteriology 175: 575-582.

Hoepffner, N., and S. Sathyendranath. 1992. Bio-optical characteristics of coastal waters: Absorption spectra of phytoplankton and pigment distribution in the western north atlantic. Limnology and Oceanography 37: 1660-1679.

Hoepffner, N., and S. Sathyendranath. 1993. Determination of the major groups of phytoplankton pigments from the absorption-spectra of total particulate matter. Journal of Geophysical Research-Oceans 98: 22789-22803.

Izydorczyk, K., M. Tarczynska, T. Jurczak, J. Mrowczynski, and M. Zalewski. 2005. Measurement of phycocyanin fluorescence as an online early warning system for cyanobacteria in reservoir intake water. Environmental Toxicology 20: 425-430.

Jupp, D.L.B., J.T.O. Kirk, and G.P. Harris. 1994. Detection, identification and mapping of cyanobacteria - using remote-sensing to measure the optical-quality of turbid inland waters. Australian Journal of Marine and Freshwater Research 45: 801-828.

Kieber, R.J., X.L. Zhou, and K. Mopper. 1990. Formation of carbonyl-compounds from UV-induced photodegradation of humic substances in natural waters - fate of riverine carbon in the sea. Limnology and Oceanography 35: 1503-1515.

Kiefer, D.A., and J.B. Soohoo. 1982. Spectral absorption by marine particles of coastal waters of Baja California. Limnology and Oceanography 27: 492-499.

Kirk, J.T.O. 1994. *Light and photosynthesis in aquatic ecosystems*, 2nd ed. Cambridge University Press.

Koponen, S., J. Vepsäläinen, J. Pullianinen, K. Kallio, T. Pyhälahti, A. Lindfors, K. Rasmus, and M. Hallikainen. 2005. Using MERIS data for the retrieval of Chl-a, CDOM, and TSS values in the Gulf of Finland and Lake Lohjanjärvi. MERIS-(A)ATSR Workshop. ESA, Frascati, Italy.

Kramer, C.J.M. 1979. Degradation by sunlight of dissolved fluorescing substances in the upper layers of the eastern atlantic-ocean. Netherlands Journal of Sea Research 13: 325-329.

Latimer, P., A. Brunsting, B.E. Pyle, and C. Moore. 1978. Effects of asphericity on single particle scattering. Applied Optics 17: 3152-3158.

Lee, T., M. Tsuzuki, T. Takeuchi, K. Yokoyama, and I. Karube. 1994. In-vivo fluorometric method for early detection of cyanobacterial waterblooms. Journal of Applied Phycology 6: 489-495.

Levin. B.R., F.M. Stewart, and L. Chao. 1977. Resource-limited growth, competition, and predation: A model and experimental studies with bacteria and bacteriophage. American Naturalist 111: 3-24.

Lewin, R.A., and P.T. Robinson. 1979. The greening of polar bears in zoos. Nature 278: 445-447.

Maranger, R., P.A. Del Giorgio, and D.F. Bird. 2002. Accumulation of damaged bacteria and viruses in lake water exposed to solar radiation. Aquatic Microbial Ecology 28: 213-227.

Maske, H., and H. Haardt. 1987. Quantitative *in vivo* absorption spectra of phytoplankton: Detrital absorption and comparison with fluorescence excitation spectra. Limnology and Oceanography 32: 620-633.

Mie, G. 1908. Contribution on optical properties of turbid solutions, with special reference to colloidal metallic solutions. Annalen der Physik vol. 25: 337-445.

Mishchenko, M.I., L.D. Travis, and A.A. Lacis. 2002. *Scattering, absorption, and emission of light by small particles*. Cambridge University Press.

Mitchell, B.G. 1990. Algorithms for determining the absorption coefficient of aquatic particulates using the quantitative filter technique (QFT). SPIE Proceedings on Ocean Optics X 1302: 137-148.

Mittenzwey, K.H., S. Ullrich, A.A. Gitelson, and K.Y. Kondratiev. 1992. Determination of chlorophyll-a of inland waters on the basis of spectral reflectance. Limnology and Oceanography 37: 147-149.

Mobley, C.D. 1994. *Light and water: Radiative transfer in natural waters*. San Diego, California: Academic Press.

Mobley, C.D. 1999. Estimation of the remote-sensing reflectance from above-surface measurements. Applied Optics 38: 7442-7455.

Moed, J.R., and G.M. Hallegraeff. 1978. Some Problems in the Estimation of Chlorophyll-*a* and Phaeopigments from Pre- and Post-acidification Spectrophotometric Measurements. Internationale Revue der Gesamten Hydrobiologie 63: 787-800.

Montagner, F. 2001. Reference model for MERIS Level 2 processing. Issue 4, rev. 1. MERIS ESL doc. nr. PO-TN-MEL-GS-0026. ACRI.

Moore, G.F., J. Aiken, and S.J. Lavender. 1999. The atmospheric correction of water colour and the quantitative retrieval of suspended particulate matter in Case II waters: application to MERIS. International Journal of Remote Sensing 20: 1713-1733.

Moore, L.R., R. Goericke, and S.W. Chisholm. 1995. Comparative physiology of synechococcus and prochlorococcus: Influence of light and temperature on growth, pigments, fluorescence and absorptive properties. Marine Ecology Progress Series 116: 259-275.

Morel, A., and A. Bricaud. 1986. Inherent properties of algal cells including picoplankton: Theoretical and experimental results, p. 521-559. *In* T. Platt and W.K.W. Li [eds.], *Photosynthetic picoplankton.* Canadian bulletin of fisheries and aquatic sciences.

Morel, A., and B. Gentili. 1991. Diffuse reflectance of oceanic waters - its dependence on sun angle as influenced by the molecular-scattering contribution. Applied Optics 30: 4427-4438.

Morel, A., and Y.H. Ahn. 1991. Optics of heterotrophic nanoflagellates and ciliates - a tentative assessment of their scattering role in oceanic waters compared to those of bacterial and algal cells. Journal of Marine Research 49: 177-202.

Morel, A., and B. Gentili. 1993. Diffuse-reflectance of oceanic waters. 2. Bidirectional aspects. Applied Optics 32: 6864-6879.

NEN. 1981. NEN 6520: Water - spectrophotometric determination of chlorophyll *a* content. Netherlands Institute for Standardization.

Noble, R.T., and J.A. Fuhrman. 1998. Use of SYBR green I for rapid epifluorescence counts of marine viruses and bacteria. Aquatic Microbial Ecology 14: 113-118.

Pel, R., H. Hoogveld, and V. Floris. 2003. Using the hidden isotopic heterogeneity in phyto- and zooplankton to unmask disparity in trophic carbon transfer. Limnology and Oceanography 48: 2200-2207.

Petzold, T.J. 1972. Volume scattering functions for selected ocean waters. Contract No. N62269-71-C-0676, UCSD, Scripps Institution of Oceanography, California, Ref. 72-78.

Petzold, T.J. 1977. Volume scattering functions for selected ocean waters., p. 152-174. *In* J.E.Tyler [ed.], *Light in the sea*. Strounburg, Pennsylvania: Dowden, Hitchinsons and Ross Inc.

Pope, R.M., and E.S. Fry. 1997. Absorption spectrum 380–700 nm of pure water. II. Integrating cavity measurements. Applied Optics 36: 8710–8723.

Porter, K.G. 1973. Selective Grazing and Differential Digestion of Algae by Zooplankton. Nature 244:179-180.

Proctor, L.M., and J.A. Fuhrman. 1990. Viral mortality of marine-bacteria and cyanobacteria. Nature 343: 60-62.

Quesada, A., and W.F. Vincent. 1993. Adaptation to the light regime within antarctic cyanobacterial mats. Verhandlungen Internationale Vereinigung für Theoretische und Angewandte Limnologie 25: 960-965.

Rast, M., J.L. Bezy, and S. Bruzzi. 1999. The ESA Medium Resolution Imaging Spectrometer MERIS – a review of the instrument and its mission. International Journal of Remote Sensing 20: 1681-1702.

Raven, J.A. 1984. A cost-benefit analysis of photon absorption by photosynthetic unicells. New Phytologist 98: 593-625.

Richman, S., and S.I. Dodson. 1983. The effect of food quality on feeding and respiration by *Daphnia* and *Diaptomus*. Limnology and Oceanography 28: 948-956.

Rijkeboer, M., F. Debles, and H.J. Gons. 1990. Laboratory scale enclosure - concept, construction and operation. Journal of Plankton Research 12: 231-244.

Rijkeboer, M., A.G. Dekker, and H.J. Gons. 1998. Subsurface irradiance reflectance spectra of inland waters differing in morphometry and hydrology. Aquatic Ecology 31: 313-323.

Rijstenbil, J.W. 2003. Effects of UVB radiation and salt stress on growth, pigments and antioxidative defence of the marine diatom *Cylindrotheca closterium*. Marine Ecology-Progress Series 254: 37-47.

Roesler, C.S. 1998. Theoretical and experimental approaches to improve the accuracy of particulate absorption coefficients derived from the quantitative filter technique. Limnology and Oceanography 43: 1649-1660.

Ruddick, K., V. De Cauwer, and B. Van Mol. 2005. Use of the near infrared similarity reflectance spectrum for the quality control of remote sensing data. SPIE International Symposium on Optics and Photonics: Remote sensing of the coastal oceanic environment, San Diego, USA.

Ruddick, K., V. De Cauwer, and B. Van Mol. 2006. Seaborne measurements of near infrared water-leaving reflectance: The similarity spectrum for turbid waters. Limnology and Oceanography 51: 1167-1179.

Safferman, R.S., and M.E. Morris. 1964. Growth characteristics of blue-green algal virus LPP-1. Journal of Bacteriology 88: 771-&.

Santer, R., and C. Schmechtig. 2000. Adjacency effects on water surfaces: Primary scattering approximation and sensitivity study. Applied Optics 39: 361-375.

Sarada, R., M.G. Pillai, and G.A. Ravishankar. 1999. Phycocyanin from *Spirulina sp.*: influence of processing of biomass on phycocyanin yield, analysis of efficacy of extraction methods and stability studies on phycocyanin. Process Biochemistry 34: 795-801.

Sathyendranath, S., L. Lazzara, and L. Prieur. 1987. Variations in the spectral values of specific absorption of phytoplankton. Limnology and Oceanography 32: 403-415.

Schalles, J.F., and Y.Z. Yacobi. 2000. Remote detection and seasonal patterns of phycocyanin, carotenoid and chlorophyll pigments in eutrophic waters. Archiv für Hydrobiologie Special Issues Advances in Limnology 55: 153-168.

Schiller, H., and R. Doerffer. 1999. Neural network for emulation of an inverse model operational derivation of case II water properties from MERIS data. International Journal of Remote Sensing 20: 1735-1746.

Schopf, J.W. 2000. The fossil record: tracing the roots of the cyanobacterial lineage, p. 13-35. *In* B.A. Whitton and M. Potts [Eds.], *The ecology of cyanobacteria: their diversity in time and space.* Dordrecht: Kluwer Academic Publishers.

Segelstein, D.J. 1981. The complex refractive index of water. MSc Thesis. Department of Physics. University of Missouri-Kansas City.

Shibata, A., K. Kogure, I. Koike, and K. Ohwada. 1997. Formation of submicron colloidal particles from marine bacteria by viral infection. Marine Ecology Progress Series 155: 303-307.

Simis, S.G.H., S.W.M. Peters, and H.J. Gons. 2005*a*. Remote sensing of the cyanobacterial pigment phycocyanin in turbid inland water. Limnology and Oceanography 50: 237-245.

Simis, S.G.H., M. Tijdens, H.L. Hoogveld, and H.J. Gons. 2005*b*. Optical changes associated with cyanobacterial bloom termination by viral lysis. Journal of Plankton Research 27: 937-949.

Smith, R.C., and K.S. Baker. 1981. Optical properties of the clearest natural waters (200-800 nm). Applied Optics 20: 177-184.

Sogandares, F.M., and E.S. Fry. 1997. Absorption spectrum (340-640 nm) of pure water. 1. Photothermal measurements. Applied Optics 36: 8699-8709.

Staehr, P.A., P. Henriksen, and S. Markager. 2002. Photoacclimation of four marine phytoplankton species to irradiance and nutrient availability. Marine Ecology-Progress Series 238: 47-59.

Stewart, D.E., and F.H. Farmer. 1984. Extraction, identification, and quantitation of phycobiliprotein pigments from phototrophic plankton. Limnology and Oceanography 29: 392-397.

Stramski, D., A. Morel, and A. Bricaud. 1988. Modeling the light attenuation and scattering by spherical phytoplanktonic cells - a retrieval of the bulk refractive-index. Applied Optics 27: 3954-3956.

Stramski, D., and D.A. Kiefer. 1991. Light-scattering by microorganisms in the open ocean. Progress in Oceanography 28: 343-383.

Stramski, D., F. Rassoulzadegan, and D.A. Kiefer. 1992. Changes in the optical-properties of a particle suspension caused by protist grazing. Journal of Plankton Research 14: 961-977.

Stramski, D., and R.A. Reynolds. 1993. Diel variations in the optical-properties of a marine diatom. Limnology and Oceanography 38: 1347-1364.

Stramski, D., and C.D. Mobley. 1997. Effects of microbial particles on oceanic optics: A database of single-particle optical properties. Limnology and Oceanography 42: 538-549.

Stramski, D., E. Boss, D. Bogucki, and K.J. Voss. 2004. The role of seawater constituents in light backscattering in the ocean. Progress in Oceanography 61: 27-56.

Stramski, D., and S.B. Wozniak. 2005. On the role of colloidal particles in light scattering in the ocean. Limnology and Oceanography 50: 1581-1591.

Suttle, C.A. 1994. The significance of viruses to mortality in aquatic microbial communities. Microbial Ecology 28: 237-243.

Tandeau de Marsac, N. 1977. Occurrence and nature of chromatic adaptation in cyanobacteria. Journal of Bacteriology 130: 82-91.

Tassan, S., and G.M. Ferrari. 1995. An alternative approach to absorption measurements of aquatic particles retained on filters. Limnology and Oceanography 40: 1358-1368.

Tassan, S., G.M. Ferrari, A. Bricaud, and M. Babin. 2000. Variability of the amplification factor of light absorption by filter-retained aquatic particles in the coastal environment. Journal of Plankton Research 22: 659-668.

Thingstad, T.F. and R. Lignell. 1997. Theoretical models for the control of bacterial growth rate, abundance, diversity and carbon demand. Aquatic Microbial Ecology 13: 19-27.

Thingstad, T.F. 2000. Elements of a theory for the mechanisms controlling abundance, diversity, and biogeochemical role of lytic bacterial viruses in aquatic systems. Limnology and Oceanography 45: 1320-1328.

Tyler, J.E. 1960. Radiance distribution as a function of depth in an underwater environment. . Bulletin of the Scripps Institution of Oceanography of the University of California 7: 363-411.

Ulloa, O., S. Sathyendranath, and T. Platt. 1994. Effect of the particle-size distribution on the backscattering ratio in seawater. Applied Optics 33: 7070-7077.

V. Esenbeck, N. 1836. Ueber einen blau-rothen Farbstoff, der sich bei der zersetzung von Oscillatorien bildet. Annalen der Pharmacie 17: 75-82.

Van Hannen, E.J., G. Zwart, M.P. Van Agterveld, H.J. Gons, J. Ebert, and H.J. Laanbroek. 1999. Changes in bacterial and eukaryotic community structure after mass lysis of filamentous cyanobacteria associated with viruses. Applied and Environmental Microbiology 65: 795-801.

Van de Hulst, H.C. 1957. *Scattering of light by small particles*. New York: Wiley.

Van Liere, L., and R.D. Gulati [eds.]. 1992. *Restoration and recovery of shallow eutrophic lake ecosystems in the Netherlands*. Developments in Hydrobiology 287. Dordrecht: Kluwer Academic Publishers.

Van Tongeren, O.F.R., L. Van Liere, R.D. Gulati, G. Postema, and J. Boesewinkel-De Bruyn. 1992. Multivariate analysis of the plankton communities in the loosdrecht lakes: Relationship with the chemical and physical environment. Hydrobiologia 233: 105–117.

Vidot, J., and R. Santer. 2005. Atmospheric correction for inland waters - application to SeaWiFS. International Journal of Remote Sensing 26: 3663-3682.

Vincent, R.K., X.M. Qin, R.M.L. Mckay, J. Miner, K. Czajkowski, J. Savino, and T. Bridgeman. 2004. Phycocyanin detection from landsat tm data for mapping cyanobacterial blooms in Lake Erie. Remote Sensing of Environment 89: 381-392.

Viskari, P.J., and C.L. Colyer. 2002. Separation and quantitation of phycobiliproteins using phytic acid in capillary electrophoresis with laser-induced fluorescence detection. Journal of Chromatography A 972: 269-276.

Viskari, P.J., and C.L. Colyer. 2003. Rapid extraction of phycobiliproteins from cultured cyanobacteria samples. Analytical Biochemistry 319: 263-271.

Volten, H., J.F. De Haan, J.W. Hovenier, R. Schreurs, W. Vassen, A.G. Dekker, H.J. Hoogenboom, F. Charlton, and R. Wouts. 1998. Laboratory measurements of angular distributions of light scattered by phytoplankton and silt. Limnology and Oceanography 43: 1180-1197.

Vos, R.J., J.H.M. Hakvoort, R.W.J. Jordans, and B.W. Ibelings. 2003. Multiplatform optical monitoring of eutrophication in temporally and spatially variable lakes. Science of the Total Environment 312: 221-243.

Wetzel, R.G. 2001. *Limnology: Lake and river ecosystems*. Third ed. San Diego, California: Academic Press.

Wilson, W.H., N.G. Carr, and N.H. Mann. 1996. The effect of phosphate status on the kinetics of cyanophage infection in the oceanic cyanobacterium synechococcus sp wh7803. Journal of Phycology 32: 506-516.

Wilson, W.H., and N.H. Mann. 1997. Lysogenic and lytic viral production in marine microbial communities. Aquatic Microbial Ecology 13: 95-100.

Wilson, W.H., S. Turner, and N.H. Mann. 1998. Population dynamics of phytoplankton and viruses in a phosphate-limited mesocosm and their effect on DMSP and DMS production. Estuarine Coastal and Shelf Science 46: 49-59.

Wyman, M., and P. Fay. 1986. Underwater light climate and the growth and pigmentation of planktonic blue-green-algae (cyanobacteria). 1. The influence of light quantity. Proceedings Of The Royal Society Of London Series B-Biological Sciences 227: 367-380.

Wyman, M., and P. Fay. 1986. Underwater light climate and the growth and pigmentation of planktonic blue-green-algae (cyanobacteria). 2. The influence of light quality. Proceedings Of The Royal Society Of London Series B-Biological Sciences 227: 381-393.

Yentsch, C.S. 1962. Measurement of visible light absorption by particulate matter in the ocean. Limnology and Oceanography 7: 207-217.

Zwart, G., M.P. Kamst-Van Agterveld, I. Van Der Werff-Staverman, F. Hagen, H.L. Hoogveld, and H.J. Gons. 2005. Molecular characterization of cyanobacterial diversity in a shallow eutrophic lake. Environmental Microbiology 7: 365-377.

SAMENVATTING

Dit proefschrift beschrijft de kleurveranderingen van water waarin een dichte populatie blauwalgen snel sterft als gevolg van een virusziekte. De hoofdvraag is daarbij of deze kleurveranderingen vanuit de ruimte (met behulp van satellieten) kunnen worden waargenomen wanneer ze in troebele, voedselrijke meren plaatsvinden. Deze identificatie richt zich onder andere op het kwantificeren van de concentratie fycocyanine, een pigment dat voornamelijk in cyanobacteriën (blauwalgen) voorkomt. Tenslotte komen de beperkingen van de satellietsensor MERIS aan bod. Deze samenvatting van het proefschrift is geschreven voor leken op het gebied van blauwalgen, virussen en aardobservatiesystemen.

Algen en cyanobacteriën

Op het land staan grassen aan het begin van een voedselketen die via uiterst inefficiënte energieverhoudingen uiteindelijk onze honger naar hamburgers stilt. Een vergelijkbare voedselketen in het water begint bij het fytoplankton (Grieks voor 'zwevende plantjes'), dat wordt begraasd door zoöplankton (weer Grieks: dierlijk en zwevend) dat op zijn beurt voedsel is voor vis, walvis, en andere kruipende en zwemmende sushivulling. Het fytoplankton omvat een diversiteit aan soorten, die gemeenschappelijk heeft dat zonlicht haar voornaamste energiebron is. Algen vormen binnen het fytoplankton de meest diverse groep en kunnen worden gezien als evolutionaire voorlopers van complexer, meercellig plantenleven. Cyanobacteriën vertegenwoordigen het primitievere deel van het fytoplankton, dat al miljarden jaren voorkomt en verantwoordelijk wordt gehouden voor de vroege zuurstofproductie op aarde. Als de tropische regenwouden de longen van de aarde zijn, dan vormt het fytoplankton in de oceanen haar kieuwen.

Cyanobacteriële groei en bloei

Cyanobacteriën danken hun naam aan hun blauwgroene (cyaan) verschijning en staan beter (maar officieel onjuist) bekend als blauwalgen. De blauwe tint onderscheidt hen van échte algen en wordt veroorzaakt door het pigment fycocyanine. Cyanobacteriën kunnen met dit pigment groengeel licht gebruiken voor de fotosynthese, wat hen een voordeel biedt in de concurrentie om licht omdat algen en planten dit licht nauwelijks gebruiken. In ondiepe, troebele plassen waar opgewoeld

slib voor een slecht doorzicht zorgt vind je daarom vaak een groot aandeel cyanobacteriën in het fytoplankton.

Een dicht bevolkt gebied als Nederland produceert nogal wat vloeibaar afval, waarvan een deel (meestal) via de waterzuivering zijn weg naar het oppervlaktewater vindt. De laatste decennia is bekend dat een overmaat fosfor en stikstof in het afvalwater sterk bijdraagt aan toename van fytoplankton in meren en plassen. Deze zogenaamde vermesting of eutrofiëring kan in extreme gevallen leiden tot fytoplanktonbloei, een sterke groene vertroebeling die op den duur kan zorgen voor een omslag van een doorgaans helder watersysteem met voornamelijk waterplanten naar een door algen en cyanobacteriën gedomineerd systeem. Daar komt bij dat een aantal zeer algemene cyanobacteriesoorten giftige stoffen kan produceren, die bij hoge dichtheden van de cyanobacterie een direct gezondheidsrisico opleveren. Er is dus voldoende reden om fytoplanktonbloei in te perken: fosfaat werd al uit wasmiddelen verbannen en het uitrijden van mest in de landbouw is streng gereguleerd. Ook het aanleggen van bufferzones rond plassen in natuurgebieden kan bijdragen aan de preventie van fytoplanktonbloei, doordat voedingsstoffen die afkomstig zijn van de landbouw het kwetsbare gebied niet meer kunnen bereiken. Echter, een keur aan maatregelen heeft tot op heden niet kunnen leiden tot daadwerkelijke vermindering van de frequentie en duur van fytoplankton- en vooral cyanobacteriebloei in Nederlandse meren. Ondertussen is de politieke druk vanuit de Europese Unie om de kwaliteit van waterlichamen nauwlettend in de gaten te houden en zo de ecologische én economische status van deze gebieden te waarborgen, toegenomen.

Virussen

Virussen zijn minuscule pakketjes genetische informatie verpakt in een eiwitmembraan. Virussen zijn strikt parasitair: ze kunnen alleen voortbestaan wanneer ze tijdig over een gastheer beschikken waarbinnen ze zich kunnen reproduceren. Wanneer virussen vrij in het milieu voorkomen hebben ze geen metabolisme, ze groeien niet en hebben geen energiebehoefte; virussen zijn daarom geen levende organismen. Bij infectie neemt de genetische code van het virus de besturing van de gastheercel over om de productie van nieuwe virussen en het langzaam kannibaliseren van de cel in gang te zetten. Uit één succesvolle infectie kunnen enkele honderden nieuwe virussen worden geproduceerd, ten koste van de gastheer. Als de gastheer een eencellig organisme is, bijvoorbeeld een alg of (cyano)bacterie, zal deze aan het eind van de reproductiecyclus van het virus sterven. De nieuwe generatie virussen komt dan vrij wanneer de celwand of het celmembraan van de gastheercel lyseert (breekt).

Zelfs met de beste lichtmicroscoop kun je virussen niet zien omdat ze zo klein zijn dat er praktisch geen interactie met lichtgolven plaatsvindt. Er zijn speciale technieken nodig, zoals het fluorescerend impregneren van virus-DNA of het gebruik van

electronenmicroscopie, om virussen zichtbaar te maken. Ecologen hebben daarom nog niet zo lang kennis van de rol van virussen in ecosystemen. Het klassieke virusonderzoek richtte zich op ziekten aan gewassen (tabaksmozaïekvirus) en mensen (pokken). Toen bekend werd dat in een normaal aquatisch milieu miljarden virussen per liter water voorkomen nam de discussie over de rol van virussen als populatieregulerend mechanisme in aquatische ecosystemen ook serieuze vormen aan.

Massale virale sterfte van cyanobacteriën

Snelle groei van een dominante gastheer geeft virussen betere gelegenheid deze te infecteren. De kans om een geschikte gastheer tegen te komen is immers groot wanneer deze het merendeel van de omringende deeltjes uitmaakt. Een gezonde, snel groeiende gastheer is daarbij een uitstekende omgeving voor het virus om zich tot grote aantallen te vermenigvuldigen. Het vrijkomen van vele virusdeeltjes bij elke succesvolle infectie kan zo leiden tot een epidemische infectiegolf, die de gastheer nagenoeg wegvaagt. De 'levenscyclus' van een virus, infectie, vermenigvuldiging, en lyse van de cel, kan zich binnen één dag voltooien. Zo is het dus mogelijk dat een bloei van een enkele cyanobacteriesoort catastrofaal ten einde komt. Vervolgens treedt dan afbraak van celresten door zogenaamde heterotrofe bacteriën op, een verbrandingsproces waarbij zuurstof wordt verbruikt. Als de hoeveelheid organisch materiaal die bij de massale lyse vrijkwam zeer groot was, kan in korte tijd zoveel zuurstof worden verbruikt dat een tekort optreedt. Vissen zullen dan aan het oppervlak naar adem moeten happen of zelfs door verstikking sterven. Plotselinge sterfte van een cyanobacteriebloei kan dus zeer negatieve gevolgen hebben, terwijl het verdwijnen van cyanobacteriën in eerste instantie makkelijk wordt opgevat als een positieve ontwikkeling van de waterkwaliteit.

Waterkleur als een indicatie voor de aanwezigheid van cyanobacteriën

De mate van absorptie van groengeel licht door het blauwe pigment fycocyanine in cyanobacteriën kan worden afgeleid uit het door een wateroppervlak gereflecteerde zonlicht. Het principe is simpel: indien uit het teruggekaatste licht veel groengeel licht mist, is er veel fycocyanine aanwezig. Het is zelfs mogelijk de bepaling vanaf zeer grote afstand te doen, bijvoorbeeld vanuit vliegtuigen of satellieten. Water is blauw, algen zijn groen, slib en organische zuren zijn geelbruin, cyanobacteriën zijn blauwgroen—zelden wordt de kleur van het water bepaald door één factor. Bij het bestuderen van waterkleur houden we bovendien rekening met licht dat wordt geabsorbeerd (bijvoorbeeld voor fotosynthese) en licht dat wordt verstrooid. De combinatie van deze processen bepaalt uiteindelijk welk deel van het spectrum van zonlicht vanuit de waterkolom wordt teruggekaatst naar het wateroppervlak en vervolgens door de atmosfeer (waar ook absorptie en verstrooiing optreden) bij een sensor terechtkomt.

Veranderingen in waterkleur bij massale virale sterfte van cyanobacteriën

In **hoofdstuk 2** van dit proefschrift beschrijven we veranderingen in de absorptie en verstrooiing van licht in water uit de Loosdrechtse Plassen. Het water werd in grote volumes (130 liter per experimentele kolom) naar het laboratorium gebracht en kreeg daar licht en voedingsstoffen toegediend om groei van cyanobacteriën te bevorderen. Binnen twee weken zagen we achtereenvolgens een toename van de populatie cyanobacteriën en een plotselinge ineenstorting van alle draadvormige cyanobacteriesoorten. Deze massale sterfte ging gepaard met een sterke opheldering van het water (het doorzicht nam toe van zo'n 20 centimeter tot anderhalve meter) en een verkleuring van het wateroppervlak van groen naar gelig. Het aantal vrij voorkomende virusdeeltjes nam tegelijkertijd sterk toe, een aanwijzing dat virusactiviteit verantwoordelijk was voor de ineenstorting. Ook werden door middel van electronenmicroscopie grote aantallen cellen gevonden die vol zaten met virussen. We zagen een verschuiving in de verhouding van fytoplanktonpigmenten: het cyanobacteriële pigment fycocyanine verdween haast volledig, terwijl slechts een deel van het pigment chlorofyl *a* verdween. Chlorofyl (bladgroen) is aanwezig in alle algen en cyanobacteriën. De verschuiving in de pigmentverhouding wees er daarom op dat specifiek de dominante cyanobacteriën uit het water verdwenen. Dit stemt overeen met de verwachting bij een epidemische virusinfectie.

Aan de hand van de waterkolomexperimenten voorspelden we dat massale (virale) sterfte van een grote populatie cyanobacteriën in de natuur vanaf een satelliet in de ruimte zichtbaar zou moeten zijn. In een tweede experimentele studie, beschreven in **hoofdstuk 3**, bestudeerden we in detail hoe het door deeltjes in het water weerkaatste licht tijdens virale sterfte van een gecultiveerde cyanobacteriesoort veranderde. Het verschil met de eerdere experimenten was dat we ons specifiek richtten op de verstrooiing van licht in de opwaartse richting, naar het wateroppervlak toe. Immers, alleen dit deel van het licht is uiteindelijk zichtbaar van boven het wateroppervlak. Wanneer lyse van een cel optreedt, valt deze in vele kleine stukjes uit elkaar. Een explosie–zoals het omslag van dit proefschrift suggereert–is het niet, maar de tijdschaal waarop de cel openbreekt en celmateriaal (waarschijnlijk zo'n 20-50 per cel) in het water verspreid worden is eerder in de orde van uren dan dagen. Volgens de natuurkundige modellen van lichtverstrooiing, zoals we die toepasten, maken de kleine vrijgekomen deeltjes het licht in het omringende medium snel diffuus. Uit onze modelsimulaties kwam dit effect wel naar voren, maar het was dermate kortdurend dat het geen geschikte optische indicator voor het in de natuur herkennen van massale lyse van cyanobacteriën bleek. We konden na deze studie wel ons vermoeden bevestigen dat een verschuivende verhouding van de pigmenten fycocyanine en chlorofyl *a* bij massale cyanobacterie-lyse uit het reflectiespectrum is af te leiden.

Detectie en kwantificatie van cyanobacteriepigmenten door aardobservatie

De satelliet ENVISAT van het Europees Ruimteagentschap (ESA) passeert Nederland elke 2 á 3 dagen rond het middaguur, en observeert daarbij de aarde vanaf 800 km hoogte met een arsenaal aan sensoren. Eén van die sensoren, de Medium Resolution Imaging Spectrometer (MERIS), meet het door land en water gereflecteerde zonlicht en stuurt deze informatie, georganiseerd in pixels van 260 bij 290 meter, naar grondstations waar deze op band wordt vastgelegd. Het project ENVISAT heeft tot doel om voor een periode van tenminste 10 jaar gebiedsdekkende studie naar diverse processen in het land- en watermilieu te faciliteren. MERIS is de eerste satelliet die op regelmatige basis overal ter wereld de detectie van fycocyanine mogelijk maakt. De sensor kan namelijk precies het geelgroene licht dat door fycocyanine wordt geabsorbeerd, meten. In **hoofdstuk 4** beschrijven we een algoritme dat MERIS gegevens gebruikt om de concentratie fycocyanine in troebele, voedselrijke wateren te schatten. Het is al langer mogelijk om met satellietbeelden de concentratie chlorofyl *a* in het water af te leiden, dus een combinatie van deze algoritmen zou nu gebruikt kunnen worden om de aanwas en sterfte van cyanobacteriën ten opzichte van ander fytoplankton te volgen.

In **hoofdstuk 5** testen we het fycocyanine-algoritme in het veld. Hiervoor werden waterkleur (gemeten vanaf een boot) en de concentraties van de belangrijkste pigmenten bij een groot aantal meren in Nederland en Spanje gemeten. Het vermoeden bestond dat het ontwikkelde algoritme weliswaar de fycocyanine concentratie correct zou voorspellen wanneer voornamelijk cyanobacteriën aanwezig waren, maar dat bij aanwezigheid van andere fytoplanktongroepen de voorspelling te hoog zou uitvallen. De lichtabsorptie door de pigmenten chlorofyl *b* en chlorofyl *c*, voornamelijk aanwezig in respectievelijk groenalgen en kiezelwieren, zou abusievelijk kunnen worden toegeschreven aan absorptie door fycocyanine. Dit effect bleek inderdaad zichtbaar, echter alleen bij relatief lage concentraties fycocyanine. Het is dus gelukt om een algoritme te ontwikkelen dat relatief gevoelig is voor de aanwezigheid van fycocyanine. De aan de hand van deze resultaten opgestelde randvoorwaarden voor gebruik van het nieuwe MERIS-algoritme laten ruimschoots toe dat de vroege ontwikkeling van cyanobacteriën in voedselrijke plassen vanuit de ruimte gevolgd kan worden.

Zonder goede satellietgegevens heb je nog niet veel aan ingewikkelde algoritmen. We voerden daarom een studie uit naar de kwaliteit van MERIS reflectiedata boven meren en plassen in Nederland, beschreven in **hoofdstuk 6**. Hieruit bleek dat MERIS weliswaar kwalitatief goede data levert, maar dat boven wateroppervlakken die zich in de nabijheid van land bevinden (meren en plassen) problemen optreden. De problemen worden veroorzaakt doordat reflectiesignalen van land en water zich in de atmosfeer mengen. Een reflectiesignatuur die gemengde eigenschappen van water en land heeft,

laat zich niet goed interpreteren met de voor pigmentbepalingen beschikbare algoritmen. In de regel geldt dat dit effect bij grotere wateroppervlakken (het IJsselmeer) niet sterk merkbaar is, maar dat bij kleine meren (zoals de Loosdrechtse Plassen) de pigmentdetectie nagenoeg onmogelijk is.

Vooruitzicht

Verdere ontwikkeling van de beschikbare satellietsensoren en de nabewerking van op afstand gemeten reflectiedata is van belang om de hier gepresenteerde gereedschappen voor waterkwaliteitsbepaling verder toe te passen. We mogen aannemen dat deze ontwikkelingen in de komende jaren zeer veel aandacht zullen krijgen, daar de waterkwaliteit van (kleine) meren en plassen voor steeds minder geld steeds beter in de gaten gehouden dient te worden. Op den duur moet het dus mogelijk zijn om de aanwezigheid van cyanobacteriën in voedselrijke, ondiepe en troebele wateren tenminste wekelijks zichtbaar te maken. Zo kan de studie naar de ontwikkeling en sterfte van cyanobacteriepopulaties in een stroomversnelling worden gebracht. Dit levert tevens op dat gezondheidsrisico's die verband houden met de aanwezigheid van cyanobacteriën tijdig onder de aandacht worden gebracht, bijvoorbeeld als aanvulling op het weerbericht, in tegenstelling tot de huidige situatie waar de waarschuwing meestal wordt gegeven nadat klachten zijn gemeld.

ACKNOWLEDGMENTS

"Beard was never the true standard of brains" (Fuller, 1608 – 1661). Developing something in rather than out of my head has taken some effort. I have certainly tried with this thesis, and I am convinced that I tried the patience of many people in the process. I wish to thank those whose support I had the privilege to receive. If you deserve to be acknowledged for making me seem more intelligent than I am as a result of this thesis, but I nevertheless failed to mention you below, please consider that at the point of writing this I did have quite some hair on my face.

First of all, my board of advisers: Herman, Steef, Riks and Bram, have done a brilliant job at making work on this thesis very rewarding. Herman gets extra credits for sharing an office with me, and both him and Steef were very brave to stay positive throughout our frequent discussions of the work, despite my general doggedness.

I spent one year at the Institute for Environmental Studies (IVM), Vrije Universiteit Amsterdam. Steef, Hans, Marieke, and Reinold deserve thanks for their useful advise during that time and I wish the 'remote sensing cluster' all the best with future theses, web maps, and spin-off companies. Beware, occupants of A603, that I will still come in unannounced and check on plant-health.

During a month at the Centre for Hydrography (CEDEX) in Madrid, Antonio made even longer days than usual, and the technicians and drivers were a great help to our cause. All associated to the remote sensing group: thanks for taking me in. Maybe some time I can come back and play with all the nice hydro plant models? There have been other labs that I got to visit in the last four years, usually for a brief discussion of mutual interests when on my way to a workshop or even a holiday, sometimes with the idea to set up something new. Keep up the good work, everyone.

Of course I spent most time at the NIOO Centre for Limnology, where I thank the Microbial Wetland Ecology department for their interest in this work, and I specifically mention the other members of the virus-hunting team: Hans, Herman, Marjolijn (and her many students). Thank you for solid and fun cooperation. To all at the CL, including the support staff and the folks at the villa, thanks for an enjoyable four years. The past and present crew of the *Luctor* as well as technicians and researchers from the NIOO Centre for Estuarine and Marine Ecology are thanked for the sharing of good food and wisdom on Lake IJsselmeer.

All who were involved in social events far away from the work environment, band members, volleyball team, drinking buddies, friends in remote places: thanks and please stay in touch! It will be great to meet you at the party and please feel welcome to visit—in France, and wherever's next.

I cannot sufficiently express my gratitude to those that steered my (early) development, supported me in many ways, and always provided a home: my parents, my sisters, their fellows and their kids: consider yourselves insufficiently thanked. The Kettunen family has offered an inspiring home (far) away from home and let Marianne run off with a guy who still doesn't speak their language–naturally, I lack the words to express my gratitude.

Marianne: science provides so little certainty. Should I shave?

CURRICULUM VITAE

Stefan Simis was born on August 8, 1978 in Purmerend, the Netherlands, where he attended primary and secondary school. After his exams in 1996 (Da Vinci College, Purmerend) he joined a combined social and natural sciences programme at the University of Amsterdam. After some trial-and-error with Physics and Philosophy, Stefan started the Biology curriculum in 1997. In 2002, he graduated as ecologist (specialization: Biodiversity and Ecosystem dynamics) having received training at the Paleoecology and Landscape Ecology department (including a six-month field training in the cloud forests of Costa Rica studying forest regrowth in relation to landscape patterns), and at the Aquatic Ecology and Ecotoxicology department (studying resource competition among benthic diatoms and cyanobacteria).

In May 2002, Stefan started as Ph.D. student at the Netherlands Institute of Ecology (NIOO-KNAW). The NIOO Centre for Limnology, and for a period of one year, the Institute for Environmental Studies (Vrije Universiteit, Amsterdam), offered a research project on optical remote sensing of mass cyanophagy, resulting in the present thesis.

Starting December 2006, Stefan will work on remote sensing of algal fluorescence at the Laboratoire d'Océanographie de Villefranche, Villefranche-sur-Mer, France.

PUBLICATIONS

Published

Simis, S.G.H., S.W.M. Peters, and H.J. Gons. 2005*a*. Remote sensing of the cyanobacterial pigment phycocyanin in turbid inland water. Limnology and Oceanography 50: 237-245.

Simis, S. G. H., M. Tijdens, H.L. Hoogveld, and H.J. Gons. 2005*b*. Optical changes associated with cyanobacterial bloom termination by viral lysis. Journal of Plankton Research 27: 937-949.

Simis, S.G.H., M. Tijdens, S.W.M. Peters, and H.J. Gons. 2005*c*. Optical characterization of cyanobacterial bloom termination. Verhandlungen Internationale Vereinigung für Theoretische und Angewandte Limnologie 29(2): 941-944.

Gons, H.J., H. Hakvoort, S.W.M. Peters, and **S.G.H. Simis**. 2005. Optical detection of cyanobacterial blooms: Shipboard observation and remote sensing, p. 177-199. *In* J. Huisman, H. C. P. Matthijs and P. M. Visser [eds.], Harmful cyanobacteria. Springer.

H.J. Gons, H.L. Hoogveld, **S.G.H. Simis**, M. Tijdens. 2006. Dynamic modelling of viral impact on cyanobacterial populations in shallow lakes: implications of burst size. Journal of the Marine Biological Association of the UK 86: 537-542.

Van der Grinten, E., M. Janssen, **S.G.H. Simis**, C. Barranguet, and W. Admiraal. 2004. Phosphate regime structures species composition in cultured phototrophic biofilms. Freshwater Biology 49: 369-381.

Van der Grinten, E., **S.G.H. Simis**, C. Barranguet, and W. Admiraal. 2004. Dominance of diatoms over cyanobacterial species in nitrogen-limited biofilms. Archiv für Hydrobiologie 161: 99-112.

Accepted for publication

Simis, S.G.H., M. Tijdens, H.L. Hoogveld, and H.J. Gons. Optical signatures of the filamentous cyanobacterium *Leptolyngbya boryana* during mass viral lysis. Limnology and Oceanography.

Simis, S.G.H., A. Ruiz-Verdú, J.A. Domínguez, R. Peña-Martinez, S.W.M. Peters, and H.J. Gons. Influence of phytoplankton pigment composition on remote sensing of cyanobacterial biomass. Remote Sensing of Environment.

Submitted

Tijdens, M. , H.L. Hoogveld, M.P. Kamst-van Agterveld, **S.G.H. Simis**, A.-C. Baudoux , and H.J. Gons. Linking viral and microbial community dynamics in a shallow, eutrophic lake.